

Wright State University

CORE Scholar

[Browse all Theses and Dissertations](#)

[Theses and Dissertations](#)

2007

Characterization and Modeling Methodology of Polytetrafluoroethylene Based Reactive Materials for the Development of Parametric Models

Stephen D. Rosencrantz
Wright State University

Follow this and additional works at: https://corescholar.libraries.wright.edu/etd_all



Part of the [Mechanical Engineering Commons](#)

Repository Citation

Rosencrantz, Stephen D., "Characterization and Modeling Methodology of Polytetrafluoroethylene Based Reactive Materials for the Development of Parametric Models" (2007). *Browse all Theses and Dissertations*. 192.

https://corescholar.libraries.wright.edu/etd_all/192

This Thesis is brought to you for free and open access by the Theses and Dissertations at CORE Scholar. It has been accepted for inclusion in Browse all Theses and Dissertations by an authorized administrator of CORE Scholar. For more information, please contact library-corescholar@wright.edu.

Characterization and Modeling Methodology of
Polytetrafluoroethylene Based Reactive Materials
for the Development of Parametric Models

A thesis submitted in partial fulfillment
of the requirements for the degree of
Master of Science in Engineering

by

Stephen D. Rosencrantz
B.S., University of Washington, 1998

2007
Wright State University

WRIGHT STATE UNIVERSITY
SCHOOL OF GRADUATE STUDIES

October 24, 2007

I HEREBY RECOMMEND THAT THE THESIS PREPARED UNDER MY SUPERVISION BY Stephen D. Rosencrantz ENTITLED Characterization and Modeling Methodology of Polytetrafluoroethylene Based Reactive Materials for the Development of Parametric Models BE ACCEPTED IN PARTIAL FULFILLMENT OF THE REQUIREMENTS FOR THE DEGREE OF Master of Science in Engineering.

Ramana V. Grandhi, Ph.D.
Thesis Director

George P. G. Huang, P.E., Ph.D.
Department Chair

Committee on
Final Examination

Ramana V. Grandhi , Ph.D.

Henry Daniel Young , Ph.D.

Ronald F. Taylor , Ph.D.

Joseph F. Thomas, Jr. , Ph.D.
Dean, School of Graduate Studies

ABSTRACT

Rosencrantz, Stephen . M.S.Egr., Department of Mechanical and Materials Engineering, Wright State University, 2007 . *Characterization and Modeling Methodology of Polytetrafluoroethylene Based Reactive Materials for the Development of Parametric Models.*

Certain materials, when impacting a target at high velocity will chemically react due to the shock wave passing through them, thereby increasing the damage done by the material. In particular, the reactive materials of interest are capable of acting as both structure and explosive, allowing them to achieve an effect similar to a High Explosive Incendiary (HEI), without the complexity and added mass of fuses.

There are a large number of materials/material combinations that could be used in reactive munitions. The purpose of this effort is to determine an efficient analytical characterization methodology that can be validated with a minimal testing effort. The data resulting from implementing this methodology for many materials would allow the development of a parametric design tool for designing effective reactive munitions using realistic damage metrics. The realistic damage data for the parametric tool could be obtained from high fidelity simulation and a minimal amount of expensive testing, using the characterization tests described here, for validation purposes.

This work presents a method for characterizing, modeling, and then validating the equation of state models of reactive materials in general and demonstrate this process specifically for an aluminum-polytetrafluoroethylene (PTFE) mixture that has been shown in previous tests to be a promising example of this kind of enhanced-lethality projectile. In this thesis a methodology is described to create a reactive material equation of state (EOS) for use in LS-DYNA which is then demonstrated by simulating characterization tests that would aid in the validation of the EOS and a realistic damage test for which test data is provided for comparison.

Contents

1	Background	1
1.1	Purpose	1
1.2	Research	4
2	Reactive Material Modeling	12
2.1	Unreacted Material JWL	15
2.1.1	Unreacted Mixture Validation	23
2.2	Reacted Products JWL	25
2.3	Reaction Rate Equation	32
3	ReactMat Software	39
3.1	Determine Unreacted Parameters Part 1	39
3.2	Determine Unreacted Parameters Part 2	42
3.3	Determine Reacted Parameters Part 1	45
3.4	Determine Reacted Parameters Part 2	47
3.5	Determine Reaction Rate Parameters	48
3.6	Resulting LS-DYNA EOS	50
4	Unreacted Material Characterization	51

CONTENTS

4.1	Simulation of Unreacted Material	
	Characterization Test	52
5	Reacted Material Characterization	75
5.1	Simulation of the Reacted Material	
	Characterization Test	76
6	Reactive Material Box Test	97
6.1	Simulation of a Reactive Projectile	
	vs. a Box	100
6.2	Test Results of a Reactive Projectile	
	Impacting a Box	127
7	Conclusions	134
A	Unreacted Characterization Model	136
B	Reacted Characterization Model	139
C	Realistic Model	143
	Bibliography	148

List of Figures

1.1	Pressure time history for 40 grams of reactive material[4].	8
1.2	Pressure time history for 40 grams of TNT[4].	9
1.3	Impulse time history for 40 grams of reactive material[4].	9
1.4	Impulse time history for 40 grams of TNT[4].	10
2.1	Wave velocity vs. particle velocity for PTFE[27].	16
2.2	Wave velocity vs. particle velocity for aluminum[27].	17
2.3	Pressure vs. specific volume plot of the JWL fit of the Hugoniot data for the unreacted material.	22
2.4	Particle velocity vs. wave velocity plot of the JWL fit of the Hugoniot data for the unreacted material.	22
2.5	Wave velocity vs. particle velocity for aluminum-PTFE mixtures[17].	24
2.6	Unreacted and reacted Hugoniot pressure data with a Rayleigh line. .	28
2.7	JWL fit of the Hugoniot data for the reacted material.	31
2.8	Arrhenius predictions of the reaction rate for several reaction extents.	34
2.9	I&G EOS predictions of the reaction rate for several reaction extents.	37
2.10	Overlay of Figures 2.8 and 2.9.	37
3.1	“Unreacted Material 1” tab.	41

LIST OF FIGURES

3.2	“Unreacted Material 2” tab.	43
3.3	“Unreacted Material 2” tab with the JWL parameters set equal to 25.	44
3.4	“Unreacted Material 2” tab with the JWL parameters optimized to provide the best fit to the Hugoniot data.	44
3.5	“Reacted Material 1” tab.	46
3.6	“Reacted Material 2” tab.	47
3.7	“Reaction Rate” tab.	49
3.8	“LS-DYNA EOS” tab.	50
4.1	Unreacted simulation Euler mesh.	53
4.2	Unreacted simulation Euler mesh, top view.	54
4.3	Unreacted simulation Euler mesh, cut in half.	55
4.4	Unreacted material characterization simulation, material locations at time = 0.00 μ s.	57
4.5	Unreacted material characterization simulation, material locations at time = 0.20 μ s.	58
4.6	Unreacted material characterization simulation, material locations at time = 0.41 μ s.	59
4.7	Unreacted material characterization simulation, material locations at time = 0.62 μ s.	60
4.8	Unreacted material characterization simulation, material locations at time = 0.83 μ s.	61
4.9	Unreacted material characterization simulation, material locations at time = 1.03 μ s.	62
4.10	Unreacted material characterization simulation, material locations at time = 1.24 μ s.	63
4.11	Unreacted material characterization simulation, material locations at time = 1.46 μ s.	64

LIST OF FIGURES

4.12	Unreacted material characterization simulation, material locations at time = 1.67 μ s.	65
4.13	Unreacted material characterization simulation, material locations at time = 1.88 μ s.	66
4.14	Unreacted material characterization simulation, pressure contours at time = 0.00 μ s.	67
4.15	Unreacted material characterization simulation, pressure contours at time = 0.20 μ s.	68
4.16	Unreacted material characterization simulation, pressure contours at time = 0.41 μ s.	68
4.17	Unreacted material characterization simulation, pressure contours at time = 0.62 μ s.	69
4.18	Unreacted material characterization simulation, pressure contours at time = 0.83 μ s.	69
4.19	Unreacted material characterization simulation, pressure contours at time = 1.03 μ s.	70
4.20	Unreacted material characterization simulation, pressure contours at time = 1.24 μ s.	70
4.21	Unreacted material characterization simulation, pressure contours at time = 1.46 μ s.	71
4.22	Unreacted material characterization simulation, pressure contours at time = 1.67 μ s.	71
4.23	Unreacted material characterization simulation, pressure contours at time = 1.88 μ s.	72
4.24	Volume fraction of an element 0.105 cm into the reactive cylinder. . .	73
4.25	Acceleration curve of a node 0.58 cm into the reactive cylinder. . . .	74
5.1	Reacted material characterization simulation euler mesh, full view. . .	77

LIST OF FIGURES

5.2	Reacted material characterization simulation euler mesh, close view. . .	78
5.3	Reacted material characterization simulation euler mesh, top view. . .	79
5.4	Reacted material characterization simulation euler parts, full view. . .	79
5.5	Reacted material characterization simulation euler parts, close view. . .	80
5.6	Reacted material characterization simulation, material locations at time = 00.00 μs	81
5.7	Reacted material characterization simulation, material locations at time = 19.40 μs	81
5.8	Reacted material characterization simulation, material locations at time = 38.80 μs	81
5.9	Reacted material characterization simulation, material locations at time = 58.20 μs	82
5.10	Reacted material characterization simulation, material locations at time = 77.60 μs	82
5.11	Reacted material characterization simulation, material locations at time = 97.00 μs	82
5.12	Reacted material characterization simulation, material locations at time = 116.4 μs	83
5.13	Reacted material characterization simulation, material locations at time = 135.8 μs	83
5.14	Reacted material characterization simulation, material locations at time = 155.2 μs	83
5.15	Reacted material characterization simulation, material locations at time = 174.6 μs	84
5.16	Reacted material characterization simulation, material locations at time = 194.0 μs	84

LIST OF FIGURES

5.17	Reacted material characterization simulation, pressure contours at time = 00.00 μs	85
5.18	Reacted material characterization simulation, pressure contours at time = 19.40 μs	85
5.19	Reacted material characterization simulation, pressure contours at time = 38.80 μs	86
5.20	Reacted material characterization simulation, pressure contours at time = 58.20 μs	86
5.21	Reacted material characterization simulation, pressure contours at time = 77.60 μs	87
5.22	Reacted material characterization simulation, pressure contours at time = 97.00 μs	87
5.23	Reacted material characterization simulation, pressure contours at time = 116.4 μs	88
5.24	Reacted material characterization simulation, pressure contours at time = 135.8 μs	88
5.25	Reacted material characterization simulation, pressure contours at time = 155.2 μs	89
5.26	Reacted material characterization simulation, pressure contours at time = 174.6 μs	89
5.27	Reacted material characterization simulation, pressure contours at time = 194.0 μs	90
5.28	Reacted material characterization simulation, percent reacted at time = 00.00 μs	91
5.29	Reacted material characterization simulation, percent reacted at time = 19.40 μs	91

LIST OF FIGURES

5.30	Reacted material characterization simulation, percent reacted at time = 38.80 μs	92
5.31	Reacted material characterization simulation, percent reacted at time = 58.20 μs	92
5.32	Reacted material characterization simulation, percent reacted at time = 77.60 μs	93
5.33	Reacted material characterization simulation, percent reacted at time = 97.00 μs	93
5.34	Reacted material characterization simulation, percent reacted at time = 116.4 μs	94
5.35	Reacted material characterization simulation, percent reacted at time = 135.8 μs	94
5.36	Reacted material characterization simulation, percent reacted at time = 155.2 μs	95
5.37	Reacted material characterization simulation, percent reacted at time = 174.6 μs	95
5.38	Reacted material characterization simulation, percent reacted at time = 194.0 μs	96
6.1	Projectile configuration.	98
6.2	Box schematic.	99
6.3	Box containing enclosed spaced plate array.	99
6.4	Airmesh used in the simulation of the box test.	101
6.5	Plates and sabot used in the simulation of the box test.	102
6.6	Plate mesh used in the simulation of the box test.	102
6.7	Projectile with reactive material used in the simulation of the box test.	103
6.8	End view of the projectile sabot mesh.	103
6.9	Eulerian mesh containing the reactive material at time = 0.0 μs	104

LIST OF FIGURES

6.10	Box test, with no reactive material shown, at time = 0.0 μs	105
6.11	Box test, with no reactive material shown, at time = 25.0 μs	106
6.12	Box test, with no reactive material shown, at time = 49.997 μs	107
6.13	Box test, with no reactive material shown, at time = 119.99 μs	108
6.14	Box test, with no reactive material shown, at time = 149.99 μs	109
6.15	Box test, with no reactive material shown, at time = 169.99 μs	110
6.16	Box test, with no reactive material shown, at time = 278.99 μs	111
6.17	Box test, with no reactive material shown, at time = 304.0 μs	112
6.18	Box test, with no reactive material shown, at time = 329.0 μs	113
6.19	Box test, with no reactive material shown, at time = 354.0 μs	114
6.20	Box test, with no reactive material shown, at time = 379.0 μs	115
6.21	Box test, with reactive material shown, at time = 0.0 μs	116
6.22	Box test, with reactive material shown, at time = 25.0 μs	117
6.23	Box test, with reactive material shown, at time = 49.997 μs	118
6.24	Box test, with reactive material shown, at time = 119.99 μs	119
6.25	Box test, with reactive material shown, at time = 149.99 μs	120
6.26	Box test, with reactive material shown, at time = 169.99 μs	121
6.27	Box test, with reactive material shown, at time = 278.99 μs	122
6.28	Box test, with reactive material shown, at time = 304.0 μs	123
6.29	Box test, with reactive material shown, at time = 329.0 μs	124
6.30	Box test, with reactive material shown, at time = 354.0 μs	125
6.31	Box test, with reactive material shown, at time = 379.0 μs	126
6.32	The front plate of the box.	128
6.33	The back plate of the box.	129
6.34	The plate array inside the box.	130
6.35	The front of the first plate in the box.	131
6.36	The back of the third plate in the box.	132

LIST OF FIGURES

6.37 Side view of the plate array inside the box. 133

List of Tables

2.1	Constituent material properties.	17
2.2	Hugoniot data for the unreacted reactive material.	18
2.3	JWL fit of the Hugoniot data for the unreacted material.	20
2.4	Unreacted reactive mixture properties.	23
2.5	Unreacted and reacted Hugoniot pressure data with a Rayleigh line. .	27
2.6	Hugoniot data for the reacted material.	29
2.7	JWL fit of the Hugoniot data for the reacted material.	30
2.8	Reaction rates from the Arrhenius equation for multiple pressures and reaction extents.	35
2.9	Reaction rates from the I&G EOS for multiple pressures and reaction extents.	36
2.10	Error between the Arrhenius and I&G EOS predicted reaction rates. .	38
6.1	Reactive projectile dimensions.	97

List of Symbols

Chapter 1

P_0	Peak pressure
T_0	Peak pressure arrival time
A	Scaling factor, that is a material dependent parameter determined by experiment

Chapter 2

P	Pressure
T	Temperature
ω	Grüneisen coefficient
C_v	Heat capacity at a constant volume
r_1	Hugoniot curve fit parameter
r_5	Hugoniot curve fit parameter
r_2	Hugoniot curve fit parameter
r_6	Hugoniot curve fit parameter
F	The Extent of Reaction $\left\{ \begin{array}{l} 0 : \text{no reaction} \\ 1 : \text{complete reaction} \end{array} \right.$
t	Time

LIST OF TABLES

V	Specific volume $\frac{\rho_0}{\rho}$
$freq$	Ignition constant
$frer$	Ignition constant
$ccrit$	Ignition constant
$eetal$	Ignition constant
$grow_1$	Growth constant
es_1	Growth constant
ar_1	Growth constant
em	Growth constant
$grow_2$	Completion constant
es_2	Completion constant
ar_2	Completion constant
en	Completion constant
U_S	Wave velocity
U_P	Particle velocity
S, C_0	Curve fit parameters
Θ_0	Activation Energy
f	Arrhenius Frequency Factor
A_p	Arrhenius Pressure Coefficient

Acknowledgements

I would like to extend my love and appreciation to my wife Erin for her incredible support. I would like to thank Dr. Grandhi for his seemingly infinite patience. I would also like to thank Dr. Ron Hinrichsen, Dr. Monty Moshier, Jeff Hess, Stephen Stratton, Brian Barlow, and Brian Choules at RHAMM Technologies for all of the guidance, support, and motivation, without which, this project would not have been completed. Last, but certainly not least, I would like to thank Dr. Dimitrios Lianos of the U.S. Army Space and Missile Defense Command who funded research of which the work presented here is a part.

Dedicated to
My wife Erin, my daughter Evelyn, and my son Alexander.

Background

1.1 Purpose

Certain materials, when impacting a target at high velocity, will chemically react due to the shock wave passing through them, thereby increasing the damage done by the projectile. While many explosives behave this way, in this thesis particular interest is in reactive materials that can act as both structure and explosive, meaning that an entire projectile could be manufactured of reactive material. This would allow the projectile to achieve a High Explosive Incendiary (HEI) - like effect without the complexity and added mass of fuses, and supporting structures.

General Sciences, Incorporated (GSI), has demonstrated the enhanced lethality of such reactive materials in ground tests at velocities of one to five km/sec. The results are intriguing in that these projectiles can inflict damage using chemical energy (CE) in addition to Kinetic Energy (KE), much like a KE projectile filled with high explosive (HE), but without the added complexity of fusing, timing and ignition mechanisms. The CE can be two to three times that of HE (due to the increased quantity of reactive material allowed by the simplification of the projectile and the elimination of the fuse) and at velocities of four to five km/sec equals the KE, thus doubling the available energy. In addition, ground tests showed that the target damage can be an order of magnitude, or more, greater than that caused by inert projectiles of equal mass and velocity. The reason for this enhancement is due to the generation of high

1.1. PURPOSE

pressures inside closed targets which can lead to increased damage.

These phenomena have been observed with targets consisting of steel plates and aluminum plate arrays, as well as with simulated missile structures and balloons. In order to incorporate this new technology into the design of new interceptor concepts with higher lethality than conventional interceptors, analytical tools are required to predict target damage beyond that measured under experimental conditions, and hopefully to predict damage on real targets in flight with warheads that may contain chem/bio agents. Testing of interceptors with reactive capabilities can be very expensive. For this reason, models are needed that include the high pressure events which are involved in the observed enhancement in opening larger holes and bent metal (petaling) on realistic target materials. The incorporation of the highly energetic chemistry and other properties of these reactive materials into current credible modeling, supported by ground test results from well-instrumented characterization experiments, will increase our confidence in predicting the behavior of reactive interceptors in terms of lethality enhancement and target kill effectiveness.

In this thesis a methodology is presented to develop an equation of state (EOS) for a reactive material. Characterization tests are described for validating the EOS, and an actual test, performed by GSI, is simulated verifying that the analytically derived EOS is reasonable for use in the development of data that could one day drive a parametric design tool. The characterization tests consist of a plane wave test to validate the unreacted material's equation of state and a cylinder test to validate the portion of the EOS used for the reaction products. Along with the discussion of the characterization tests, a discussion of the measurements that need to be made during the test and the necessary data reduction to validate the equation of state of the reactive material are presented.

Although physics-based models may be most appropriate for in-depth, detailed

1.1. PURPOSE

understanding of specific events, they are not appropriate for use in lethality and vulnerability studies where vehicle or munition probabilities of kill are desired. Such studies require simulating many thousands of independent events where the target model (presented in detail) is attacked by the threat from many aspects, at many different velocities. For this type of analysis, a quick-running, yet accurate parametric model is more appropriate.

Empirically based parametric models for explosive events from conventional energetic materials like TNT, RDX, HMX, etc. have been available for use for several years. Codes such as BLAST-X[3] and CONWEP[5] were created by performing hundreds of arena tests with several different configurations of energetic materials (mass, size, shape, casing materials, etc.) and measuring pressure time histories at many radial distances from the blast center. Curve fits were then performed and the parametric models were created.

The larger purpose, of which this project is a part, is the development of a Polytetrafluoroethylene (PTFE) based reactive projectile performance database and a fast-running parametric model based on the database. The methodology presented here would allow the analytical derivation of equations of state for various PTFE based reactive materials. The developed equations of state need to be sufficiently accurate to demonstrate the differences between mixtures of various material compositions. The goal is not to develop an exact analytical representation of each material but to capture the trends in performance (penetration, pressure generated, impulse, etc.) created by different reactive mixtures on realistic targets. This methodology is sufficiently simple to implement for a wide variety of reactive material mixtures, allowing the generation of LS-DYNA simulations of a variety of reactive material projectile impacts on various realistic three dimensional targets chosen to evaluate the performance of the reactive projectiles.

1.2 Research

A literature search was performed and one of the first items that was found was a review of reactive material research that was produced by the National Research Council's Committee on Advanced Energetic Materials and Manufacturing Technologies[10]. The committee reviewed U.S. R&D, published papers, and technology assessments and suggested specific opportunities, strategies, and priorities for government sponsorship of technologies and manufacturing process development. In summary, the committee's recommendations for reactive materials were:

- i. Many trade-off studies should be conducted before reactive materials can move forward.
- ii. The possibility of more advanced applications (such as liners and cases) should be explored.
- iii. Appropriate analytical tools should be developed and used, along with critical experiments, to determine applicability.
- iv. Other materials such as thermoplastics should be investigated in greater detail with lower processing temperatures to allow the use of other metals.
- v. Requirements regarding the material properties of reactive materials should be correlated with results of realistic warhead tests including probability of kill.
- vi. Greater emphasis should be given to materials engineering research and deployment methods to improve the lethality of reactive materials against both soft and hard targets.

The search also revealed that work has been performed or is being performed by each of the DoD services, DoE labs, their contractors and academic institutions funded by AFOSR.

Without exception each of the efforts identified is focused on using Eulerian finite volume techniques to model (in a macro-mechanical sense) the reactive material's characteristics. Typical of these macro-mechanical Eulerian codes is the Second-order Hydrodynamic Automatic Mesh Refinement Code (SHAMRC). SHAMRC is a government-owned Eulerian CFD code that requires the use of tens of millions of cells to model reactive material events. It has two possibilities for Equations of State, 1) a reactive flow model of the combustion processes and 2) a particulate combustion model. One notable exception to the Eulerian macro-mechanical methods is an effort being performed by a consortium of universities led by Georgia Tech and funded by AFOSR's Multidisciplinary University Research Initiative (MURI) program[11]. In this project, entitled Multifunctional Energetic Structural Materials, the university team is performing molecular modeling as well as macro-mechanical modeling of reactive materials.

These molecular level and mesh intensive Eulerian techniques require high performance, massively parallel computer resources in order to solve the tens of millions of equations. Rather than focus this physics-based research on the Eulerian finite volume techniques, it was decided that coupled Euler-Lagrange and coupled SPH(smoothed particle hydrodynamic)-Lagrange methods should be investigated. The reasoning behind this decision was that targets could be more readily modeled in the Lagrangian domain, while the reactive materials could be most effectively modeled in the Eulerian domain or as SPH particles. Computer resources to solve these problems were anticipated to be an order of magnitude less than the other methods. A search of existing codes (CTH, DYNA3D, SHAMRC, AUTODYN, LS-DYNA) that can perform these coupled techniques revealed that LS-DYNA is the only one that could do the job in a fully 3-dimensional way that was readily available. Therefore, LS-DYNA was chosen as the tool that would be used for the simulations in this project.

1.2. RESEARCH

LS-DYNA is a commercial finite-element code derived from the public domain DYNA3D software created at Lawrence Livermore National Laboratory. LS-DYNA is developed and supported by the Livermore Software Technology Corporation (LSTC) and is a fully functional finite element package capable of Lagrange, Euler, coupled Euler-Lagrange, and implicit simulations. The LS-DYNA engine is also the explicit analysis package for a number of other finite element tools including NASTRAN and ANSYS.

For this thesis, the particular reactive material of interest is an aluminum-PTFE mixture that has been shown in previous tests to be a promising example of a reactive material enhanced-lethality projectile. In the fall of 1999, GSI performed a limited number of 40 gram reactive material tests in an instrumented, nitrogen-filled chamber and collected pressure and temperature data during the events[4]. Figure 1.1 shows a typical pressure time history for this event. Based on these early trials with 40 grams of reactive material in the nitrogen-filled tank, it was hypothesized that much of the extensive damage seen from the reactive material is due to the large impulse imparted to the structure. It was decided to compare the pressure time history of the reactive material event with a similar 40 gram Trinitrotoluene (TNT) event as predicted by the CONWEP code. Figure 1.2 shows the predicted pressure time history for 40 grams of TNT. Note the difference in the time scales of the two plots. The TNT peak pressure is approximately 189 psi, but the pulse lasts only 0.00056 seconds. The reactive material peak pressure is approximately 31 psi, but the pulse lasts over 0.4 seconds.

When the areas under the curves are computed by integrating the pressure time histories, the impulses of the events are obtained. Figures 1.3 and 1.4 show the impulse time histories for the reactive material and TNT events, respectively. Note that the total impulse for the TNT is on the order of 0.01 psi-sec while the reactive material's total impulse is over two orders of magnitude larger at about 6 psi-sec. This is

1.2. RESEARCH

a significant observation. The pressure time history for conventional explosive materials (as used in CONWEP) was found to have a form governed by an exponentially decaying term as seen in equation 1.1 [5].

$$P(t) = P_0 \left(1 - \frac{t}{t_0}\right) e^{-A \frac{t}{t_0}} \quad (1.1)$$

Where:

P_0 = Peak pressure

t_0 = Peak pressure arrival time.

A = Blast scaling factor, that is a material dependent parameter determined by experiment

Figure 1.2 clearly shows the exponential decay form for pressure decay for TNT described in equation 1.1. The form of the pressure time history for the reactive material (Figure 1.1) does not appear to be exponential at all. Although this is only a single data set, it suggests that the CONWEP and BLAST-X codes are not appropriate for modeling the pressure and impulse time histories for reactive materials.

Gerald I. Kerley has done extensive work in the development of very high fidelity reactive equations of state for pure PTFE and aluminum-PTFE mixtures for NSWC, Dahlgren Division[16, 17, 18]. Kerley's models were developed for use with the PANDA code that he developed for Sandia National Laboratory for the purpose of understanding the reactive nature of PTFE based mixtures[14].

In his final paper Kerley begins to look into, and model, the micro-structural properties of the aluminum-PTFE. The method used by Kerley is too intensive to implement for simulations with large or complicated targets to generate the first look approximation that is needed from the EOS generated in this project. Some of Kerley's conclusions, however, are both reassuring as to the probability of success of

1.2. RESEARCH

this effort and emphasize some of the limitations that must be kept in mind when interpreting the results of less detailed material models. One finding is that “the ideal mixture approximation, in which both mixture components have the same pressure and temperature, gives surprisingly good results for the average mixture properties, except near the shock front”[18]. Near the shock front, “This phenomenon is not so important for high-density mixtures, but it has a profound effect on the final shock state for porous mixtures”[18].

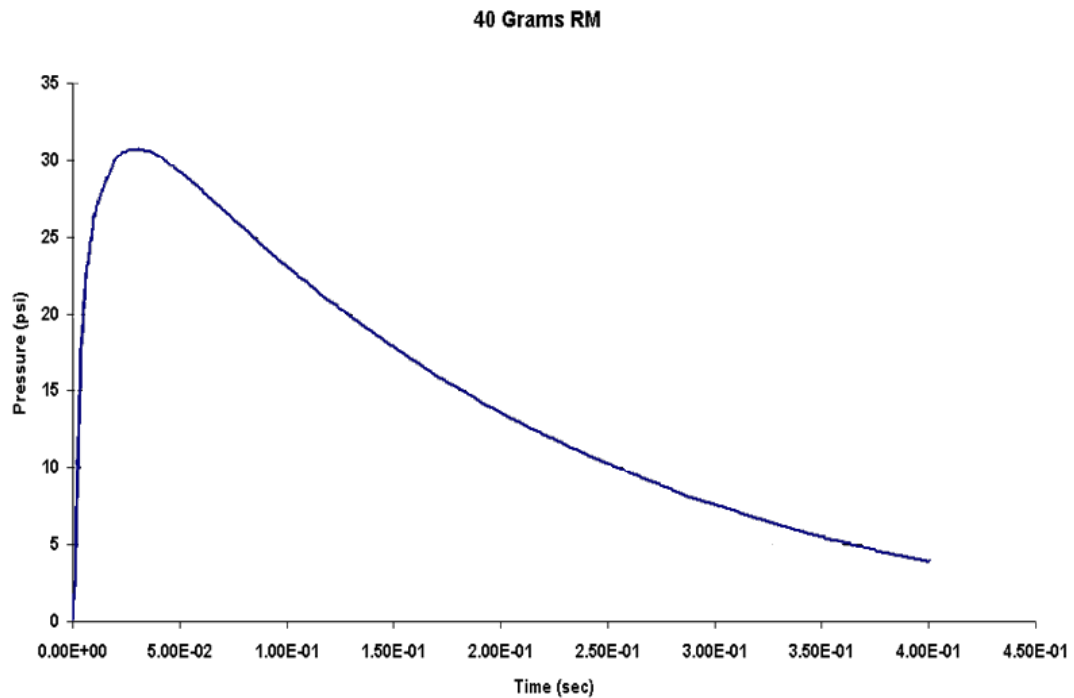


Figure 1.1: Pressure time history for 40 grams of reactive material[4].

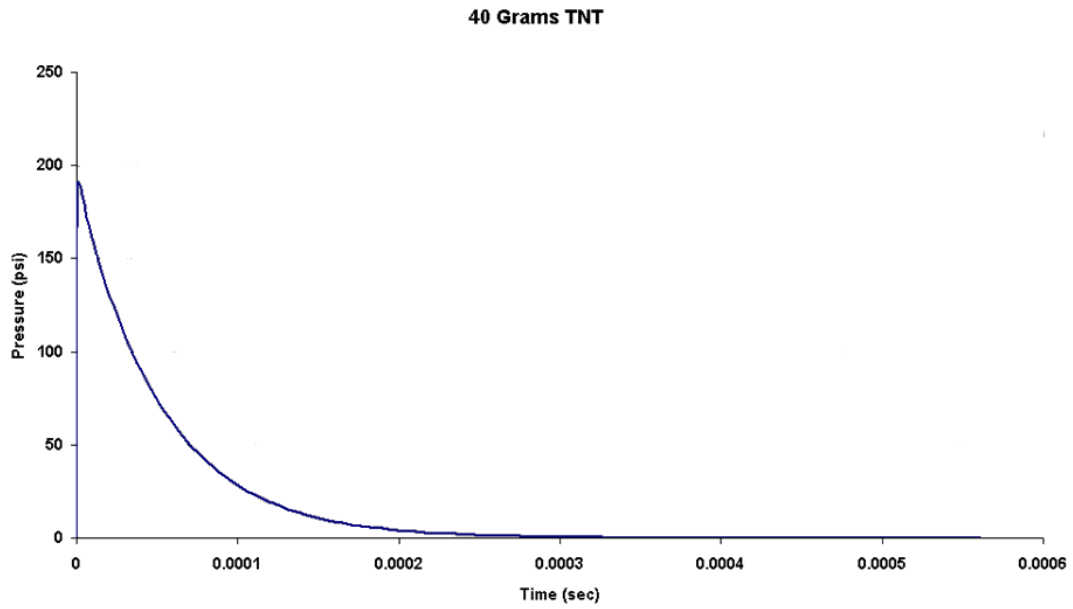


Figure 1.2: Pressure time history for 40 grams of TNT[4].

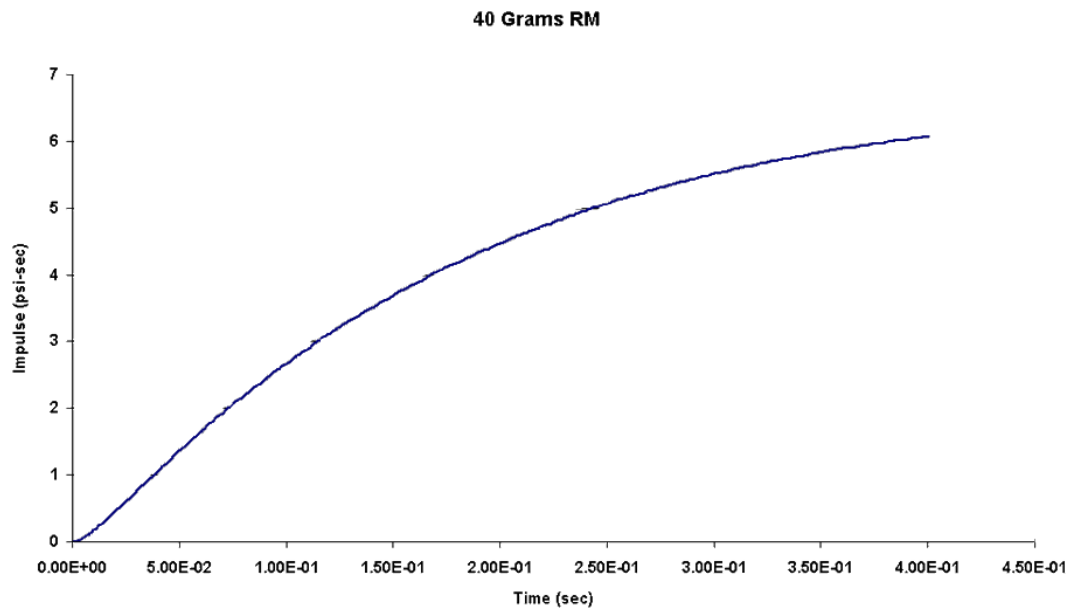


Figure 1.3: Impulse time history for 40 grams of reactive material[4].

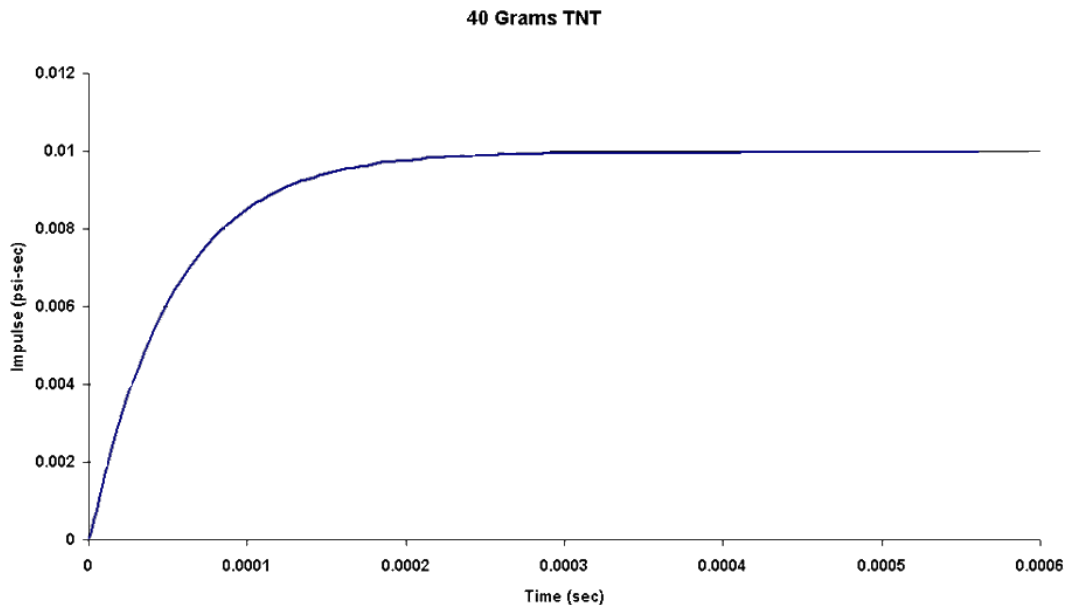


Figure 1.4: Impulse time history for 40 grams of TNT[4].

In Kerley's work with aluminum and PTFE he primarily used PANDA to develop equations of state for the Eulerian finite element software package CTH created by Sandia National Laboratories[16, 17, 18]. Initially this project looked at using CTH, but found that it was inappropriate for many of the realistic targets that would ultimately be desirable, such as the box model with internal plates described in Chapter 6. For example, it is inappropriate to model parts of a target some distance from the point of impact in the Eulerian domain as stiffness and bending are not well modeled. A combination of Eulerian and Lagrangian techniques is most appropriate for the simulations desired as the target can be best modeled in the Lagrangian domain and the reactive material best modeled in the Euler domain. In the past, Euler-Lagrange coupling has been accomplished using CTH to develop pressures which are then input into a solely Lagrangian LS-DYNA model, enabling a one-way coupling. As an improvement and simplification of this process, LS-DYNA is now capable of fully (two-way) coupled Euler-Lagrange simulations. While LS-DYNA does not have material EOSs that are as complex as those available in CTH (such as the Sesame

1.2. RESEARCH

models), the level of fidelity of LS-DYNA's EOS's was found to be sufficient given the constraints of this project.

Reactive Material Modeling

This chapter describes the EOS and material model chosen to model the reactive aluminum-PTFE material discussed in this thesis using LS-DYNA. This chapter also describes the methodology developed to determine the parameters for the EOS. The methodology for generating the EOS presented here involves the creation of a material in the Euler domain using the “IGNITION AND GROWTH OF REACTION IN HE” (I&G) equation of state (EOS) and a “MAT ELASTIC PLASTIC HYDRO” material model for the reactive material[21]. For the equation of state of the reactive material the I&G EOS model was chosen to accurately model the properties of the reactive material both before and after its reaction. The I&G EOS model represents the behavior of the unreacted material, in this case a pressed mixture of PTFE, and aluminum, with a Jones-Wilkins-Lee (JWL) equation. A second JWL equation is used to describe the behavior of the reacted material which consists of $\text{AlF}_4(\text{gas})$, $\text{AlF}(\text{gas})$, $\text{C}_3(\text{gas})$, $\text{C}(\text{gas})$, $\text{F}(\text{gas})$, $\text{C}_2(\text{gas})$, $\text{CF}(\text{gas})$, $\text{C}_5(\text{gas})$, and $\text{C}(\text{solid})$. Finally a pressure based rate equation governs the rate of the reaction that converts unreacted material into reaction products. This EOS has been used previously to model explosives such as PBXW-115 [23]. Equation 2.1 is the form of the JWL equation used by LS-DYNA’s I&G EOS model for both unreacted and reacted materials[21].

$$P = r_1 \exp^{-r_5 V} + r_2 \exp^{-r_6 V} + \omega C_v \frac{T}{V} \quad (2.1)$$

Where:

P = Pressure

V = Specific volume, $\frac{1}{\rho}$

T = Temperature

ω = Grüneisen coefficient

C_v = Heat capacity at a constant volume

r_1, r_5, r_2, r_6 = Hugoniot curve fit parameters

LS-DYNA's I&G EOS model reaction rate equation consists of three parts. The first part of the equation determines the reaction rate just after the shock wave passes, the second part determines the reaction rate during a period of slow growth of the reaction, and the third part determines the reaction rate during the rapid completion of the reaction. Equation 2.2 is the form of the reaction rate equation used by LS-DYNA's I&G EOS model [21].

$$\frac{\partial F}{\partial t} = \underbrace{freq (1 - F)^{frer} (V^{-1} - 1 - ccrit)^{eetal}}_{\text{Ignition}} + \underbrace{grow_1 (1 - F)^{es1} F^{ar1} P^{em}}_{\text{Growth}} + \underbrace{grow_2 (1 - F)^{es2} F^{ar2} P^{en}}_{\text{Completion}} \quad (2.2)$$

Where:

$$F = \text{Extent of reaction} \begin{cases} 0 & : \text{ no reaction} \\ 1 & : \text{ complete reaction} \end{cases}$$

t = Time

V = Specific volume $\frac{\rho_0}{\rho}$

P = Pressure

$freq, frer, ccrit, eetal$ = Ignition constants

$grow_1, es_1, ar_1, em$ = Growth constants

$grow_2, es_2, ar_2, en$ = Completion constants

Three additional parameters not shown in Equation 2.2 need to be input when using the I&G EOS; $fm\text{ig}$, $fm\text{gr}$, and $fm\text{ngr}$. When $F \geq fm\text{ig}$ the ‘‘Ignition’’ portion of Equation 2.2 is set to zero. When $F \geq fm\text{gr}$ the ‘‘Growth’’ portion of Equation 2.2 is set to zero. When $F \leq fm\text{ngr}$ the ‘‘Completion’’ portion of Equation 2.2 is set to zero[21]. These parameters allow the user to model the reaction’s stages (ignition, growth, and completion) differently.

2.1 Unreacted Material JWL

To create a JWL equation for the unreacted material, a method described in Meyers' Dynamic Behavior of Materials was used to generate Hugoniot data for the mixture[28]. The JWL equation can then be fit to the Hugoniot data. Basic shock data is available for both unreacted PTFE and aluminum, as well as numerous other elements and compounds in the Los Alamos Shock Hugoniot Data Volume[27]. This Hugoniot data for the various materials is available in the form of particle velocity vs. wave velocity data. For each of the components of the mixture, a line was fit through the particle velocity vs. wave velocity data. Where the line has the form[28]:

$$U_S = SU_P + C_0 \tag{2.3}$$

Where:

U_S = Wave velocity

U_P = Particle velocity

S, C_0 = Curve fit parameters

The data and the resulting lines are shown in Figure 2.1 for PTFE and Figure 2.2 for aluminum. Next the Grüneisen coefficient must be obtained or estimated for each material. As described by Meyers the Grüneisen coefficient is a constant that represents the relationship between vibrational frequencies and volume[28]. If measured data is not available then the Grüneisen coefficient can be estimated, as has been done here, using Equation 2.4[28].

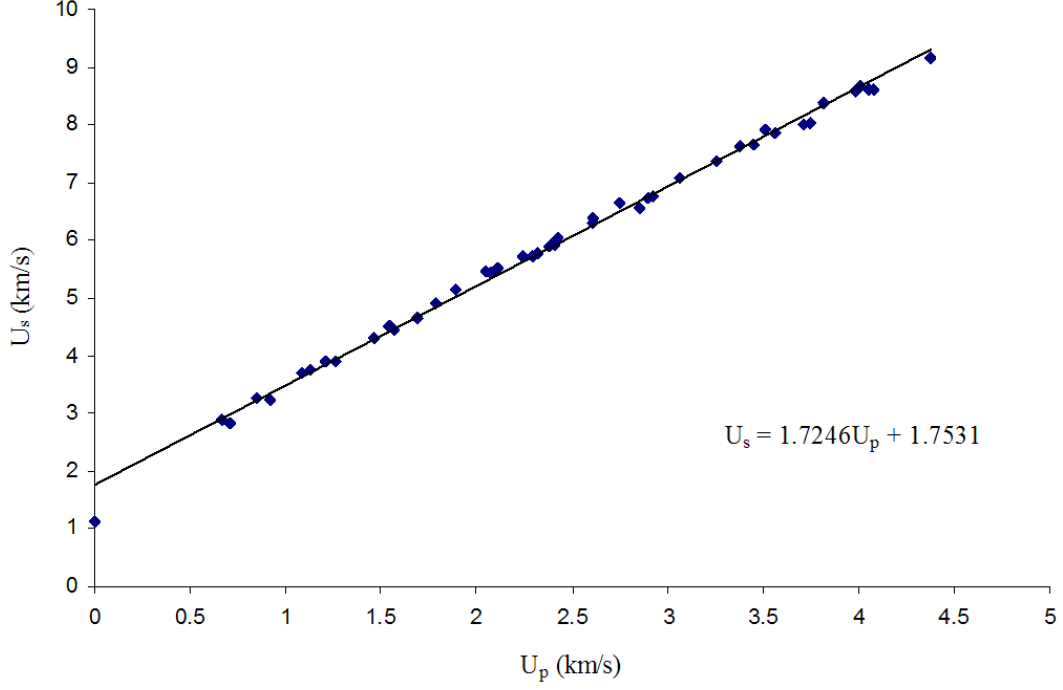


Figure 2.1: Wave velocity vs. particle velocity for PTFE[27].

$$\omega \cong 2S - 1 \quad (2.4)$$

Where:

ω = Grüneisen Coefficient

The remaining required parameters, the density and the heat capacity at constant volume, can either be looked up or measured. In this case the density and heat capacity were looked up for each of the materials resulting in the final set of data shown in Table 2.1 below.

To generate the properties of the mixture, the properties for each material are mass averaged and converted to the gram-centimeter-microsecond set of units that is used for all of the models developed in this thesis. The final values are $C_0 = 3.1814E - 1 \left(\frac{\text{cm}}{\mu\text{s}} \right)$, $S = 1.5504$, $\rho_0 = 2.3909 \left(\frac{\text{g}}{\text{cm}^3} \right)$, $C_v = 9.9300E - 6 \left(\frac{100\text{KJ}}{\text{g}\cdot\text{K}} \right)$, and

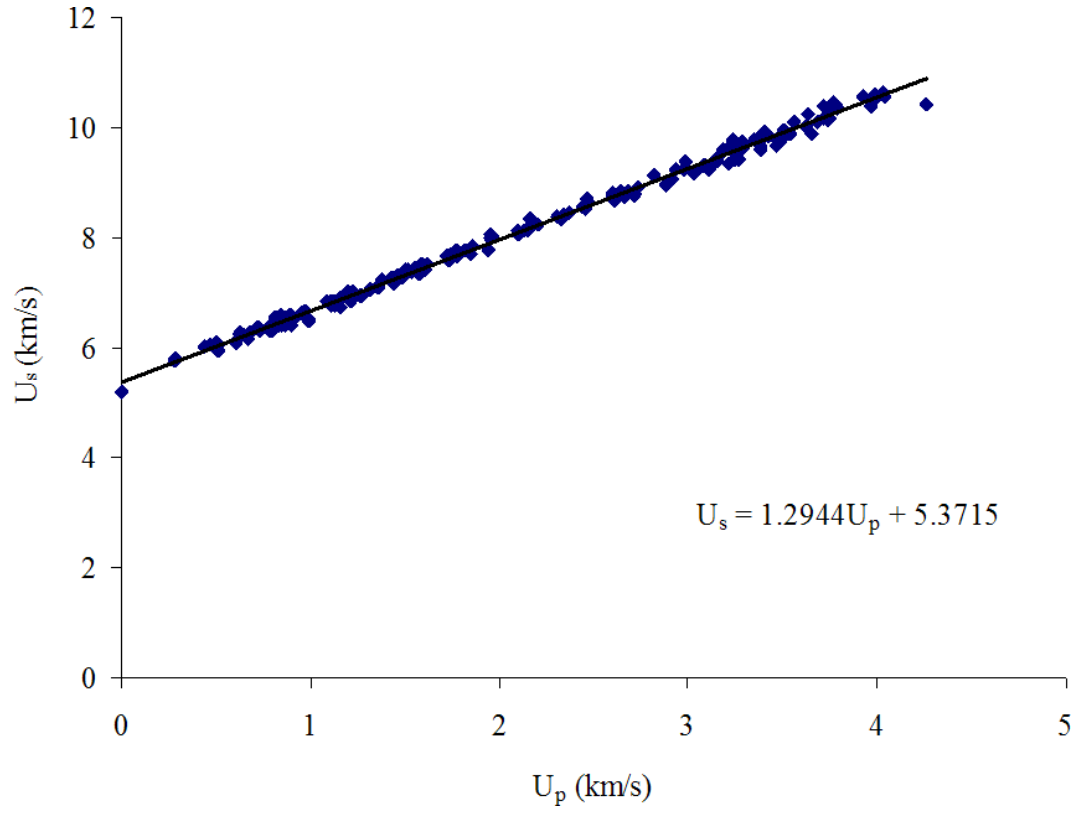


Figure 2.2: Wave velocity vs. particle velocity for aluminum[27].

Table 2.1: Constituent material properties.

Materials	$C_0 \left(\frac{m}{s}\right)$	S	$\rho_0 \left(\frac{kg}{m^3}\right)$	$C_v \left(\frac{J}{g \cdot K}\right)$	ω
aluminum	5370	1.29	2784	0.90	1.58
PTFE	1840	1.71	2150	1.05	2.42

2.1. UNREACTED MATERIAL JWEL

$\omega = 2.1008$. Using these values, the Hugoniot data for the reactive mixture can be created using the following procedure. Create a range of particle velocity values and use C_0 and S to calculate a corresponding set of wave velocity values using Equation 2.3. Next the basic shock parameter relations shown in Equations 2.5, 2.6, and 2.7 are used to calculate the necessary pressure, density, and temperature data respectively[28].

$$P = (C_0 U_P + S U_P^2) \quad (2.5)$$

$$\rho = \frac{\rho_0}{\left(1 - \frac{U_P}{U_S}\right)} \quad (2.6)$$

$$T = \frac{U_P^2}{2C_V} + T_0 \quad (2.7)$$

This then results in the Hugoniot data for the unreacted reactive mixture shown in Table 2.2.

Table 2.2: Hugoniot data for the unreacted reactive material.

$U_P \left(\frac{\text{cm}}{\mu\text{s}}\right)$	$U_S \left(\frac{\text{cm}}{\mu\text{s}}\right)$	$P \text{ (100GPa)}$	$\rho_0 \left(\frac{\text{g}}{\text{cm}^3}\right)$	$T \text{ (K)}$
0.0	3.181×10^{-1}	0.0	2.391	0.0
8.247×10^{-3}	3.309×10^{-1}	6.525×10^{-3}	2.452	3.425
1.649×10^{-2}	3.437×10^{-1}	1.356×10^{-2}	2.511	1.370×10^1
2.474×10^{-2}	3.565×10^{-1}	2.109×10^{-2}	2.569	3.082×10^1
3.299×10^{-2}	3.693×10^{-1}	2.913×10^{-2}	2.625	5.480×10^1
4.124×10^{-2}	3.821×10^{-1}	3.767×10^{-2}	2.680	8.562×10^1
4.948×10^{-2}	3.949×10^{-1}	4.672×10^{-2}	2.733	1.233×10^2
5.773×10^{-2}	4.076×10^{-1}	5.627×10^{-2}	2.785	1.678×10^2
6.598×10^{-2}	4.204×10^{-1}	6.632×10^{-2}	2.836	2.192×10^2
7.423×10^{-2}	4.332×10^{-1}	7.688×10^{-2}	2.885	2.774×10^2
8.247×10^{-2}	4.460×10^{-1}	8.795×10^{-2}	2.933	3.425×10^2
9.072×10^{-2}	4.588×10^{-1}	9.952×10^{-2}	2.980	4.144×10^2
9.897×10^{-2}	4.716×10^{-1}	1.116×10^{-1}	3.026	4.932×10^2

Continued on next page...

2.1. UNREACTED MATERIAL JWL

$U_P \left(\frac{\text{cm}}{\mu\text{s}} \right)$	$U_S \left(\frac{\text{cm}}{\mu\text{s}} \right)$	$P \text{ (100GPa)}$	$\rho_0 \left(\frac{\text{g}}{\text{cm}^3} \right)$	$T \text{ (K)}$
1.072×10^{-1}	4.844×10^{-1}	1.242×10^{-1}	3.071	5.788×10^2
1.155×10^{-1}	4.972×10^{-1}	1.372×10^{-1}	3.114	6.713×10^2
1.237×10^{-1}	5.099×10^{-1}	1.508×10^{-1}	3.157	7.706×10^2
1.320×10^{-1}	5.227×10^{-1}	1.649×10^{-1}	3.198	8.768×10^2
1.402×10^{-1}	5.355×10^{-1}	1.795×10^{-1}	3.239	9.898×10^2
1.485×10^{-1}	5.483×10^{-1}	1.946×10^{-1}	3.279	1.110×10^3
1.567×10^{-1}	5.611×10^{-1}	2.102×10^{-1}	3.317	1.236×10^3
1.649×10^{-1}	5.739×10^{-1}	2.263×10^{-1}	3.355	1.370×10^3
1.732×10^{-1}	5.867×10^{-1}	2.429×10^{-1}	3.392	1.510×10^3
1.814×10^{-1}	5.994×10^{-1}	2.600×10^{-1}	3.429	1.658×10^3
1.897×10^{-1}	6.122×10^{-1}	2.777×10^{-1}	3.464	1.812×10^3
1.979×10^{-1}	6.250×10^{-1}	2.958×10^{-1}	3.499	1.973×10^3
2.062×10^{-1}	6.378×10^{-1}	3.144×10^{-1}	3.533	2.141×10^3
2.144×10^{-1}	6.506×10^{-1}	3.336×10^{-1}	3.566	2.315×10^3
2.227×10^{-1}	6.634×10^{-1}	3.532×10^{-1}	3.599	2.497×10^3
2.309×10^{-1}	6.762×10^{-1}	3.733×10^{-1}	3.631	2.685×10^3
2.392×10^{-1}	6.890×10^{-1}	3.940×10^{-1}	3.662	2.880×10^3
2.474×10^{-1}	7.017×10^{-1}	4.151×10^{-1}	3.693	3.082×10^3
2.557×10^{-1}	7.145×10^{-1}	4.368×10^{-1}	3.723	3.291×10^3
2.639×10^{-1}	7.273×10^{-1}	4.589×10^{-1}	3.753	3.507×10^3
2.722×10^{-1}	7.401×10^{-1}	4.816×10^{-1}	3.782	3.730×10^3
2.804×10^{-1}	7.529×10^{-1}	5.048×10^{-1}	3.810	3.959×10^3
2.887×10^{-1}	7.657×10^{-1}	5.284×10^{-1}	3.838	4.196×10^3
2.969×10^{-1}	7.785×10^{-1}	5.526×10^{-1}	3.865	4.439×10^3
3.052×10^{-1}	7.912×10^{-1}	5.773×10^{-1}	3.892	4.689×10^3
3.134×10^{-1}	8.040×10^{-1}	6.025×10^{-1}	3.918	4.946×10^3

Using the Hugoniot data we can now fit the parameters r_1 , r_5 , r_2 , r_6 , and ω of the JWL form shown in Equation 2.1. Doing this results in the JWL parameters $r_1 = 2.2937$, $r_2 = 2.0093$, $r_5 = 45.2922$, $r_6 = 51.5454$, and $\omega = 7.7642$. A series of pressure values predicted by the Hugoniot data and the JWL equation are shown along with the square of the error between them in Table 2.3 for comparison purposes. Figure 2.3 shows a comparison of the original Hugoniot's pressure vs. volume (P-V) curve and the P-V curve produced by the JWL equation. Figure 2.4 shows a comparison of the

2.1. UNREACTED MATERIAL JWL

original Hugoniot's particle vs wave velocity curve and curve described by the JWL equation. Figure 2.3 and Figure 2.4 show two of the more common ways of looking at the Hugoniot in two dimensions. Both plots show the original Hugoniot data from Table 2.2 compared with the JWL fit Hugoniot data from Table 2.3 for the purposes of illustrating the quality of the fit that was achieved. Figure 2.3 shows a good fit at higher pressures where the reaction rate is much greater. Figure 2.4 shows that at velocities greater than $3.0 \times 10^{-1} \left(\frac{\text{cm}}{\mu\text{s}} \right)$, the fit matches very well.

Table 2.3: JWL fit of the Hugoniot data for the unreacted material.

Hugoniot Pressure (Real) (100GPa)	JWL Estimated Pressure (100GPa)	Error (<i>Estimate</i> - <i>Real</i>) ²
0.0	4.910×10^{-20}	2.411×10^{-39}
6.525×10^{-3}	2.708×10^{-4}	3.912×10^{-5}
1.356×10^{-2}	1.109×10^{-3}	1.549×10^{-4}
2.109×10^{-2}	2.554×10^{-3}	3.436×10^{-4}
2.913×10^{-2}	4.639×10^{-3}	5.997×10^{-4}
3.767×10^{-2}	7.400×10^{-3}	9.163×10^{-4}
4.672×10^{-2}	1.087×10^{-2}	1.285×10^{-3}
5.627×10^{-2}	1.507×10^{-2}	1.697×10^{-3}
6.632×10^{-2}	2.005×10^{-2}	2.142×10^{-3}
7.688×10^{-2}	2.581×10^{-2}	2.608×10^{-3}
8.795×10^{-2}	3.240×10^{-2}	3.086×10^{-3}
9.952×10^{-2}	3.983×10^{-2}	3.563×10^{-3}
1.116×10^{-1}	4.812×10^{-2}	4.028×10^{-3}
1.242×10^{-1}	5.731×10^{-2}	4.469×10^{-3}
1.372×10^{-1}	6.741×10^{-2}	4.877×10^{-3}
1.508×10^{-1}	7.844×10^{-2}	5.240×10^{-3}
1.649×10^{-1}	9.043×10^{-2}	5.549×10^{-3}
1.795×10^{-1}	1.034×10^{-1}	5.797×10^{-3}
1.946×10^{-1}	1.173×10^{-1}	5.974×10^{-3}
2.102×10^{-1}	1.323×10^{-1}	6.077×10^{-3}
2.263×10^{-1}	1.482×10^{-1}	6.099×10^{-3}
2.429×10^{-1}	1.652×10^{-1}	6.038×10^{-3}
2.600×10^{-1}	1.833×10^{-1}	5.893×10^{-3}
2.777×10^{-1}	2.024×10^{-1}	5.666×10^{-3}

Continued on next page. . .

2.1. UNREACTED MATERIAL JWL

Hugoniot Pressure (Real) (100GPa)	JWL Estimated Pressure (100GPa)	Error (<i>Estimate - Real</i>) ²
2.958×10^{-1}	2.226×10^{-1}	5.359×10^{-3}
3.144×10^{-1}	2.439×10^{-1}	4.977×10^{-3}
3.336×10^{-1}	2.663×10^{-1}	4.528×10^{-3}
3.532×10^{-1}	2.898×10^{-1}	4.023×10^{-3}
3.733×10^{-1}	3.144×10^{-1}	3.473×10^{-3}
3.940×10^{-1}	3.402×10^{-1}	2.896×10^{-3}
4.151×10^{-1}	3.671×10^{-1}	2.309×10^{-3}
4.368×10^{-1}	3.952×10^{-1}	1.733×10^{-3}
4.589×10^{-1}	4.244×10^{-1}	1.193×10^{-3}
4.816×10^{-1}	4.548×10^{-1}	7.176×10^{-4}
5.048×10^{-1}	4.864×10^{-1}	3.368×10^{-4}
5.284×10^{-1}	5.192×10^{-1}	8.506×10^{-5}
5.526×10^{-1}	5.532×10^{-1}	3.651×10^{-7}
5.773×10^{-1}	5.884×10^{-1}	1.241×10^{-4}
6.025×10^{-1}	6.249×10^{-1}	5.011×10^{-4}

2.1. UNREACTED MATERIAL JWL

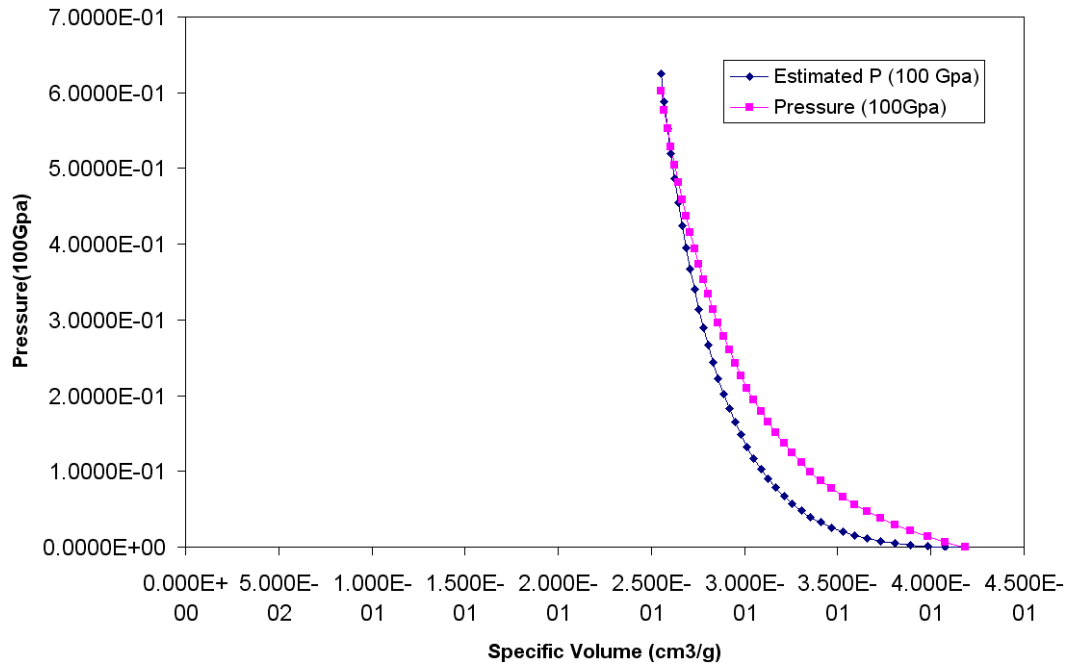


Figure 2.3: Pressure vs. specific volume plot of the JWL fit of the Hugoniot data for the unreacted material.

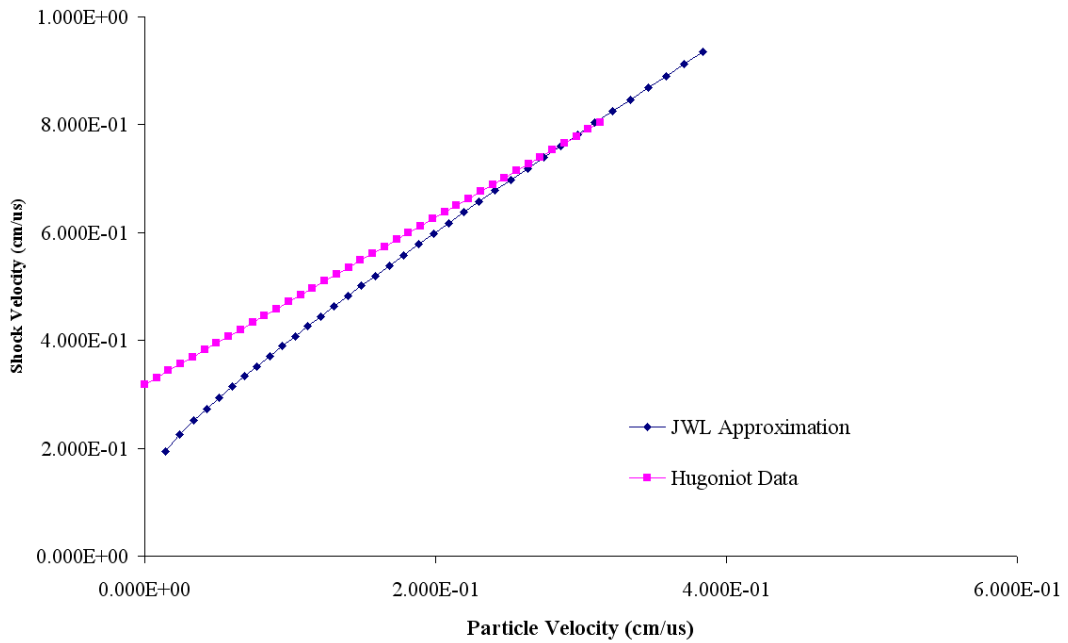


Figure 2.4: Particle velocity vs. wave velocity plot of the JWL fit of the Hugoniot data for the unreacted material.

2.1.1 Unreacted Mixture Validation

As a first order check of the reasonableness of the technique of combining the properties of the various constitutive materials, we applied the same technique to several compositions of aluminum-PTFE reactive material. The results were then compared to the more robust methodology accomplished by Kerley[17]. Recall that the basic properties for aluminum and PTFE are in Table 2.1. Using these properties we have found the properties of several different mixtures of aluminum and PTFE as shown in Table 2.4.

Table 2.4: Unreacted reactive mixture properties.

Materials	C_0 ($\frac{\text{km}}{\text{s}}$)	S	ρ_0 ($\frac{\text{g}}{\text{cm}^3}$)	C_v ($\frac{\text{MJ}}{\text{kg}\cdot\text{K}}$)	ω
100% Al 0% PTFE	5.370	1.290	2.784	9.000×10^{-4}	1.580
90% Al 10% PTFE	5.017	1.332	2.721	9.150×10^{-4}	1.664
75% Al 25% PTFE	4.488	1.395	2.626	9.375×10^{-4}	1.790
50% Al 50% PTFE	3.605	1.500	2.467	9.750×10^{-4}	2.000
26.45% Al 73.55% PTFE	2.774	1.599	2.318	1.010×10^{-3}	2.198
10% Al 90% PTFE	2.193	1.668	2.213	1.035×10^{-3}	2.336
0% Al 100% PTFE	1.840	1.710	2.150	1.050×10^{-3}	2.420

If we plot the data in Table 2.4 on top of the data obtained by Kerley we get the plot shown in Figure 2.5. Our data matches up well at higher particle velocities and accurately preserves the overall trend of the changing mixture. At lower particle velocities the aluminum-PTFE mixtures show very non-linear behavior. This is due to the “large difference between the compressibility” of aluminum and PTFE noted by Kerley[17]. This methodology is therefore going to be more accurate for high pressures where the compressibility of the constituent components is more similar. Fortunately the minimum reactive projectile velocity of interest is on the order of one kilometer per second or higher and again the purpose of reactive material models developed with this methodology is to show the difference in different reactive mixtures rather

2.1. UNREACTED MATERIAL JWL

than determine exactly what will happen with a specific mixture in a real-world environment. It is worth noting that the curve fit found for the unreacted material results in a shock vs. particle velocity curve more like Kerley's curves than the straight line a better JWL fit might have predicted, as is shown in Figure 2.4, indicating the fit may be better than the P-V curve, shown in Figure 2.3, might have indicated by itself.

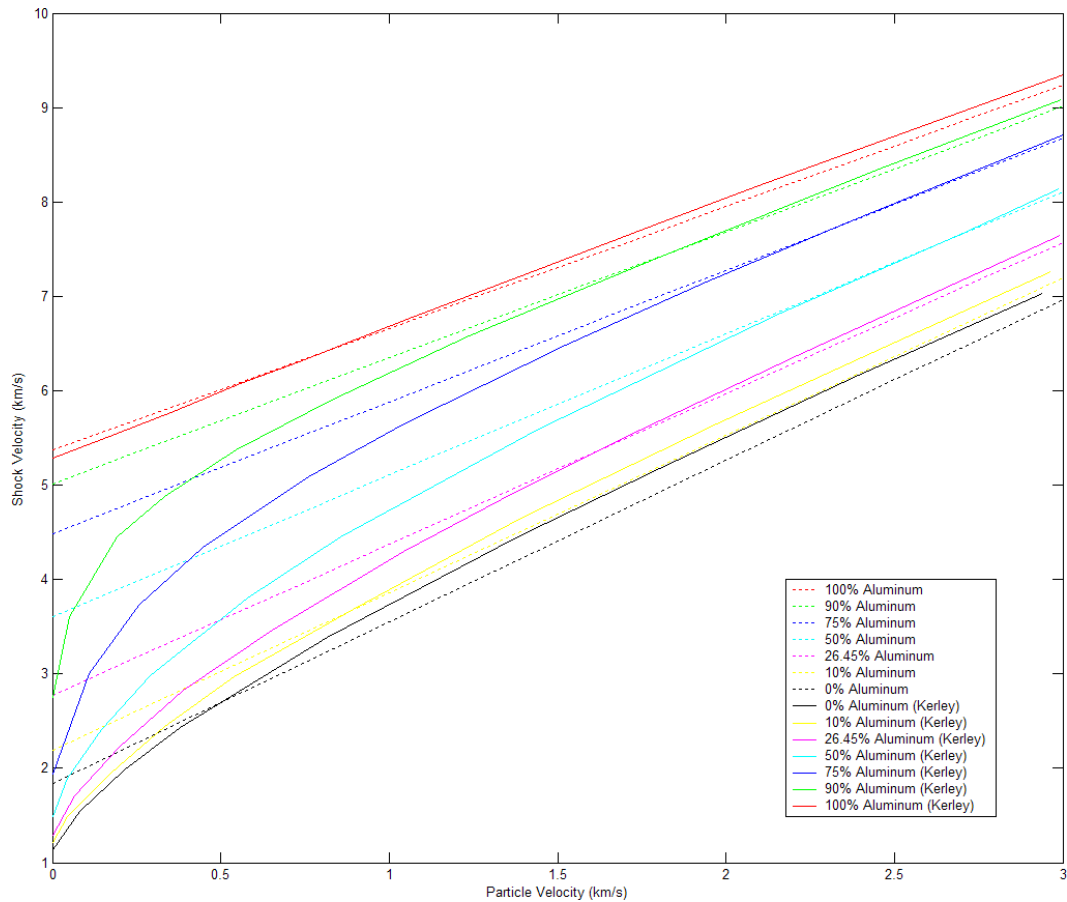


Figure 2.5: Wave velocity vs. particle velocity for aluminum-PTFE mixtures[17].

2.2 Reacted Products JWEL

To create a JWEL equation for the reacted material, we began by picking an impact velocity of interest based on the test data described in Chapter 6. The impact velocity and explosive density used here are $U_P = 3.134 \times 10^{-1} \left(\frac{\text{cm}}{\mu\text{s}} \right)$ and $\rho = 2.391 \left(\frac{\text{g}}{\text{cm}^3} \right)$ respectively. Next, data from the unreacted Hugoniot is needed. This data, the unreacted wave velocity $U_s = 8.040 \times 10^{-1} \left(\frac{\text{cm}}{\mu\text{s}} \right)$, the pressure $P = 7.812 \times 10^{-1} (100\text{Gpa})$, the temperature $T = 5.239 \times 10^3 (\text{K})$, and the internal energy $E_i = 5.202 \times 10^{-2} \left(100 \frac{\text{KJ}}{\text{g}} \right)$ calculated using Equation 2.8, along with the energy created by the reaction, essentially defines the initial state of the reacted gas just after reaction.

$$E = U_P^2 + C_{v_{\text{unreacted}}} T_0 \quad (2.8)$$

Where:

U_P = Particle velocity in the unreacted material $\left(\frac{\text{cm}}{\mu\text{s}} \right)$.

$C_{v_{\text{unreacted}}}$ = Heat Capacity of the unreacted material at a constant volume $\left(100 \frac{\text{KJ}}{\text{g} \cdot \text{K}} \right)$.

T_0 = Initial Temperature of the unreacted Material (prior to impact) (K).

Using this data, the second version of NASA Glenn's computer program Chemical Equilibrium with Applications (CAE2) was run using the CEAgui (graphical user interface) program. This program allows the calculation of the heat of reaction and the heat capacity of the reaction products, given the unreacted mixture and its initial conditions. The heat of reaction was found to be $Q = 1.35 \times 10^{-2} \left(100 \frac{\text{KJ}}{\text{g}} \right)$ and the heat capacity of the reaction products was found to be $C_{v_{\text{reacted}}} = 1.457 \times 10^{-5} \left(100 \frac{\text{KJ}}{\text{g} \cdot \text{K}} \right)$. Using the heat of reaction, we can use the polytropic gas law described in Reference [28] to calculate the pressure vs. particle velocity curves. The polytropic gas law is shown in Equation 2.9 [28]. The polytropic gas constant is calculated using an

2.2. REACTED PRODUCTS JWL

equation from Table 10.3 in Reference [28], the equation is shown below as Equation 2.10 and the constant that was calculated is $\gamma = 4.894$. Table 2.5 shows pressure data for a variety of particle velocities for the unreacted material as calculated in Section 2.1, the reacted material as calculated using Equation 2.10, and the Rayleigh line. This data is depicted graphically in Figure 2.6. The Rayleigh line goes through the Chapman-Jouguet point on the reacted Hugoniot and the Von Neumann point on the unreacted Hugoniot. The Chapman-Jouguet point represents the pressure and wave speed of the reaction products. The Von Neumann point is the pressure and wave speed of the initial wave through the unreacted material. Between these two points the reaction is occurring and converting unreacted material into reacted material.

$$P\rho^{-\gamma} = K \quad (2.9)$$

Where:

γ = Polytropic Gas Constant.

P = Pressure (100Gpa).

ρ = Density ($\frac{\text{g}}{\text{cm}^3}$).

K = Constant.

$$\gamma = \sqrt{\frac{U_S^2}{2Q + 1}} \quad (2.10)$$

Where:

γ = Polytropic Gas Constant.

U_S = Wave speed in the unreacted material (detonation velocity) ($\frac{\text{cm}}{\mu\text{s}}$).

Q = Heat of reaction ($100\frac{\text{KJ}}{\text{g}}$).

2.2. REACTED PRODUCTS JWL

Table 2.5: Unreacted and reacted Hugoniot pressure data with a Rayleigh line.

Particle Velocity $\left(\frac{\text{cm}}{\mu\text{s}}\right)$	Unreacted Hugoniot Pressure (100GPa)	Reacted Hugoniot Pressure (100GPa)	Rayleigh Line Pressure (100GPa)
0	0	0.125639315	0
2.00×10^{-2}	1.67×10^{-2}	1.28×10^{-1}	3.76×10^{-2}
4.00×10^{-2}	3.64×10^{-2}	1.37×10^{-1}	7.53×10^{-2}
6.00×10^{-2}	5.90×10^{-2}	1.51×10^{-1}	1.13×10^{-1}
8.00×10^{-2}	8.46×10^{-2}	1.71×10^{-1}	1.51×10^{-1}
1.00×10^{-1}	1.13×10^{-1}	1.96×10^{-1}	1.88×10^{-1}
1.20×10^{-1}	1.45×10^{-1}	2.27×10^{-1}	2.26×10^{-1}
1.40×10^{-1}	1.79×10^{-1}	2.64×10^{-1}	2.63×10^{-1}
1.60×10^{-1}	2.17×10^{-1}	3.06×10^{-1}	3.01×10^{-1}
1.80×10^{-1}	2.57×10^{-1}	3.54×10^{-1}	3.39×10^{-1}
2.00×10^{-1}	3.00×10^{-1}	4.07×10^{-1}	3.76×10^{-1}
2.20×10^{-1}	3.47×10^{-1}	4.67×10^{-1}	4.14×10^{-1}
2.40×10^{-1}	3.96×10^{-1}	5.31×10^{-1}	4.52×10^{-1}
2.60×10^{-1}	4.48×10^{-1}	6.02×10^{-1}	4.89×10^{-1}
2.80×10^{-1}	5.04×10^{-1}	6.78×10^{-1}	5.27×10^{-1}
3.00×10^{-1}	5.62×10^{-1}	7.60×10^{-1}	5.65×10^{-1}
3.20×10^{-1}	6.23×10^{-1}	8.47×10^{-1}	6.02×10^{-1}
3.40×10^{-1}	6.87×10^{-1}	9.40×10^{-1}	6.40×10^{-1}

The Chapman-Jouguet pressure is certainly a pressure that occurs for the reaction products so we can use it along with the polytropic gas constant, the Chapman-Jouguet particle velocity, and the heat of reaction to calculate the density of the reaction products at the Chapman-Jouguet point ρ_{cj} using Equation 2.11. The Chapman-Jouguet pressure and density are then used with Equation 2.9 to calculate the value of K for the impact velocity. The calculated value of K is $K = 1.420 \times 10^{-3}$ and the value of the Chapman-Jouguet parameters for the initial velocity are pressure,

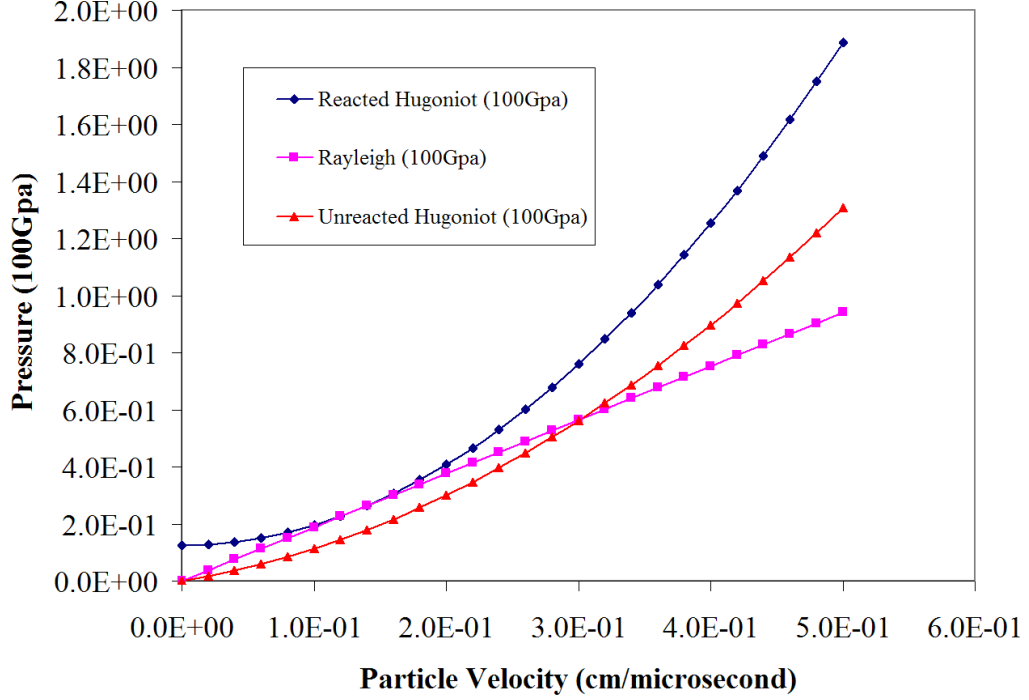


Figure 2.6: Unreacted and reacted Hugoniot pressure data with a Rayleigh line.

$P_{cj} = 2.513 \times 10^{-1}$ (100Gpa); the particle velocity, $U_{cj} = 1.335 \times 10^{-1}$ $\left(\frac{\text{cm}}{\mu\text{s}}\right)$; and the density, $\rho_{cj} = 2.879$ $\left(\frac{\text{g}}{\text{cm}^3}\right)$.

$$\rho_{cj} = \frac{P_{cj}}{(\gamma - 1) \left(\frac{U_{cj}^2}{2} + Q \right)} \quad (2.11)$$

Where:

ρ_{cj} = Chapman-Jouguet density $\left(\frac{\text{g}}{\text{cm}^3}\right)$.

P_{cj} = Chapman-Jouguet Pressure (100GPa).

γ = Polytropic Gas Constant.

U_{cj} = Chapman-Jouguet Particle Velocity $\left(\frac{\text{cm}}{\mu\text{s}}\right)$.

Q = Heat of Reaction $\left(100\frac{\text{KJ}}{\text{g}}\right)$.

2.2. REACTED PRODUCTS JWL

Finally, Equations 2.9, 2.5, 2.6, and 2.7 were used to generate Hugoniot data for the given initial velocity. This data is shown in Table 2.6. From this data we can optimize the coefficients of the JWL equation to best fit the Hugoniot data. The parameters found are $r_1 = 4.7356 \times 10^5$, $r_2 = 3.0620 \times 10^1$, $r_5 = 5.0467 \times 10^1$, $r_6 = 4.9234$, and $\omega = 3.1403 \times 10^{-1}$. The pressures calculated using the JWL equation and the parameters are shown along with the original Hugoniot pressures in Table 2.7. A P-V plot is shown in Figure 2.7 for both the derived Hugoniot and the JWL equation, to show the quality of the JWL fit for the reacted material.

Table 2.6: Hugoniot data for the reacted material.

Pressure (100GPa)	Specific Volume $\left(\frac{\text{cm}^3}{\text{g}}\right)$	Detonation Velocity $\left(\frac{\text{cm}}{\mu\text{s}}\right)$	Particle Ve- locity $\left(\frac{\text{cm}}{\mu\text{s}}\right)$	Temperature (K)
2.51×10^{-1}	3.47×10^{-1}	7.87×10^{-1}	1.34×10^{-1}	6.04×10^3
2.43×10^{-1}	3.50×10^{-1}	7.74×10^{-1}	1.31×10^{-1}	6.00×10^3
2.35×10^{-1}	3.52×10^{-1}	7.60×10^{-1}	1.29×10^{-1}	5.95×10^3
2.26×10^{-1}	3.55×10^{-1}	7.47×10^{-1}	1.27×10^{-1}	5.91×10^3
2.18×10^{-1}	3.58×10^{-1}	7.33×10^{-1}	1.24×10^{-1}	5.87×10^3
2.09×10^{-1}	3.60×10^{-1}	7.18×10^{-1}	1.22×10^{-1}	5.83×10^3
2.01×10^{-1}	3.63×10^{-1}	7.04×10^{-1}	1.19×10^{-1}	5.79×10^3
1.93×10^{-1}	3.67×10^{-1}	6.89×10^{-1}	1.17×10^{-1}	5.74×10^3
1.84×10^{-1}	3.70×10^{-1}	6.74×10^{-1}	1.14×10^{-1}	5.70×10^3
1.76×10^{-1}	3.74×10^{-1}	6.58×10^{-1}	1.12×10^{-1}	5.66×10^3
1.68×10^{-1}	3.77×10^{-1}	6.43×10^{-1}	1.09×10^{-1}	5.61×10^3
1.59×10^{-1}	3.81×10^{-1}	6.26×10^{-1}	1.06×10^{-1}	5.57×10^3
1.51×10^{-1}	3.85×10^{-1}	6.10×10^{-1}	1.03×10^{-1}	5.52×10^3
1.42×10^{-1}	3.90×10^{-1}	5.92×10^{-1}	1.01×10^{-1}	5.48×10^3
1.34×10^{-1}	3.95×10^{-1}	5.75×10^{-1}	9.75×10^{-2}	5.43×10^3
1.26×10^{-1}	4.00×10^{-1}	5.57×10^{-1}	9.44×10^{-2}	5.38×10^3
1.17×10^{-1}	4.06×10^{-1}	5.38×10^{-1}	9.12×10^{-2}	5.34×10^3
1.09×10^{-1}	4.12×10^{-1}	5.18×10^{-1}	8.79×10^{-2}	5.29×10^3
1.01×10^{-1}	4.19×10^{-1}	4.98×10^{-1}	8.45×10^{-2}	5.24×10^3
9.21×10^{-2}	4.26×10^{-1}	4.77×10^{-1}	8.09×10^{-2}	5.19×10^3
8.38×10^{-2}	4.35×10^{-1}	4.54×10^{-1}	7.71×10^{-2}	5.14×10^3
7.54×10^{-2}	4.44×10^{-1}	4.31×10^{-1}	7.31×10^{-2}	5.09×10^3
6.70×10^{-2}	4.55×10^{-1}	4.06×10^{-1}	6.90×10^{-2}	5.04×10^3

Continued on next page...

2.2. REACTED PRODUCTS JWL

Pressure (100GPa)	Specific Volume $\left(\frac{\text{cm}^3}{\text{g}}\right)$	Detonation Velocity $\left(\frac{\text{cm}}{\mu\text{s}}\right)$	Particle Ve- locity $\left(\frac{\text{cm}}{\mu\text{s}}\right)$	Temperature (K)
5.86×10^{-2}	4.68×10^{-1}	3.80×10^{-1}	6.45×10^{-2}	4.98×10^3
5.03×10^{-2}	4.83×10^{-1}	3.52×10^{-1}	5.97×10^{-2}	4.93×10^3
4.19×10^{-2}	5.01×10^{-1}	3.21×10^{-1}	5.45×10^{-2}	4.87×10^3
3.35×10^{-2}	5.24×10^{-1}	2.87×10^{-1}	4.88×10^{-2}	4.81×10^3
2.51×10^{-2}	5.56×10^{-1}	2.49×10^{-1}	4.22×10^{-2}	4.74×10^3
1.68×10^{-2}	6.04×10^{-1}	2.03×10^{-1}	3.45×10^{-2}	4.68×10^3
8.38×10^{-3}	6.96×10^{-1}	1.44×10^{-1}	2.44×10^{-2}	4.60×10^3

Table 2.7: JWL fit of the Hugoniot data for the reacted material.

Hugoniot Pressure (Real) (100GPa)	JWL Estimated Pressure (100GPa)	Error $(\text{Estimate} - \text{Real})^2$
2.51×10^{-1}	2.49×10^{-1}	3.30×10^{-6}
2.43×10^{-1}	2.42×10^{-1}	1.66×10^{-6}
2.35×10^{-1}	2.34×10^{-1}	6.59×10^{-7}
2.26×10^{-1}	2.26×10^{-1}	1.52×10^{-7}
2.18×10^{-1}	2.18×10^{-1}	4.52×10^{-10}
2.09×10^{-1}	2.10×10^{-1}	8.59×10^{-8}
2.01×10^{-1}	2.02×10^{-1}	3.06×10^{-7}
1.93×10^{-1}	1.93×10^{-1}	5.77×10^{-7}
1.84×10^{-1}	1.85×10^{-1}	8.31×10^{-7}
1.76×10^{-1}	1.77×10^{-1}	1.02×10^{-6}
1.68×10^{-1}	1.69×10^{-1}	1.12×10^{-6}
1.59×10^{-1}	1.60×10^{-1}	1.11×10^{-6}
1.51×10^{-1}	1.52×10^{-1}	9.94×10^{-7}
1.42×10^{-1}	1.43×10^{-1}	8.00×10^{-7}
1.34×10^{-1}	1.35×10^{-1}	5.57×10^{-7}
1.26×10^{-1}	1.26×10^{-1}	3.10×10^{-7}
1.17×10^{-1}	1.18×10^{-1}	1.10×10^{-7}
1.09×10^{-1}	1.09×10^{-1}	5.55×10^{-9}
1.01×10^{-1}	1.00×10^{-1}	4.19×10^{-8}
9.21×10^{-2}	9.16×10^{-2}	2.46×10^{-7}
8.38×10^{-2}	8.30×10^{-2}	6.19×10^{-7}

Continued on next page...

2.2. REACTED PRODUCTS JWL

Hugoniot Pressure (Real) (100GPa)	JWL Estimated Pressure (100GPa)	Error ($Estimate - Real$) ²
7.54×10^{-2}	7.43×10^{-2}	1.12×10^{-6}
6.70×10^{-2}	6.57×10^{-2}	1.66×10^{-6}
5.86×10^{-2}	5.72×10^{-2}	2.07×10^{-6}
5.03×10^{-2}	4.88×10^{-2}	2.18×10^{-6}
4.19×10^{-2}	4.06×10^{-2}	1.76×10^{-6}
3.35×10^{-2}	3.26×10^{-2}	8.25×10^{-7}
2.51×10^{-2}	2.50×10^{-2}	6.61×10^{-9}
1.68×10^{-2}	1.81×10^{-2}	1.85×10^{-6}
8.38×10^{-3}	1.21×10^{-2}	1.37×10^{-5}

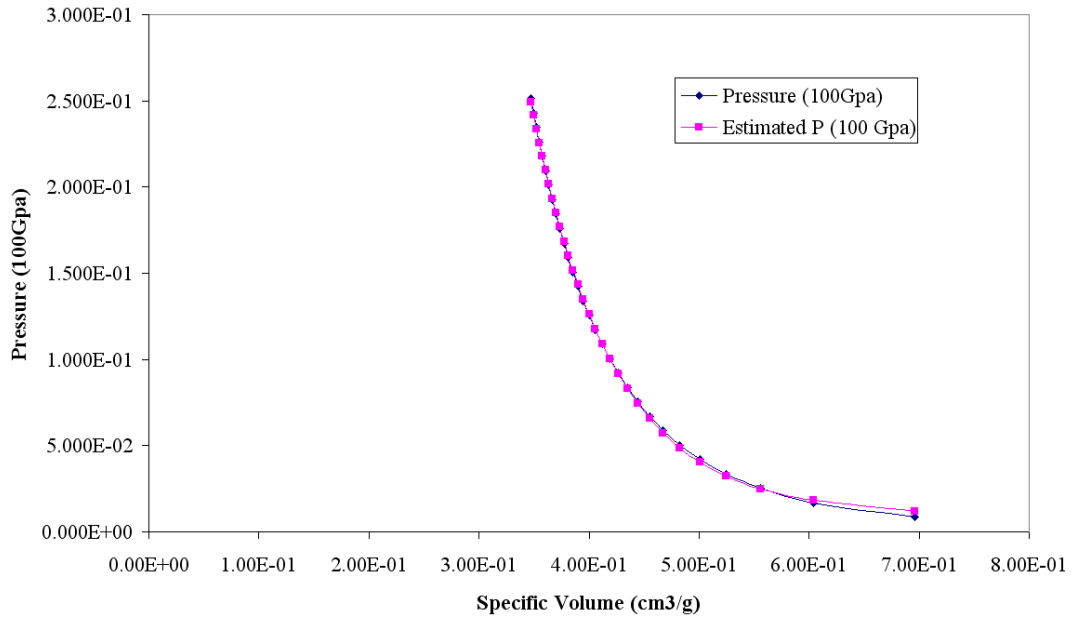


Figure 2.7: JWL fit of the Hugoniot data for the reacted material.

2.3 Reaction Rate Equation

In reference [16], Kerley showed that the decomposition of pure PTFE can be described by an Arrhenius rate law shown in Equation 2.12.

$$\frac{d\lambda}{dt} = (1 - \lambda) F e^{\frac{-\Theta_0(1+A_P P)}{T}} \quad (2.12)$$

Where:

$$F = \text{Extent of reaction} \begin{cases} 0 & : \text{no reaction} \\ 1 & : \text{complete reaction} \end{cases}$$

t = Time

P = Pressure

T = Temperature

Θ_0 = Activation energy

f = Arrhenius Frequency factor

A_P = Arrhenius Pressure coefficient

For pure PTFE, Kerley found the activation energy to be $\Theta_0 = 3.25\text{eV}$, the frequency factor to be $F = 8.4 \times 10^{16}\text{s}^{-1}$, and the pressure coefficient to be $A_P = 1.2 \times 10^{-2} \frac{1}{\text{GPa}}$. According to Kerley “The fact that the above activation energy is so close to a typical C-C bond energy (3.6 eV), shows that breaking of C-C bonds in the polymer chain is the rate-determining step in both thermal degradation (formation of C_2F_4 monomer molecules) and complete dissociation” [16]. We assume, as Kerley did in his work, that as a first approximation we can use the same reaction rate for our aluminum-PTFE mixtures that we use for pure PTFE, because the activation energies should be roughly the same [16]. It is worth noting some of the limitations of this assumption as Kerley did:

“There are two difficulties with the above argument, both of which were

2.3. REACTION RATE EQUATION

noted in Ref. [7]. The first is that hot spots, produced by shock interactions between the PTFE and Al particles, could lower the threshold for reaction and change the macroscopic reaction rate law, just as occurs in heterogeneous explosives. Understanding this mechanism is the principal goal of the present work. In addition, the rate of diffusion of reactant species to the Al-PTFE interface could also limit the reaction rate. We have not attempted to explore the second effect in this study”[16]

The reaction rate equation (Equation 2.2) included in the I&G EOS model is significantly different in form from the Arrhenius rate equation shown in Equation 2.12. To determine the parameters needed for the I&G EOS model version we first note that F and t in Equation 2.12 are the same as F and t in Equation 2.2, respectively. Only one of either the growth or completion portions of Equation 2.2 are necessary to accurately approximate Equation 2.12, so $fm\grave{x}ig$, $fm\grave{x}gr$, and $fm\grave{n}gr$ were set equal to 0. This will prevent ignition and growth portions of Equation 2.2 from turning on, and will also cause the completion portion of the equation to contribute the full reaction rate from start to finish.

The Hugoniot data from Table 2.2 was used to obtain compatible sets of values consisting of pressure, temperature, and specific volume at several extents of the reaction (different percentages of material reacted). This data is shown in Table 2.8. These values were then used to calculate the reaction rate $\frac{dF}{dt}$ for the Arrhenius rate law used by Kerley (Equation 2.12) these rates are shown in Table 2.8 and Figure 2.8. The parameters in the completion portion of the I&G EOS reaction rate equation were then optimized to give the nearly matching rates shown in Table 2.9 and Figure 2.9. The square of the error in the rates is shown in Table 2.10 and Figure 2.10, it can be seen that the I&G and Arrhenius rates overlap nearly exactly. The optimized parameters found were $grow_2 = 8.5991 \times 10^{13} (100 GPa^{-en} \mu s^{-1})$, $es_2 = 1.0020$, $ar_2 =$

2.3. REACTION RATE EQUATION

6.3067×10^{-5} , $en = 2.6963 \times 10^1$, $fm_{xig} = 0.0$, $fm_{xgr} = 0.0$, and $fm_{ngr} = 0.0$. The rest of the parameters were irrelevant because of the values chosen for fm_{xig} , fm_{xgr} , and fm_{ngr} which, as mentioned previously, were set equal to 0.

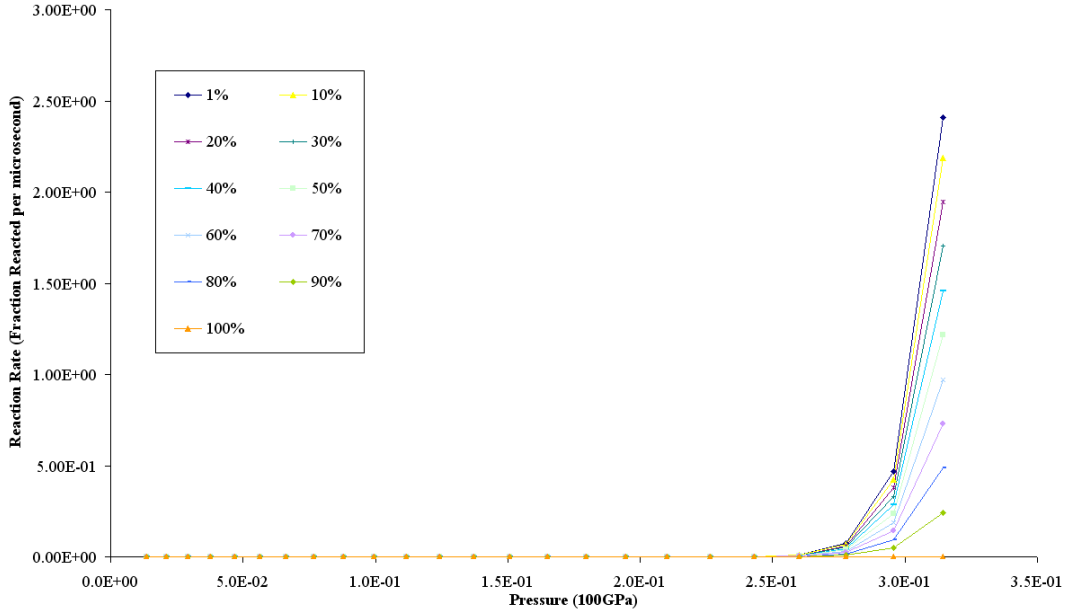


Figure 2.8: Arrhenius predictions of the reaction rate for several reaction extents.

2.3. REACTION RATE EQUATION

Table 2.8: Reaction rates from the Arrhenius equation for multiple pressures and reaction extents.

Pressure (100GPa)	Reaction Extents										
	1%	10%	20%	30%	40%	50%	60%	70%	80%	90%	100%
1.36E-02	0.00E+00	0.00E+00	0.00E+00	0.00E+00	0.00E+00	0.00E+00	0.00E+00	0.00E+00	0.00E+00	0.00E+00	0.00E+00
2.11E-02	0.00E+00	0.00E+00	0.00E+00	0.00E+00	0.00E+00	0.00E+00	0.00E+00	0.00E+00	0.00E+00	0.00E+00	0.00E+00
2.91E-02	3.87E-299	3.52E-299	3.13E-299	2.74E-299	2.35E-299	1.96E-299	1.57E-299	1.17E-299	7.83E-300	3.91E-300	0.00E+00
3.77E-02	9.70E-190	8.82E-190	7.84E-190	6.86E-190	5.88E-190	4.90E-190	3.92E-190	2.94E-190	1.96E-190	9.80E-191	1.09E-205
4.67E-02	4.32E-130	3.93E-130	3.49E-130	3.05E-130	2.62E-130	2.18E-130	1.74E-130	1.31E-130	8.72E-131	4.36E-131	4.84E-146
5.63E-02	5.43E-94	4.94E-94	4.39E-94	3.84E-94	3.29E-94	2.74E-94	2.20E-94	1.65E-94	1.10E-94	5.49E-95	6.09E-110
6.63E-02	1.79E-70	1.62E-70	1.44E-70	1.26E-70	1.08E-70	9.02E-71	7.21E-71	5.41E-71	3.61E-71	1.80E-71	2.00E-86
7.69E-02	2.72E-54	2.47E-54	2.20E-54	1.92E-54	1.65E-54	1.37E-54	1.10E-54	8.23E-55	5.49E-55	2.74E-55	3.05E-70
8.79E-02	1.13E-42	1.02E-42	9.10E-43	7.96E-43	6.82E-43	5.69E-43	4.55E-43	3.41E-43	2.27E-43	1.14E-43	1.26E-58
9.95E-02	4.77E-34	4.33E-34	3.85E-34	3.37E-34	2.89E-34	2.41E-34	1.93E-34	1.44E-34	9.63E-35	4.82E-35	5.35E-50
1.12E-01	1.83E-27	1.67E-27	1.48E-27	1.30E-27	1.11E-27	9.27E-28	7.41E-28	5.56E-28	3.71E-28	1.85E-28	2.06E-43
1.24E-01	2.55E-22	2.32E-22	2.06E-22	1.80E-22	1.55E-22	1.29E-22	1.03E-22	7.73E-23	5.16E-23	2.58E-23	2.86E-38
1.37E-01	3.18E-18	2.89E-18	2.57E-18	2.25E-18	1.93E-18	1.61E-18	1.29E-18	9.64E-19	6.43E-19	3.21E-19	3.57E-34
1.51E-01	6.59E-15	5.99E-15	5.33E-15	4.66E-15	3.99E-15	3.33E-15	2.66E-15	2.00E-15	1.33E-15	6.66E-16	7.39E-31
1.65E-01	3.49E-12	3.17E-12	2.82E-12	2.47E-12	2.11E-12	1.76E-12	1.41E-12	1.06E-12	7.05E-13	3.52E-13	3.91E-28
1.80E-01	6.43E-10	5.84E-10	5.19E-10	4.55E-10	3.90E-10	3.25E-10	2.60E-10	1.95E-10	1.30E-10	6.49E-11	7.21E-26
1.95E-01	5.17E-08	4.70E-08	4.18E-08	3.65E-08	3.13E-08	2.61E-08	2.09E-08	1.57E-08	1.04E-08	5.22E-09	5.79E-24
2.10E-01	2.14E-06	1.95E-06	1.73E-06	1.52E-06	1.30E-06	1.08E-06	8.66E-07	6.50E-07	4.33E-07	2.17E-07	2.40E-22
2.26E-01	5.22E-05	4.74E-05	4.22E-05	3.69E-05	3.16E-05	2.64E-05	2.11E-05	1.58E-05	1.05E-05	5.27E-06	5.85E-21
2.43E-01	8.22E-04	7.47E-04	6.64E-04	5.81E-04	4.98E-04	4.15E-04	3.32E-04	2.49E-04	1.66E-04	8.30E-05	9.22E-20
2.60E-01	9.04E-03	8.22E-03	7.30E-03	6.39E-03	5.48E-03	4.57E-03	3.65E-03	2.74E-03	1.83E-03	9.13E-04	1.01E-18
2.78E-01	7.38E-02	6.70E-02	5.96E-02	5.21E-02	4.47E-02	3.72E-02	2.98E-02	2.23E-02	1.49E-02	7.45E-03	8.27E-18
2.96E-01	4.68E-01	4.26E-01	3.79E-01	3.31E-01	2.84E-01	2.37E-01	1.89E-01	1.42E-01	9.46E-02	4.73E-02	5.25E-17
3.14E-01	2.41E+00	2.19E+00	1.95E+00	1.70E+00	1.46E+00	1.22E+00	9.73E-01	7.29E-01	4.86E-01	2.43E-01	2.70E-16

In this table E represents a short hand for scientific notation. So $1.34E - 1$ is equivalent to 1.34×10^{-1} .

2.3. REACTION RATE EQUATION

Table 2.9: Reaction rates from the I&G EOS for multiple pressures and reaction extents.

Pressure (100GPa)	Reaction Extents													
	1%	10%	20%	30%	40%	50%	60%	70%	80%	90%	100%			
1.36E-02	3.69E-37	3.35E-37	2.98E-37	2.61E-37	2.24E-37	1.86E-37	1.49E-37	1.12E-37	7.45E-38	3.73E-38	4.11E-53			
2.11E-02	5.53E-32	5.02E-32	4.47E-32	3.91E-32	3.35E-32	2.79E-32	2.23E-32	1.67E-32	1.12E-32	5.58E-33	6.15E-48			
2.91E-02	3.34E-28	3.04E-28	2.70E-28	2.36E-28	2.02E-28	1.69E-28	1.35E-28	1.01E-28	6.75E-29	3.37E-29	3.72E-44			
3.77E-02	3.43E-25	3.12E-25	2.77E-25	2.43E-25	2.08E-25	1.73E-25	1.39E-25	1.04E-25	6.93E-26	3.46E-26	3.82E-41			
4.67E-02	1.14E-22	1.03E-22	9.19E-23	8.04E-23	6.89E-23	5.74E-23	4.59E-23	3.44E-23	2.30E-23	1.15E-23	1.27E-38			
5.63E-02	1.71E-20	1.56E-20	1.38E-20	1.21E-20	1.04E-20	8.66E-21	6.92E-21	5.19E-21	3.46E-21	1.73E-21	1.91E-36			
6.63E-02	1.44E-18	1.31E-18	1.17E-18	1.02E-18	8.74E-19	7.29E-19	5.83E-19	4.37E-19	2.91E-19	1.46E-19	1.61E-34			
7.69E-02	7.75E-17	7.04E-17	6.26E-17	5.48E-17	4.70E-17	3.91E-17	3.13E-17	2.35E-17	1.57E-17	7.82E-18	8.62E-33			
8.79E-02	2.91E-15	2.64E-15	2.35E-15	2.06E-15	1.76E-15	1.47E-15	1.17E-15	8.81E-16	5.87E-16	2.94E-16	3.24E-31			
9.95E-02	8.14E-14	7.40E-14	6.58E-14	5.76E-14	4.93E-14	4.11E-14	3.29E-14	2.47E-14	1.64E-14	8.22E-15	9.06E-30			
1.12E-01	1.78E-12	1.62E-12	1.44E-12	1.26E-12	1.08E-12	9.01E-13	7.21E-13	5.41E-13	3.60E-13	1.80E-13	1.99E-28			
1.24E-01	3.18E-11	2.89E-11	2.57E-11	2.25E-11	1.93E-11	1.60E-11	1.28E-11	9.62E-12	6.42E-12	3.21E-12	3.54E-27			
1.37E-01	4.73E-10	4.30E-10	3.82E-10	3.34E-10	2.87E-10	2.39E-10	1.91E-10	1.43E-10	9.55E-11	4.78E-11	5.26E-26			
1.51E-01	6.03E-09	5.48E-09	4.87E-09	4.26E-09	3.65E-09	3.04E-09	2.43E-09	1.83E-09	1.22E-09	6.09E-10	6.71E-25			
1.65E-01	6.70E-08	6.09E-08	5.41E-08	4.73E-08	4.06E-08	3.38E-08	2.71E-08	2.03E-08	1.35E-08	6.76E-09	7.45E-24			
1.80E-01	6.59E-07	5.99E-07	5.32E-07	4.66E-07	3.99E-07	3.33E-07	2.66E-07	2.00E-07	1.33E-07	6.65E-08	7.33E-23			
1.95E-01	5.81E-06	5.28E-06	4.70E-06	4.11E-06	3.52E-06	2.94E-06	2.35E-06	1.76E-06	1.17E-06	5.87E-07	6.47E-22			
2.10E-01	4.65E-05	4.23E-05	3.76E-05	3.29E-05	2.82E-05	2.35E-05	1.88E-05	1.41E-05	9.39E-06	4.69E-06	5.17E-21			
2.26E-01	3.40E-04	3.09E-04	2.75E-04	2.41E-04	2.06E-04	1.72E-04	1.37E-04	1.03E-04	6.87E-05	3.44E-05	3.79E-20			
2.43E-01	2.30E-03	2.09E-03	1.86E-03	1.62E-03	1.39E-03	1.16E-03	9.28E-04	6.96E-04	4.64E-04	2.32E-04	2.56E-19			
2.60E-01	1.44E-02	1.31E-02	1.16E-02	1.02E-02	8.73E-03	7.27E-03	5.82E-03	4.36E-03	2.91E-03	1.45E-03	1.60E-18			
2.78E-01	8.43E-02	7.67E-02	6.82E-02	5.96E-02	5.11E-02	4.26E-02	3.41E-02	2.56E-02	1.70E-02	8.52E-03	9.39E-18			
2.96E-01	4.64E-01	4.22E-01	3.75E-01	3.28E-01	2.81E-01	2.34E-01	1.87E-01	1.41E-01	9.37E-02	4.68E-02	5.16E-17			
3.14E-01	2.41E+00	2.19E+00	1.95E+00	1.70E+00	1.46E+00	1.22E+00	9.73E-01	7.30E-01	4.86E-01	2.43E-01	2.68E-16			

In this table E represents a short hand for scientific notation. So $1.34E-1$ is equivalent to 1.34×10^{-1} .

2.3. REACTION RATE EQUATION

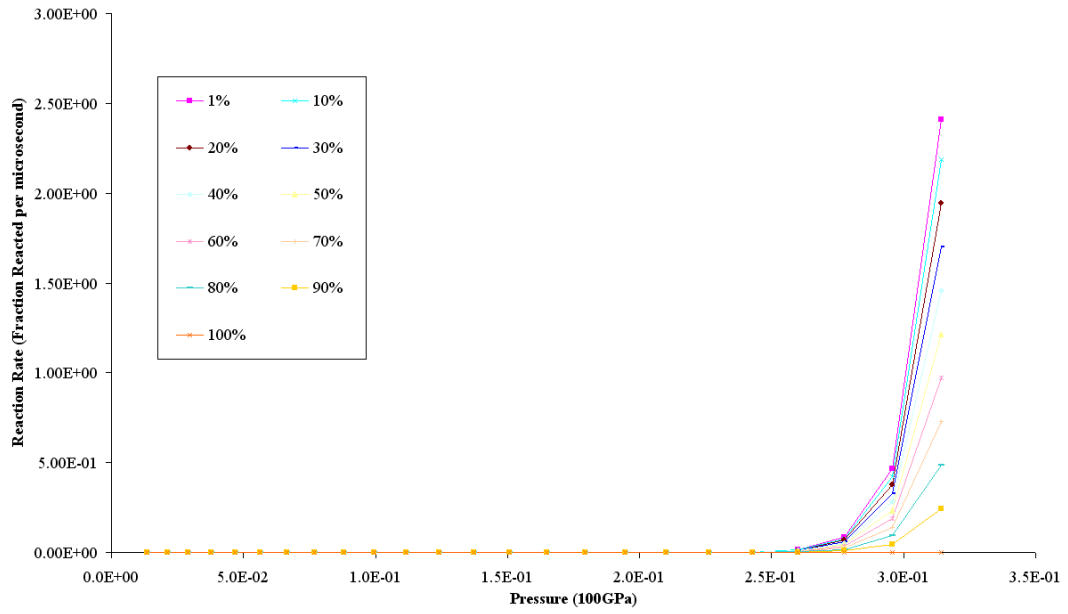


Figure 2.9: I&G EOS predictions of the reaction rate for several reaction extents.

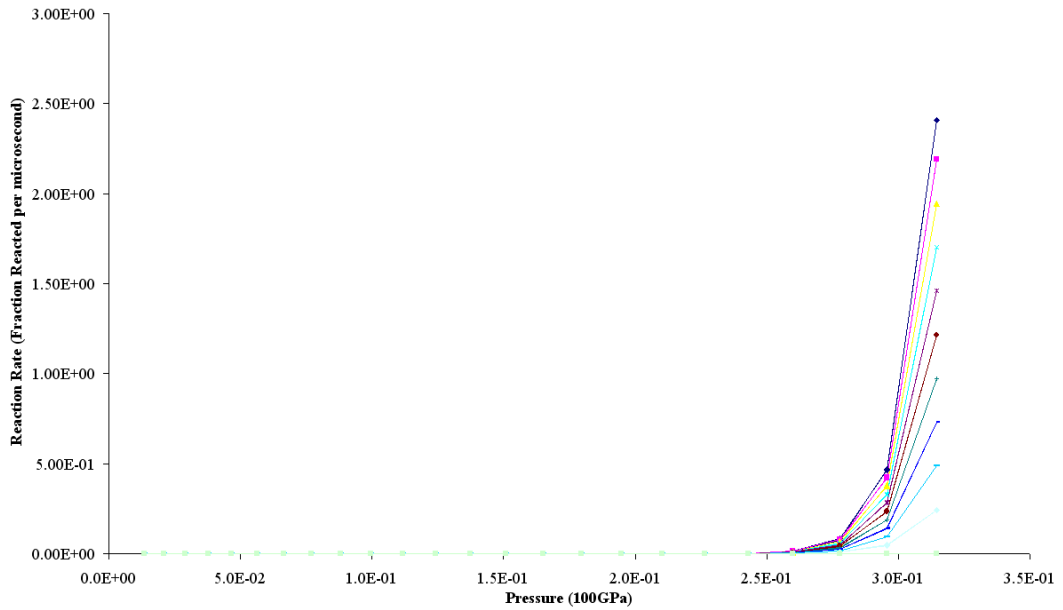


Figure 2.10: Overlay of Figures 2.8 and 2.9.

2.3. REACTION RATE EQUATION

Table 2.10: Error between the Arrhenius and I&G EOS predicted reaction rates.

Pressure (100GPa)	Reaction Extents										
	1%	10%	20%	30%	40%	50%	60%	70%	80%	90%	100%
1.36E-02	1.36E-73	1.12E-73	8.89E-74	6.80E-74	5.00E-74	3.47E-74	2.22E-74	1.25E-74	5.55E-75	1.39E-75	1.69E-105
2.11E-02	3.05E-63	2.52E-63	1.99E-63	1.53E-63	1.12E-63	7.79E-64	4.99E-64	2.80E-64	1.25E-64	3.12E-65	3.78E-95
2.91E-02	1.12E-55	9.22E-56	7.29E-56	5.58E-56	4.10E-56	2.85E-56	1.82E-56	1.02E-56	4.55E-57	1.14E-57	1.38E-87
3.77E-02	1.18E-49	9.72E-50	7.68E-50	5.88E-50	4.32E-50	3.00E-50	1.92E-50	1.08E-50	4.80E-51	1.20E-51	1.46E-81
4.67E-02	1.29E-44	1.07E-44	8.44E-45	6.46E-45	4.75E-45	3.30E-45	2.11E-45	1.19E-45	5.27E-46	1.32E-46	1.60E-76
5.63E-02	2.94E-40	2.43E-40	1.92E-40	1.47E-40	1.08E-40	7.49E-41	4.79E-41	2.70E-41	1.20E-41	2.99E-42	3.64E-72
6.63E-02	2.08E-36	1.72E-36	1.36E-36	1.04E-36	7.65E-37	5.31E-37	3.40E-37	1.91E-37	8.49E-38	2.12E-38	2.58E-68
7.69E-02	6.00E-33	4.96E-33	3.92E-33	3.00E-33	2.21E-33	1.53E-33	9.80E-34	5.51E-34	2.45E-34	6.12E-35	7.44E-65
8.79E-02	8.45E-30	6.99E-30	5.52E-30	4.23E-30	3.11E-30	2.16E-30	1.38E-30	7.76E-31	3.45E-31	8.62E-32	1.05E-61
9.95E-02	6.62E-27	5.48E-27	4.33E-27	3.31E-27	2.43E-27	1.69E-27	1.08E-27	6.08E-28	2.70E-28	6.76E-29	8.21E-59
1.12E-01	3.18E-24	2.63E-24	2.08E-24	1.59E-24	1.17E-24	8.12E-25	5.20E-25	2.92E-25	1.30E-25	3.25E-26	3.94E-56
1.24E-01	1.01E-21	8.34E-22	6.59E-22	5.04E-22	3.71E-22	2.57E-22	1.65E-22	9.26E-23	4.12E-23	1.03E-23	1.25E-53
1.37E-01	2.24E-19	1.85E-19	1.46E-19	1.12E-19	8.22E-20	5.71E-20	3.65E-20	2.05E-20	9.13E-21	2.28E-21	2.77E-51
1.51E-01	3.63E-17	3.00E-17	2.37E-17	1.82E-17	1.33E-17	9.26E-18	5.93E-18	3.33E-18	1.48E-18	3.70E-19	4.50E-49
1.65E-01	4.48E-15	3.70E-15	2.93E-15	2.24E-15	1.65E-15	1.14E-15	7.32E-16	4.12E-16	1.83E-16	4.57E-17	5.55E-47
1.80E-01	4.33E-13	3.58E-13	2.83E-13	2.17E-13	1.59E-13	1.10E-13	7.07E-14	3.98E-14	1.77E-14	4.42E-15	5.36E-45
1.95E-01	3.32E-11	2.74E-11	2.17E-11	1.66E-11	1.22E-11	8.46E-12	5.42E-12	3.05E-12	1.35E-12	3.38E-13	4.11E-43
2.10E-01	1.97E-09	1.63E-09	1.28E-09	9.83E-10	7.22E-10	5.02E-10	3.21E-10	1.81E-10	8.02E-11	2.01E-11	2.43E-41
2.26E-01	8.30E-08	6.86E-08	5.42E-08	4.15E-08	3.05E-08	2.12E-08	1.35E-08	7.62E-09	3.39E-09	8.46E-10	1.03E-39
2.43E-01	2.18E-06	1.80E-06	1.42E-06	1.09E-06	8.00E-07	5.55E-07	3.55E-07	2.00E-07	8.88E-08	2.22E-08	2.67E-38
2.60E-01	2.87E-05	2.38E-05	1.88E-05	1.44E-05	1.06E-05	7.33E-06	4.69E-06	2.64E-06	1.17E-06	2.93E-07	3.47E-37
2.78E-01	1.12E-04	9.28E-05	7.34E-05	5.62E-05	4.13E-05	2.86E-05	1.83E-05	1.03E-05	4.57E-06	1.14E-06	1.25E-36
2.96E-01	2.03E-05	1.64E-05	1.29E-05	9.88E-06	7.28E-06	5.08E-06	3.28E-06	1.86E-06	8.42E-07	2.16E-07	8.03E-37
3.14E-01	5.91E-08	2.44E-07	2.26E-07	1.69E-07	1.10E-07	6.05E-08	2.61E-08	7.00E-09	3.19E-10	6.32E-10	3.99E-36

In this table E represents a short hand for scientific notation. So $1.34E - 1$ is equivalent to 1.34×10^{-1} .

ReactMat Software

The ReactMat software described in this chapter was developed as a part of this project to provide a tool for stepping through the methodology outlined in this thesis. It allows calculation of various unreacted mixtures and provides a means to optimize the various JWL and I&G reaction rate parameters. In the end, ReactMat produces a fully formatted IGNITION AND GROWTH OF REACTION IN HE record that can be directly copied into the user's LS-DYNA keyword file.

The tabs in the program are meant to be stepped through from left to right and each tab from top to bottom. Frequently, later functions and fields will require data from previous fields/tabs, so working out of order is not recommended.

3.1 Determine Unreacted Parameters Part 1

The first tab, shown in Figure 3.1, in ReactMat allows the user to calculate the reactive material mixture properties and enter the minimum and maximum particle velocities (impact velocities) of interest. ReactMat maintains an internal database of reactive material properties so the user does not have to continually reenter the values for individual materials. Previously stored materials are listed by name in the drop down box labeled "Load a previously saved material:". To load a constituent material from ReactMat's database, select it from the drop down box and click the

3.1. DETERMINE UNREACTED PARAMETERS PART 1

“Load” button, the material name and properties will be filled in the fields below. To add a material to ReactMat’s database, enter the material’s properties and name into the material property fields named “Material Name:”, “C0:”, “S:”, “p0:”, “Cv:”, and “w:” and press the “Save Material in Database” button. Materials in the database must have unique names or they will be overwritten. To delete a material from the database, ensure its name is in the “Material Name:” field and press the “Delete Material from Database” button. Once one of the constitutive materials that the user would like to be in the resulting reactive mixture is displayed in the material property fields, all that is required to add the material to the mixture is to specify the percent of the total mixture that the current component composes by weight and press the “Add Material to Reactive Mixture” button. To remove a constituent material from the mixture, simply select the row in the mixture table and press the “Remove Material from Reactive Mixture” button. Once all the components have been added to the mixture, all that remains is to calculate the mixture properties by clicking the “Calculate Reactive Mixture Properties” button. At this point it is necessary to enter the minimum and maximum particle velocities before clicking the “Calculate Unreacted Hugoniot Data from Reactive Mixture Properties” button and continuing on to the second tab discussed in the next section.

3.1. DETERMINE UNREACTED PARAMETERS PART 1

ReactMat

RIHAMM TECHNOLOGIES, LLC FEA MODELING AND SIMULATION EXPERTS

Status: Reading in the Unreacted_Material_Properties.txt file.

Unreacted Material 1 | Unreacted Material 2 | Reacted Material 1 | Reacted Material 2 | Reaction Rate | LS-DYNA EOS

Load a previously saved material:

Material Name:

C0: cm/us

S:

p0: g/cm³

Cv: 100KJ/g*K

w:

Percent of total material by weight (0 - 100):

Weight %	Material Name	C0 (cm/us)	S	p0 (g/cm ³)	Cv (100KJ/g*K)	w
						2.42

C0 (cm/us)	S	p0 (g/cm ³)	Cv (100KJ/g*K)	w

Minimum Particle Velocity of Interest: cm/us

Maximum Particle Velocity of Interest: cm/us

Figure 3.1: “Unreacted Material 1” tab.

3.2 Determine Unreacted Parameters Part 2

The second tab in the ReactMat program, shown in Figure 3.2 helps the user to optimize the JWL parameters for the unreacted materials. When the “Calculate Unreacted Hugoniot Data from Reactive Mixture Properties” button on the previous tab is pressed ReactMat calculates and fills in the first six columns in the “Unreacted Hugoniot table” using the reactive material properties and particle velocities from the previous page. The user can fill in the remaining columns of the table by entering initial guesses for the values of “r1:”, “r2:”, “r5:”, “r6:”, and “w:” and pressing the “Calculate JWL Pressures and Error” button. It doesn’t really matter at this point what the user chooses for guesses, with the exception that they should be greater than zero. The user can get an idea of the quality of the initial guess by looking at the “Sum of Error²” field and by clicking the “Plot Pressure Vs. Specific Volume” which will create a P-V plot with both the Hugoniot and JWL Pressures. An example of this is shown in Figure 3.3. The next step is to press the “Optimize JWL Parameters” button, which will use a modified Newton’s Method to minimize the error between the pressures predicted by the JWL equation and the Hugoniot pressures by changing the JWL parameters. An example of the result of this optimization along with the corresponding plot is shown in Figure 3.4.

3.2. DETERMINE UNREACTED PARAMETERS PART 2

ReactMat

RHAMM
TECHNOLOGIES, LLC FEA MODELING AND SIMULATION EXPERTS

Status: Reading in the Unreacted_Material_Properties.txt file.

Unreacted Material 1 Unreacted Material 2 Reacted Material 1 Reacted Material 2 Reaction Rate LS-DYNA EOS

Unreacted Hugoniot Data

Up (cm/us)	Us (cm/us)	p (g/cm ³)	T (K)	E (100KJ/g)	P (100 GPa)	JWL P (100 GPa)	Error	Error^2

Unreacted JWL Parameters

r1:

r2:

r5:

r6:

w:

Sum of Error²:

Calculate JWL Pressures and Error

Optimize JWL Parameters

Plot Pressure Vs. Specific Volume

Figure 3.2: “Unreacted Material 2” tab.

3.2. DETERMINE UNREACTED PARAMETERS PART 2

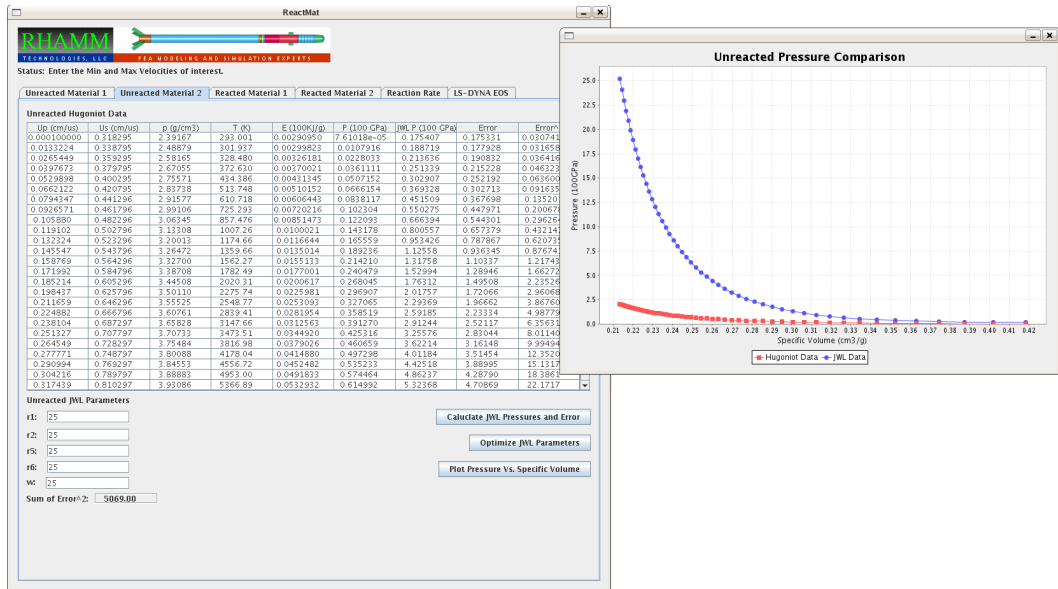


Figure 3.3: “Unreacted Material 2” tab with the JWL parameters set equal to 25.

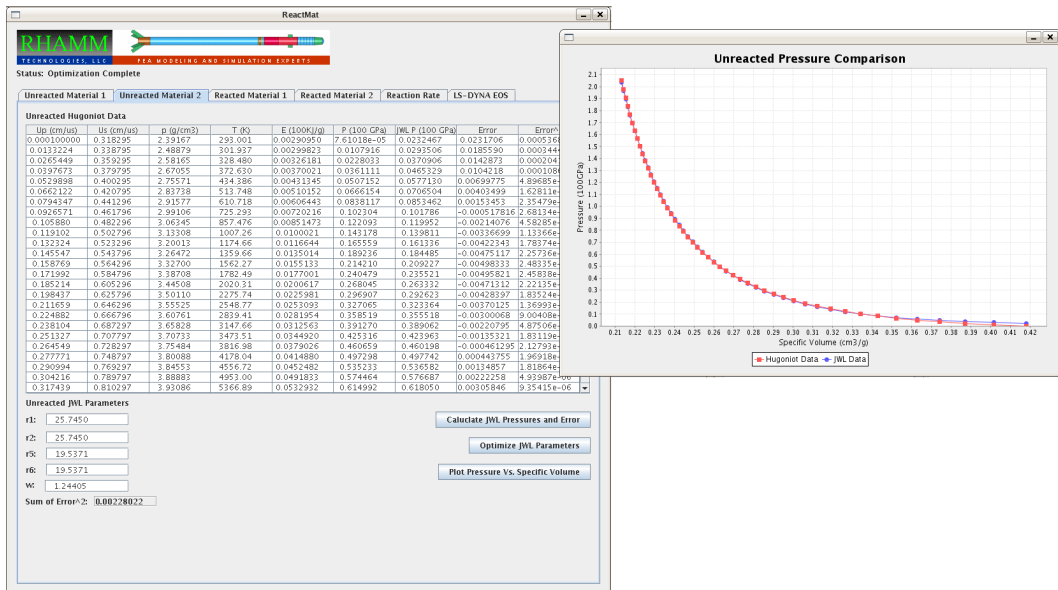


Figure 3.4: “Unreacted Material 2” tab with the JWL parameters optimized to provide the best fit to the Hugoniot data.

3.3 Determine Reacted Parameters Part 1

The third tab of the ReactMat program, shown in Figure 3.5, allows entry of the basic data needed to determine the Hugoniot data for the reacted material. When the “Look Up Unreacted Data” button is pressed, ReactMat looks up the unreacted Hugoniot data for the impact (particle) velocity entered in the “Impact Velocity (cm/us):” field. This data can then be used with the CAE program to determine the unburned and burned gas enthalpies along with the heat capacity of the reaction products. Pressing the “Calculate Additional Parameters” button will then cause ReactMat to calculate the Polytropic Gas Constant, the internal energy of the fully expanded gasses, and the heat of reaction. The Chapman-Jouget parameters, the detonation velocity, and the constant K can now be calculated by pressing the “Determine Chapman-Jouget Parameters” button. Finally, pressing the “Calculate the Reacted Hugoniot Data” button causes the ReactMat program to calculate the Hugoniot data for the reacted material and fill in the table on tab 4.

3.3. DETERMINE REACTED PARAMETERS PART 1

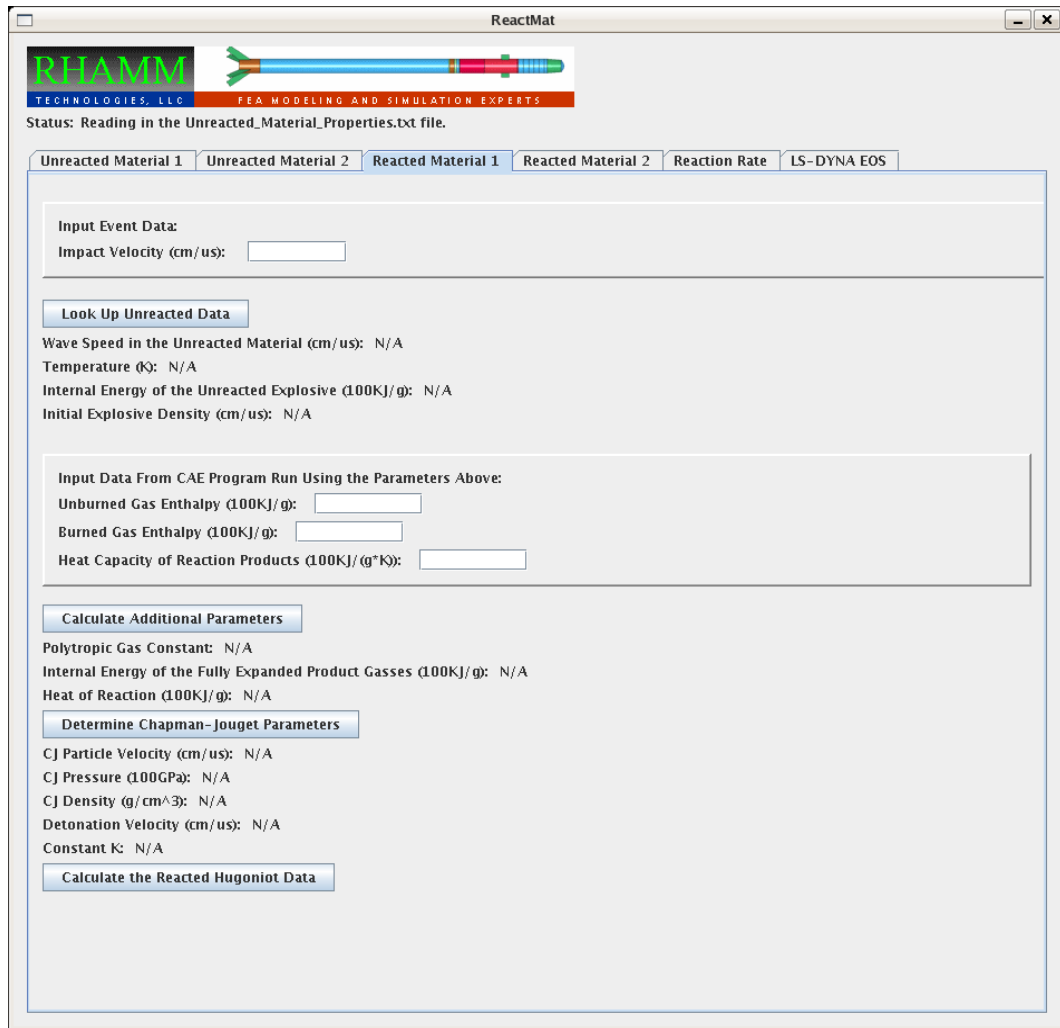


Figure 3.5: "Reacted Material 1" tab.

3.4 Determine Reacted Parameters Part 2

Tab 4, shown in Figure 3.6, is nearly identical to tab 2, with the exception being that we are now optimizing the JWL parameters for the reacted material. The interface itself operates identically.

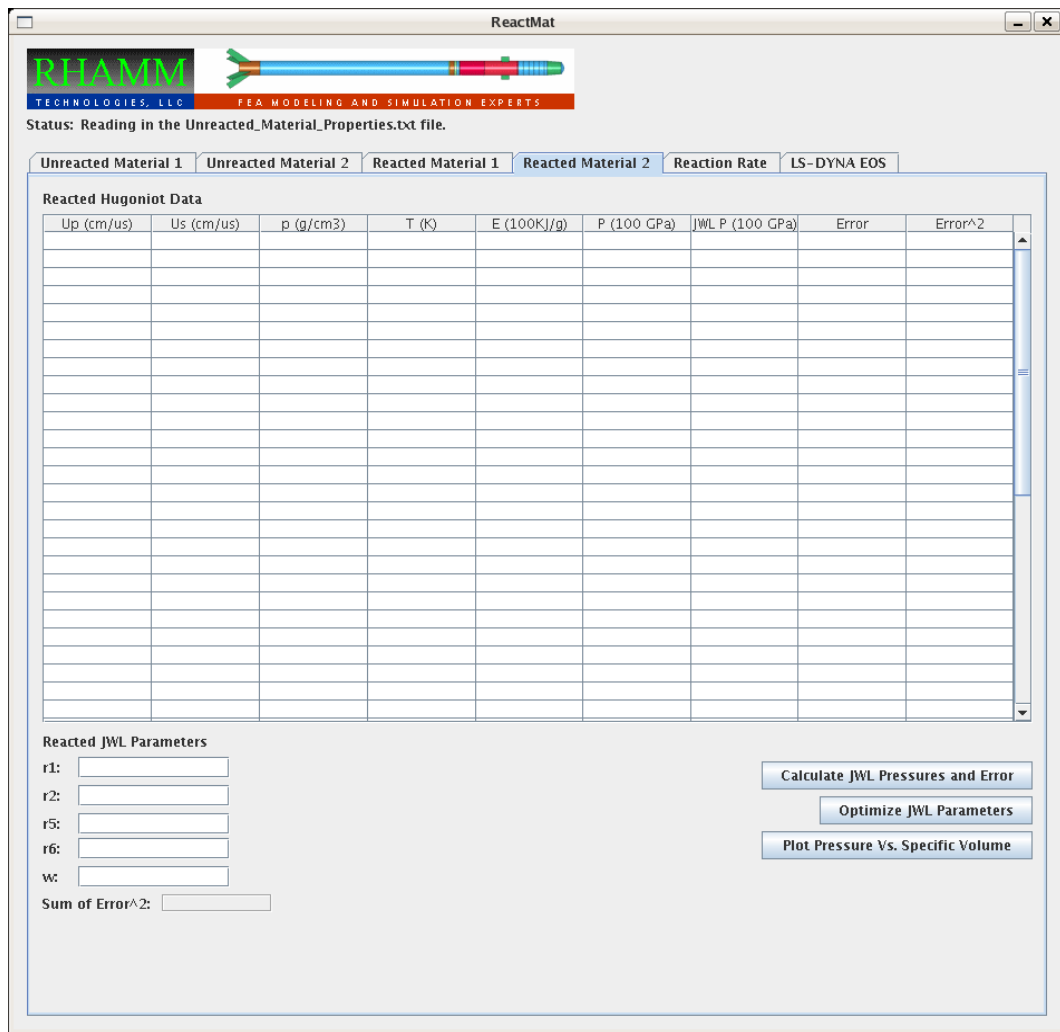


Figure 3.6: “Reacted Material 2” tab.

3.5 Determine Reaction Rate Parameters

Tab 5, shown in Figure 3.7, is included in the ReactMat software to aid in the conversion of an Arrhenius rate equation into the rate equation form found in LS-DYNA's I&G EOS. If the user needs to convert from some other rate equation form, it will need to be done offline and then the resulting reaction parameters typed into the "LS-DYNA Rate Equation Parameters:" fields. Once good values for the reaction rate are in these fields the user can proceed to tab 6, to get a fully formatted I&G EOS record without pressing any other buttons. If the user does need to convert an Arrhenius rate equation, then he/she would begin by clicking the "Get Hugoniot to Populate the Table Below" button. This will grab data from tab 2 and insert it into the table. The Arrhenius parameters can then be entered and the "Calculate the Arrhenius Rate Values in the Table Above" button can be pressed to populate the "Arrhenius Rate" column of the table. Once this is done, the procedure is much like tab 2. Initial guesses are plugged into the "LS-DYNA Rate Equation Parameters:" section and the rates are calculated by pressing the "Calculate LS-DYNA Reaction Rates and Error" button. Because of the complex nature of the I&G rate equation, individual parameters can be selected for optimization by checking the boxes to the left of the values. The checked parameters can then be optimized by pressing the "Optimize LS-DYNA Reaction Rate Parameters" button.

3.5. DETERMINE REACTION RATE PARAMETERS

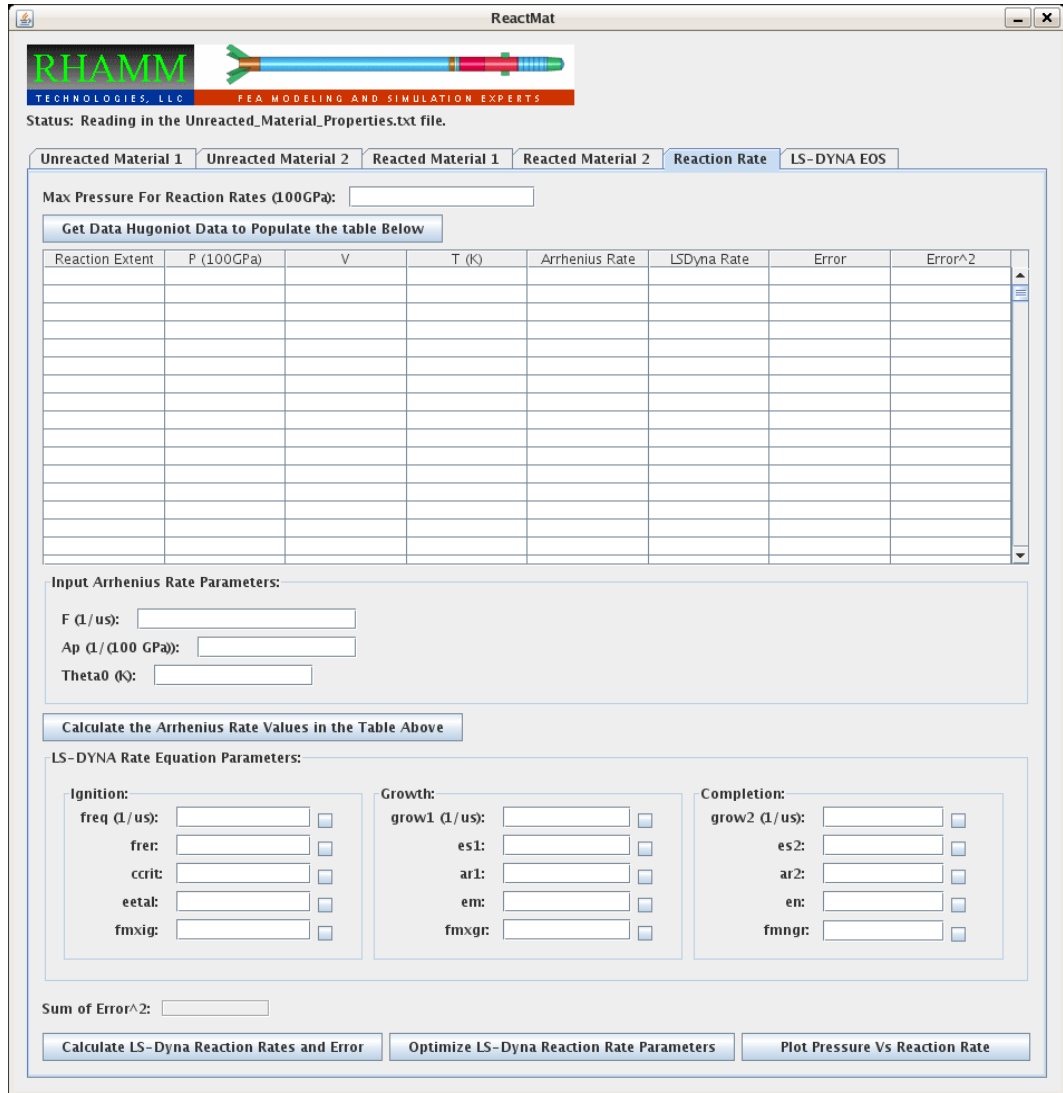


Figure 3.7: "Reaction Rate" tab.

3.6 Resulting LS-DYNA EOS

The sole purpose of Tab 6, shown in Figure 3.8 is to collect unreacted JWL, reacted JWL, and reaction rate parameters from tabs 2, 4, 5 respectively and format them into an IGNITION AND GROWTH OF REACTION IN HE EOS record that can be copied and pasted directly into an LS-DYNA keyword file.

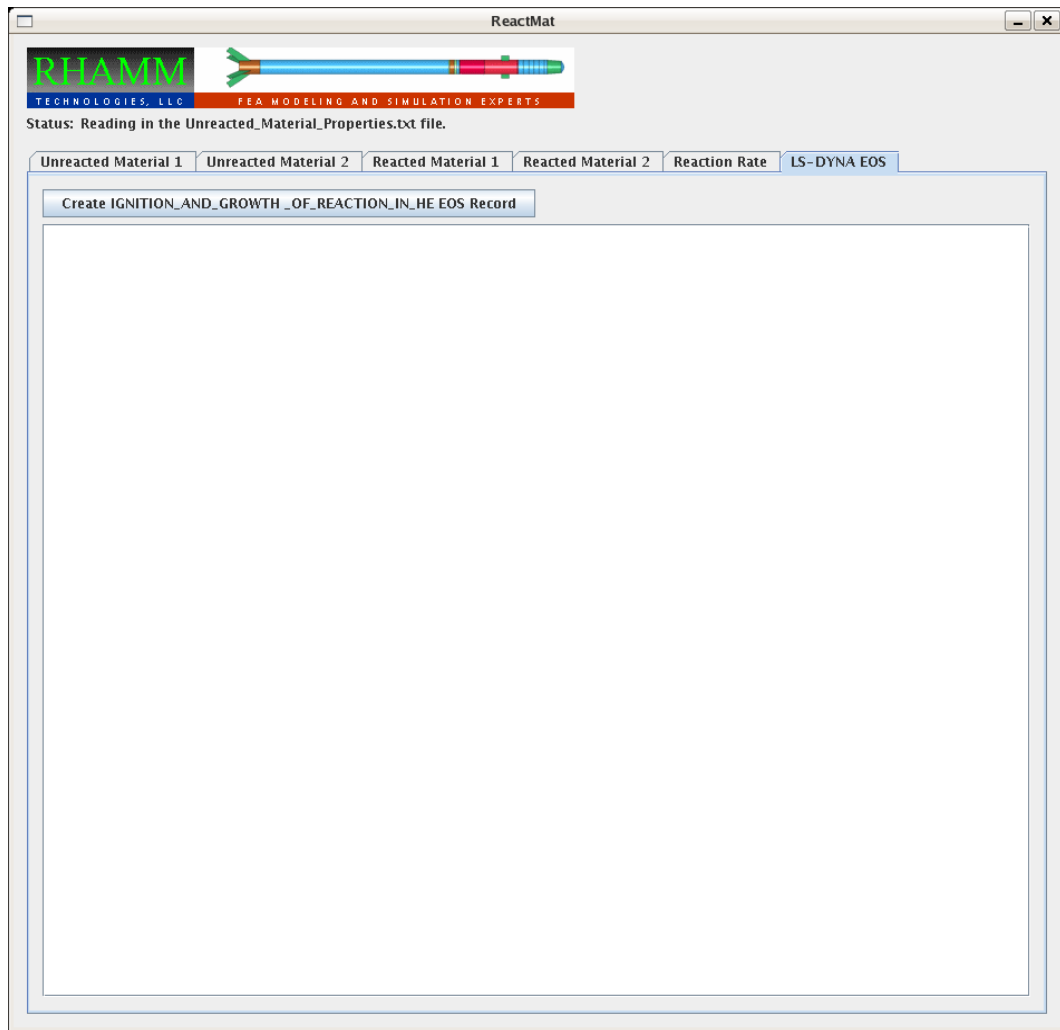


Figure 3.8: “LS-DYNA EOS” tab.

Unreacted Material Characterization

This chapter describes a test with the purpose of characterizing the unreacted state of the reactive material. A simulation of the characterization test is then performed to show that the equation of state developed in chapter 2 is modeling the unreacted material as expected.

To experimentally characterize the unreacted material, a plane pressure wave is generated by an inert projectile, accelerated by a gas gun or explosive means, impacting a sample of the reactive material. It is important that the edges of the reactive material sample are more distant from the center of the sample than the impacted side of the sample is from the opposing side. If this is the case, then waves radiating from the sides of the material will not reach the center of the opposing side before the plane wave, and can be ignored. The initial velocity of the projectile is measured before impact, and the time of impact is calculated. Some means of detecting motion on the other side of the reactive sample is then used to measure the time taken for the wave to travel the thickness of the sample. This is done for multiple projectile velocities to properly characterize the particle vs. wave velocity data which is then used to develop the Hugoniot data as in Section 2.1.

4.1 Simulation of Unreacted Material Characterization Test

This test was modeled entirely in a three-dimensional Euler domain. The model consists of a solid cylinder 1.36 cm high and 2.54 cm in diameter, and is shown in Figure 4.1. A top view is shown in Figure 4.2. The elements are all single point integration multi-material Euler element. The Euler domain has no boundary conditions so material is free to flow out of the model through any of the sides of the domain. The outer material is a vacuum material described by the *MAT VACUUM TITLE record. Inside, as shown in the cut away view in Figure 4.3, there is a solid cylinder of copper (blue) and a solid cylinder of the reactive material (red). Both cylinders are 0.6351 cm long and 2.434 cm in diameter. The material properties of both cylinders are described using LS-DYNA's *MAT ELASTIC PLASTIC HYDRO TITLE record. The copper cylinder is using a Grüneisen EOS defined by the *EOS GRUNEISEN TITLE and the reactive material is using the *EOS IGNITION AND GROWTH OF REACTION IN HE TITLE EOS. The copper cylinder has been given an initial velocity of one kilometer per second.

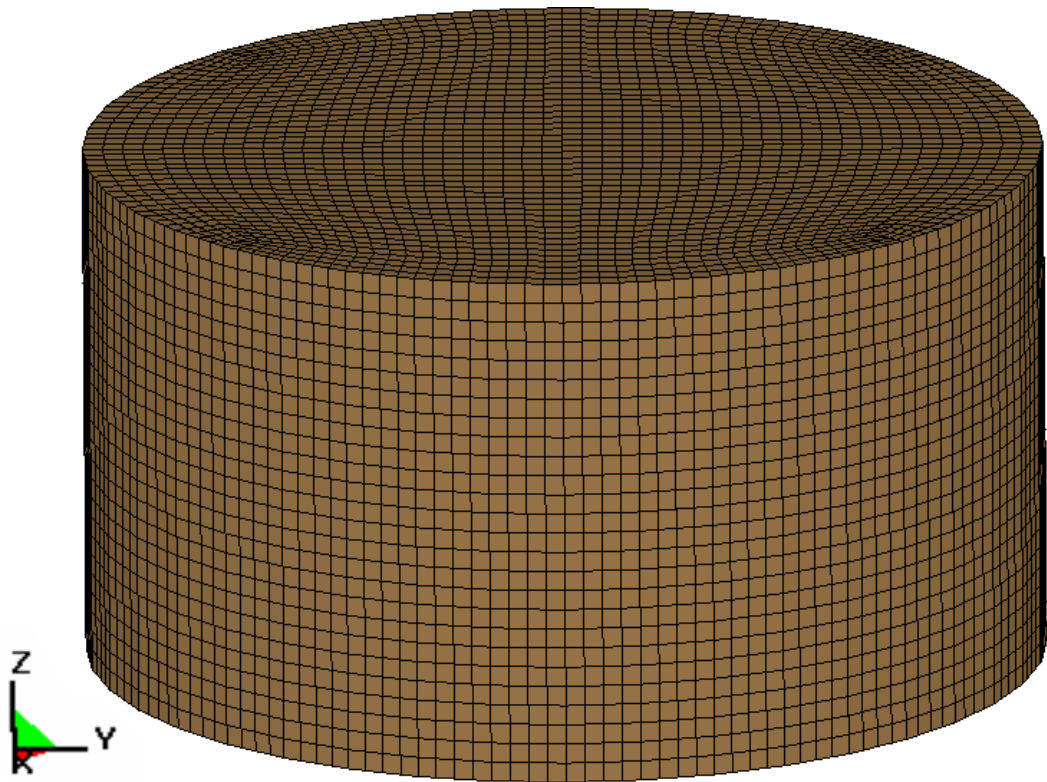


Figure 4.1: Unreacted simulation Euler mesh.

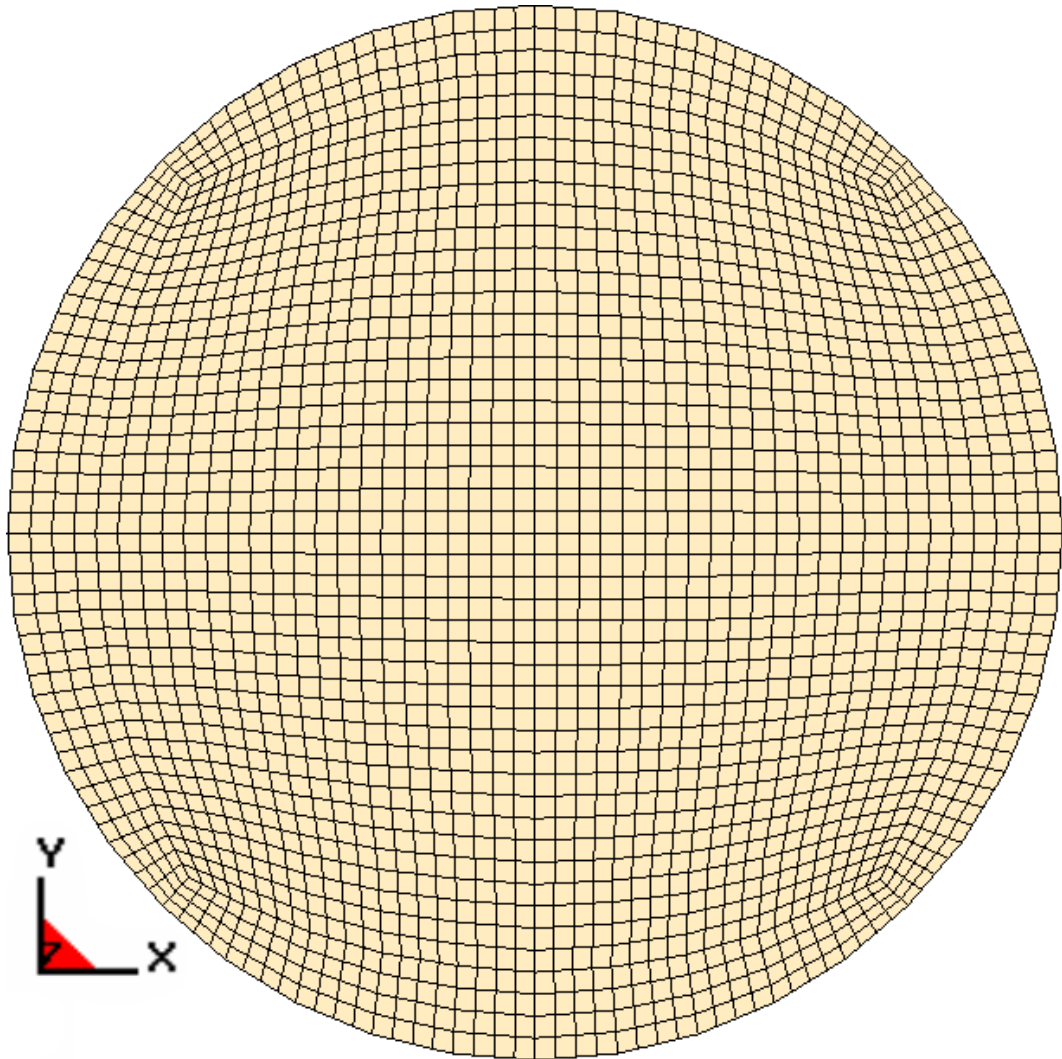


Figure 4.2: Unreacted simulation Euler mesh, top view.

4.1. SIMULATION OF UNREACTED MATERIAL
CHARACTERIZATION TEST

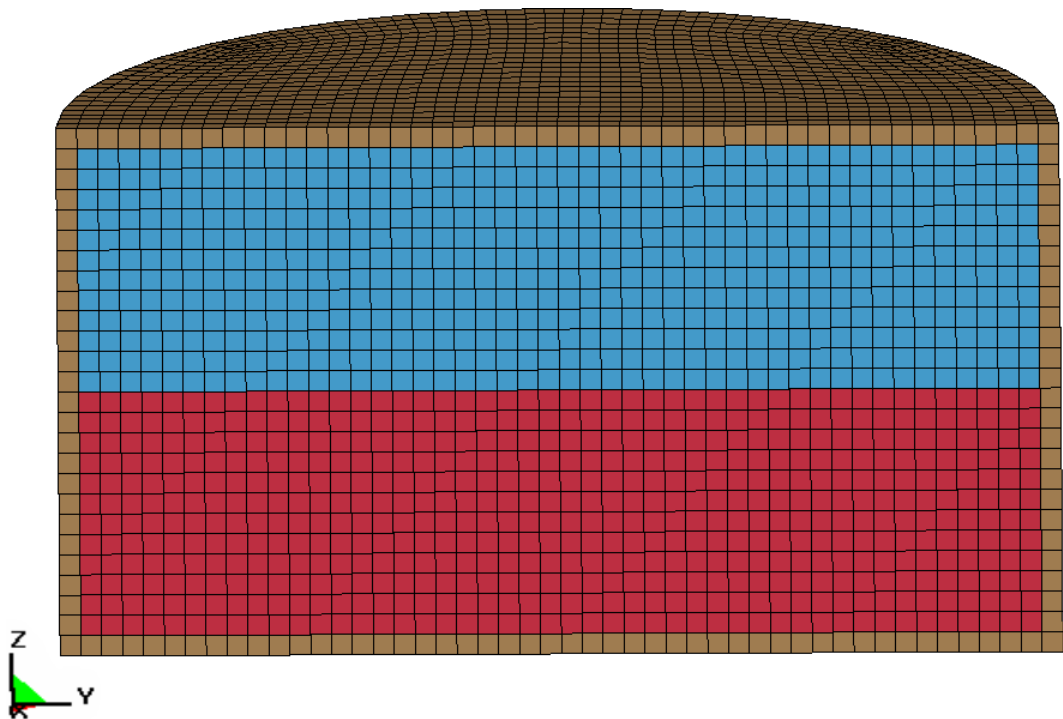


Figure 4.3: Unreacted simulation Euler mesh, cut in half.

4.1. SIMULATION OF UNREACTED MATERIAL CHARACTERIZATION TEST

Figures 4.4 through 4.13 depict the material positions and shapes over time. The blue material is the copper projectile and the red material is the reactive material. LS-PREPOST, LSTC's pre- and post-processor, provides the ability to plot a fluid in an Eulerian simulation as a solid by internally meshing, in the post-processor, the different Eulerian materials locations with tetrahedrons. This is what the material position figures show. The actual Eulerian elements, which are not shown, are hexahedrons. It is clearer to see the position and movement of the fluids when the mesh is shown, so while the tetrahedral mesh is merely an artifact of the method of visualization, it is shown for clarity. Over time one can see the blue projectile moving downward and impacting the red reactive material. The blue projectile deforms slightly at the interface between the two materials. The red material ultimately begins to react and begins to expand rapidly. On the side of the reactive material opposite the projectile, the reaction begins to show in Figure 4.13.

4.1. SIMULATION OF UNREACTED MATERIAL CHARACTERIZATION TEST

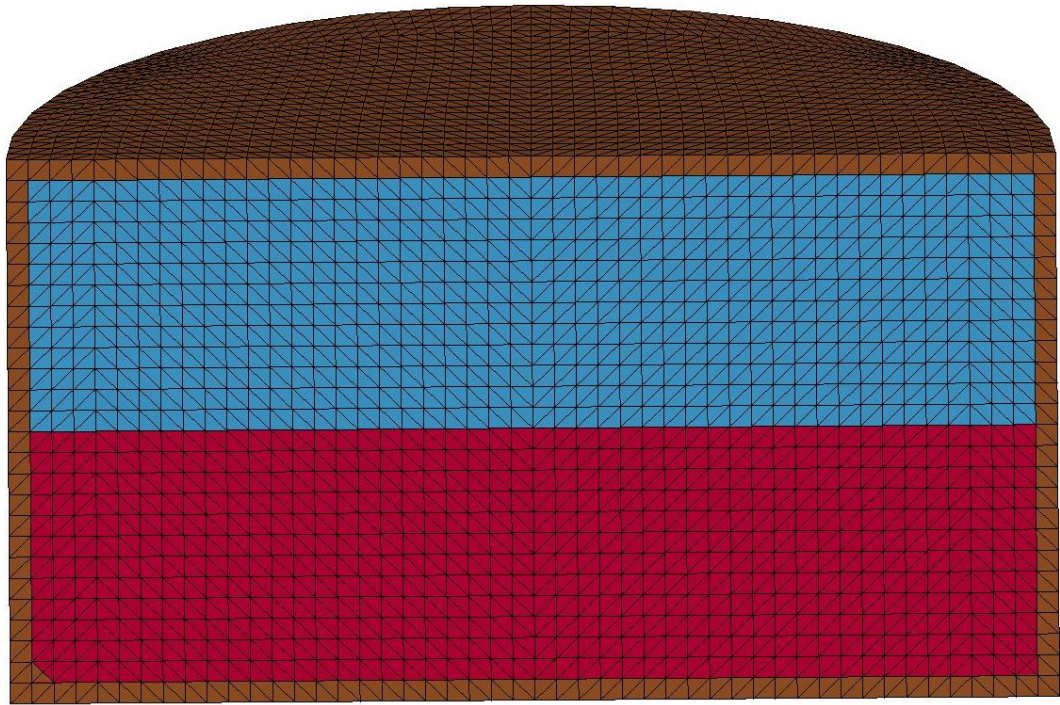


Figure 4.4: Unreacted material characterization simulation, material locations at time $= 0.00 \mu s$.

4.1. SIMULATION OF UNREACTED MATERIAL
CHARACTERIZATION TEST

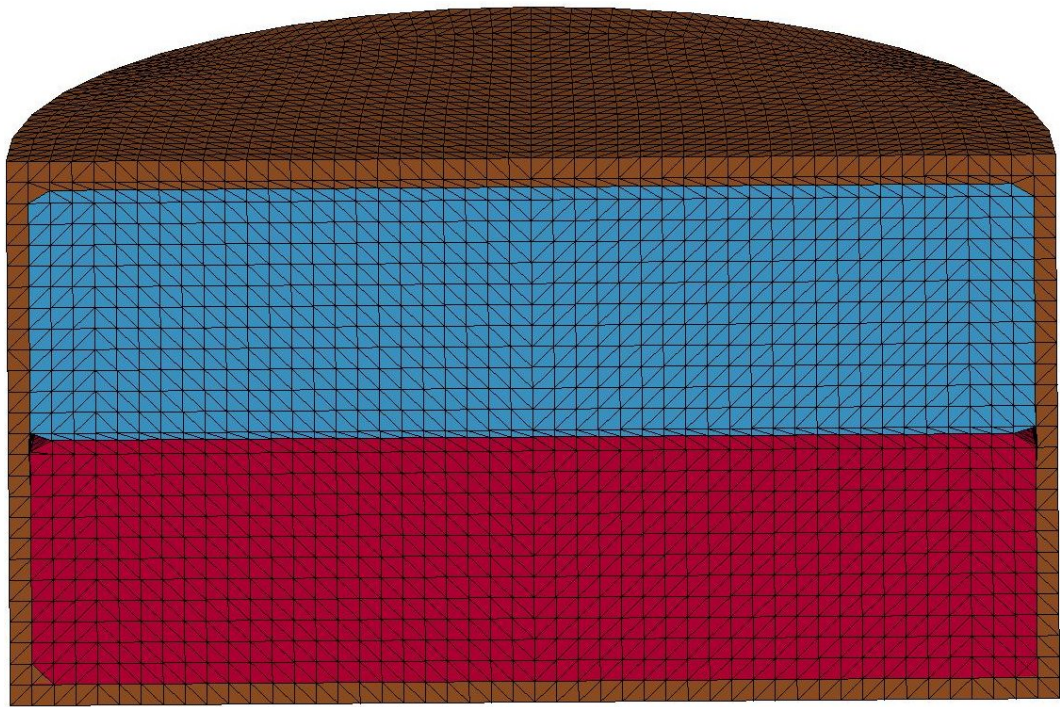


Figure 4.5: Unreacted material characterization simulation, material locations at time $= 0.20 \mu s$.

4.1. SIMULATION OF UNREACTED MATERIAL
CHARACTERIZATION TEST

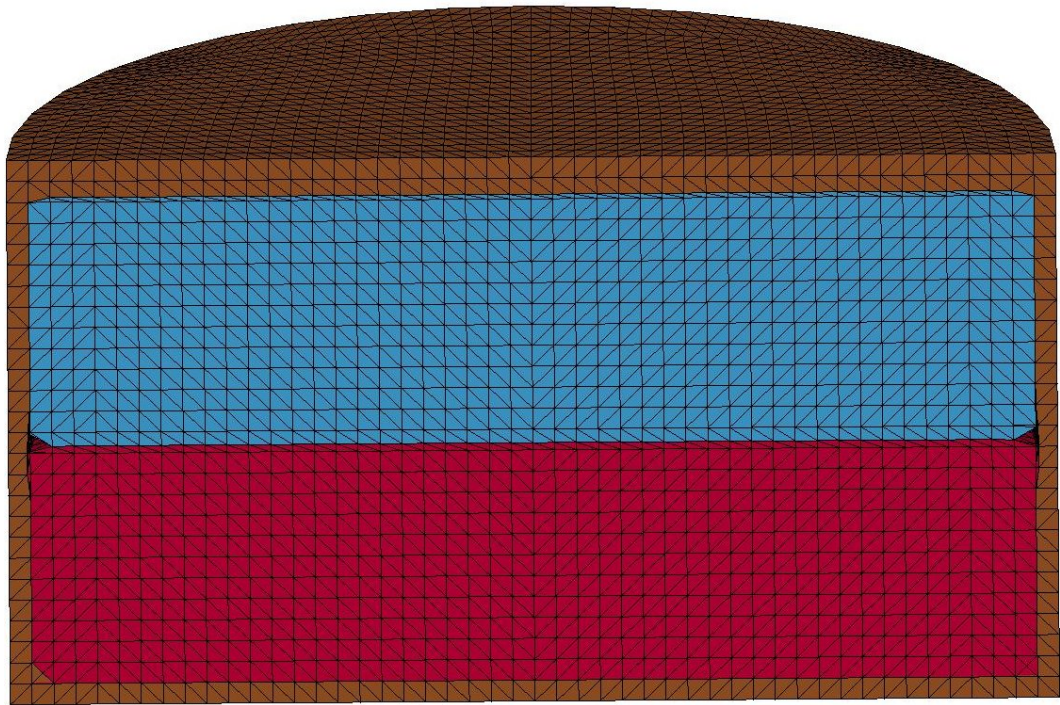


Figure 4.6: Unreacted material characterization simulation, material locations at time $= 0.41 \mu s$.

4.1. SIMULATION OF UNREACTED MATERIAL
CHARACTERIZATION TEST

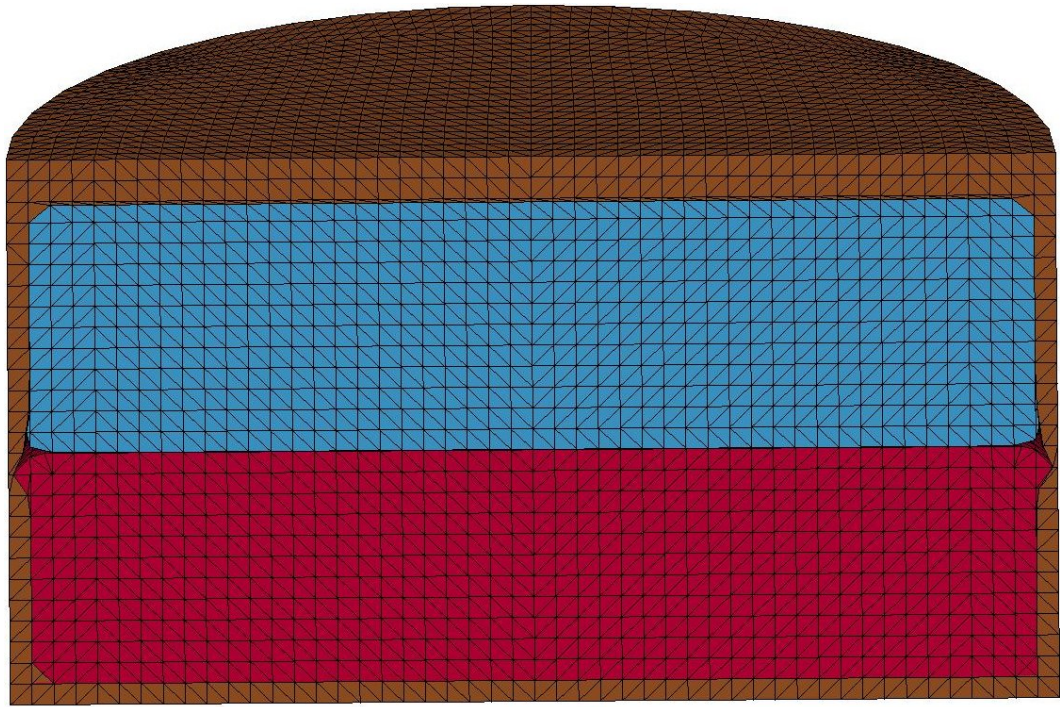


Figure 4.7: Unreacted material characterization simulation, material locations at time $t = 0.62 \mu s$.

4.1. SIMULATION OF UNREACTED MATERIAL
CHARACTERIZATION TEST

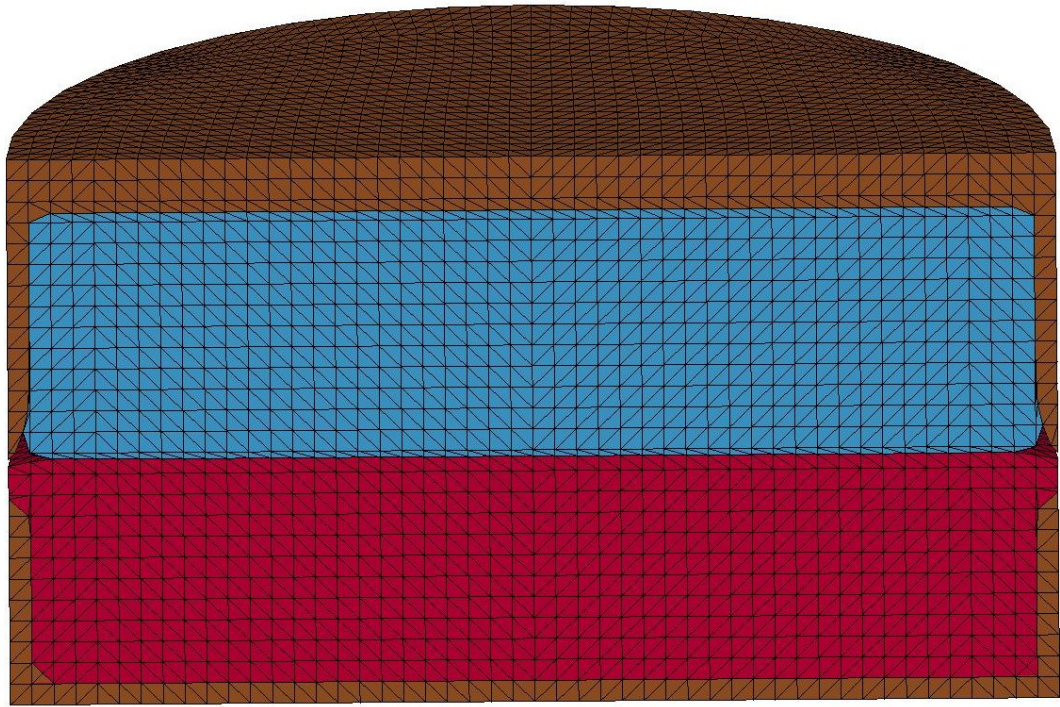


Figure 4.8: Unreacted material characterization simulation, material locations at time $= 0.83 \mu s$.

4.1. SIMULATION OF UNREACTED MATERIAL
CHARACTERIZATION TEST

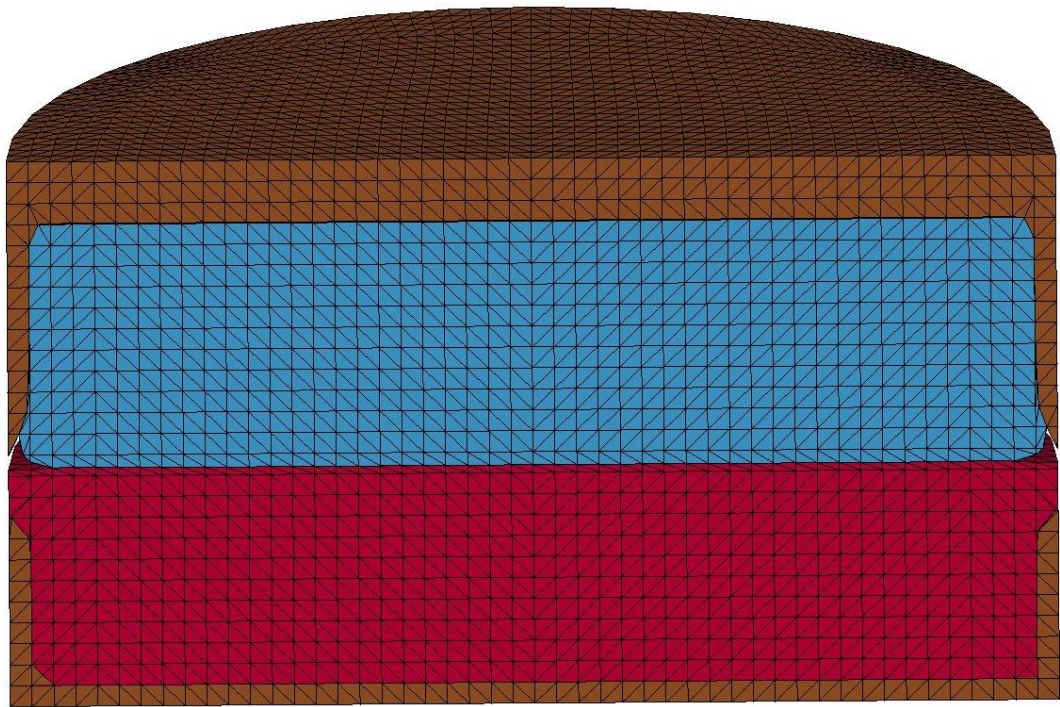


Figure 4.9: Unreacted material characterization simulation, material locations at time $= 1.03 \mu s$.

4.1. SIMULATION OF UNREACTED MATERIAL
CHARACTERIZATION TEST

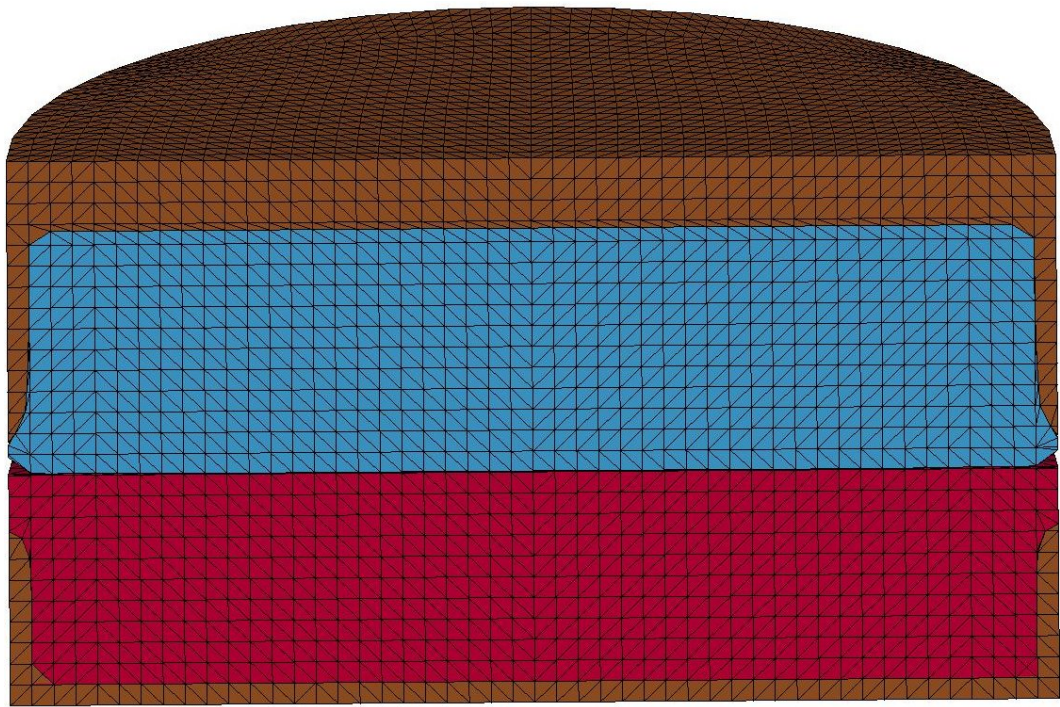


Figure 4.10: Unreacted material characterization simulation, material locations at time = $1.24 \mu\text{s}$.

4.1. SIMULATION OF UNREACTED MATERIAL
CHARACTERIZATION TEST

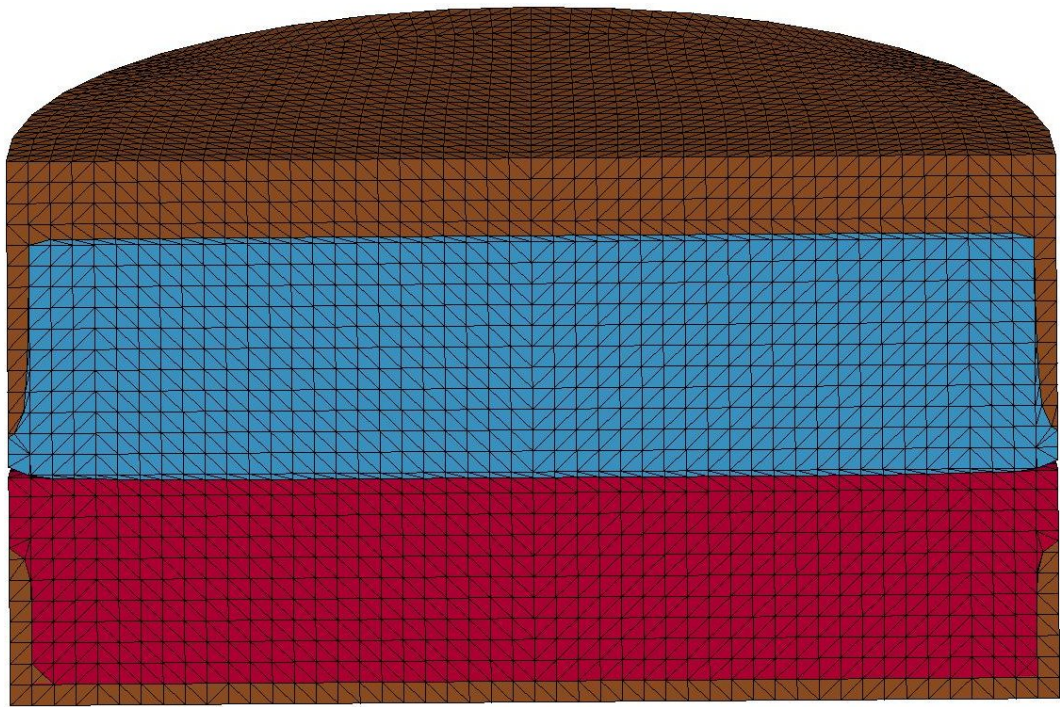


Figure 4.11: Unreacted material characterization simulation, material locations at time = $1.46 \mu\text{s}$.

4.1. SIMULATION OF UNREACTED MATERIAL
CHARACTERIZATION TEST

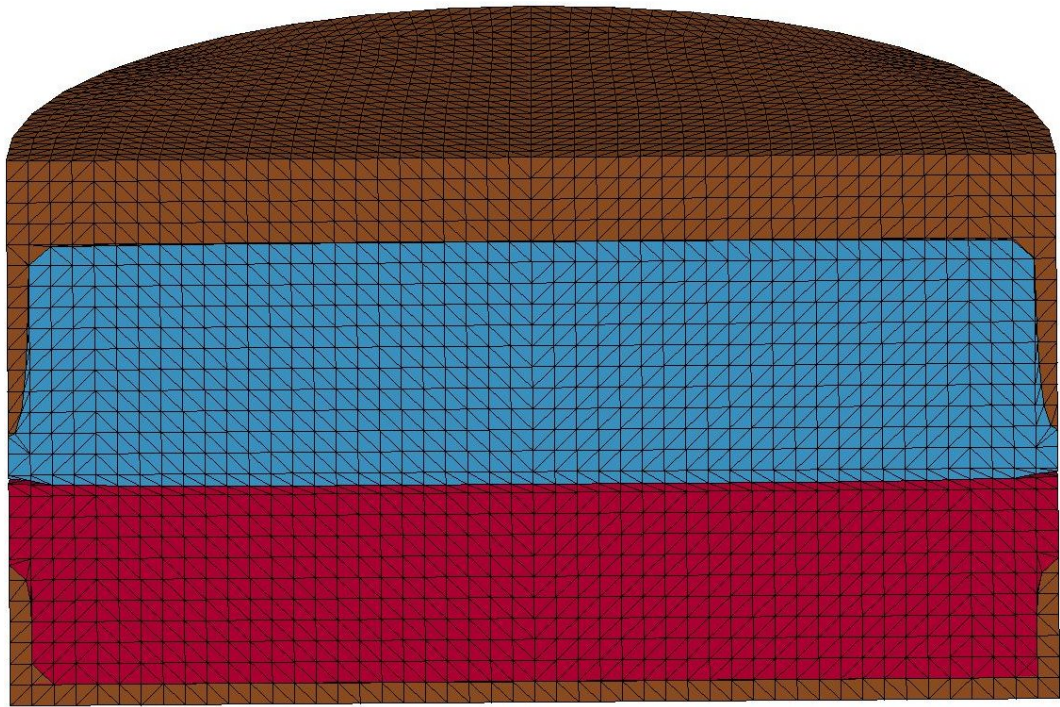


Figure 4.12: Unreacted material characterization simulation, material locations at time = $1.67 \mu\text{s}$.

4.1. SIMULATION OF UNREACTED MATERIAL
CHARACTERIZATION TEST

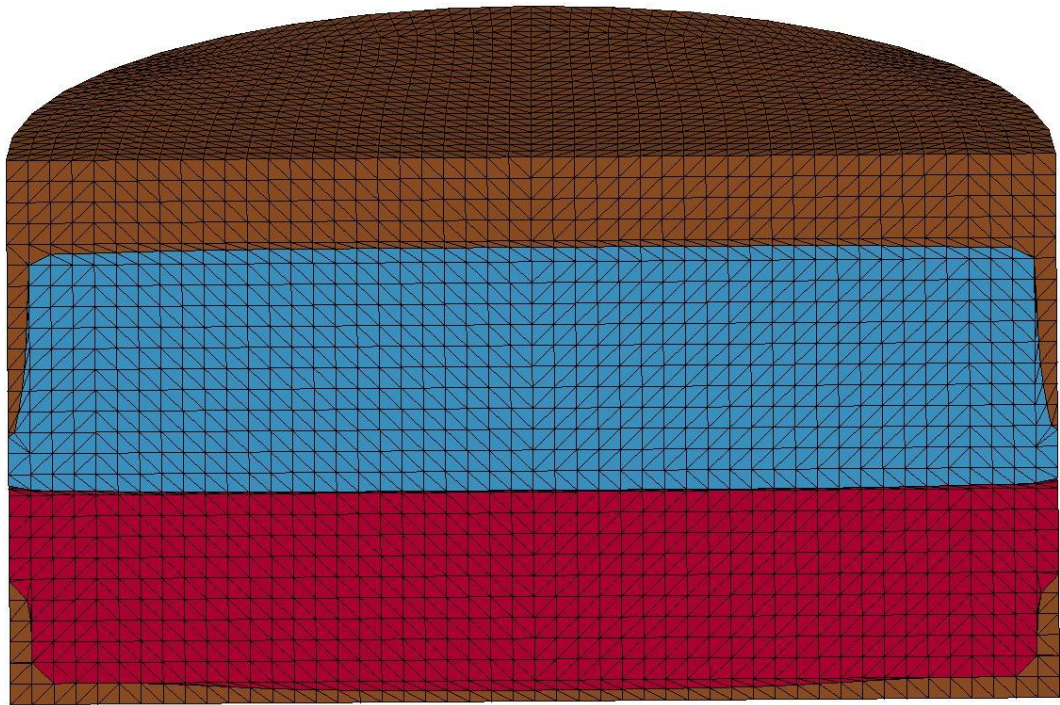


Figure 4.13: Unreacted material characterization simulation, material locations at time = $1.88 \mu\text{s}$.

4.1. SIMULATION OF UNREACTED MATERIAL CHARACTERIZATION TEST

Figures 4.14 through 4.23 depict the pressure in the reactive material. The projectile and vacuum have been excluded from these plots for clarity. Please note that the pressure scales change with each time step to provide the maximum clarity. These figures also confirm that, as desired, the plane pressure wave first reaches the opposite side in the center.

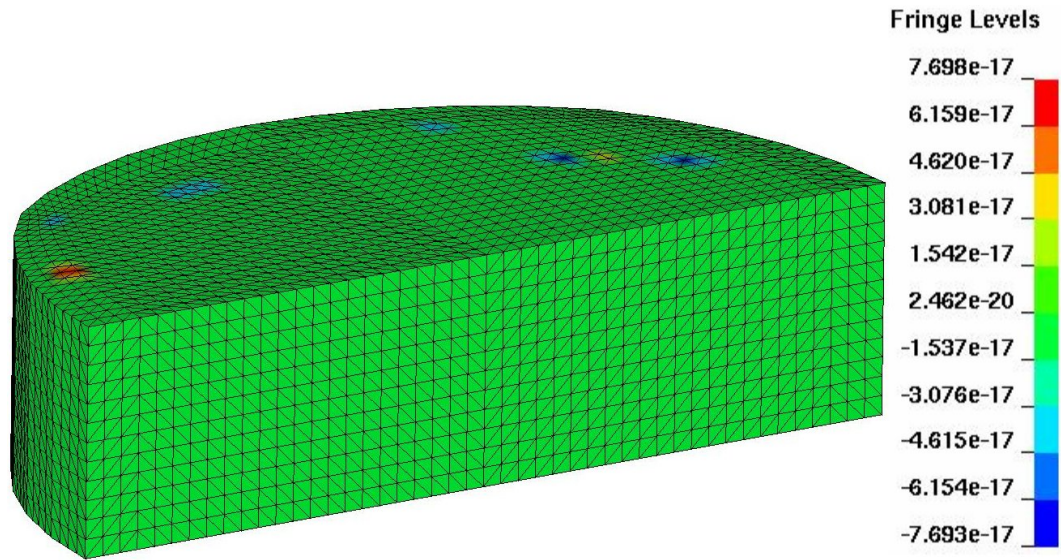


Figure 4.14: Unreacted material characterization simulation, pressure contours at time = $0.00 \mu\text{s}$.

4.1. SIMULATION OF UNREACTED MATERIAL CHARACTERIZATION TEST

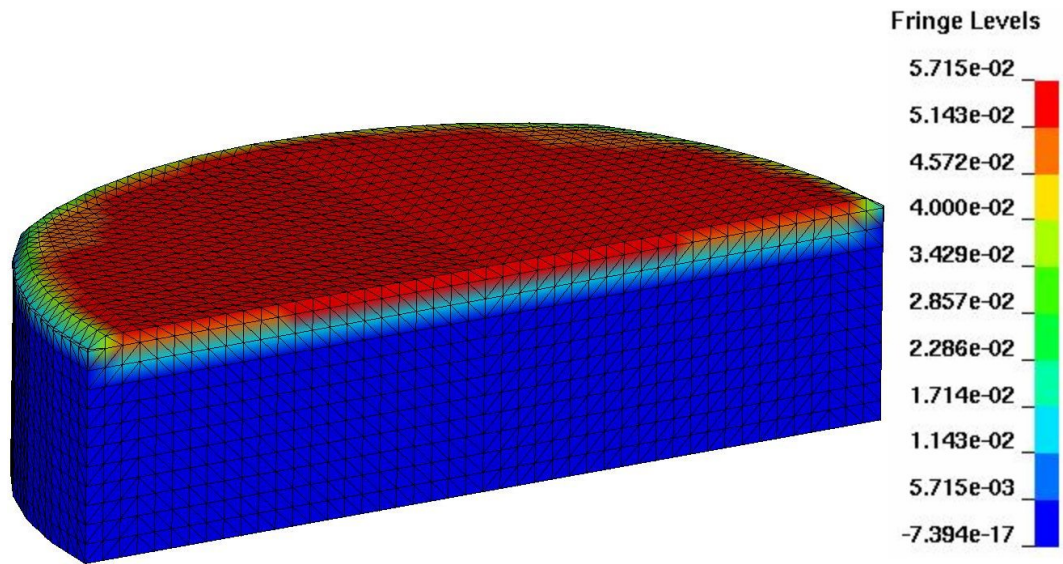


Figure 4.15: Unreacted material characterization simulation, pressure contours at time = $0.20 \mu\text{s}$.

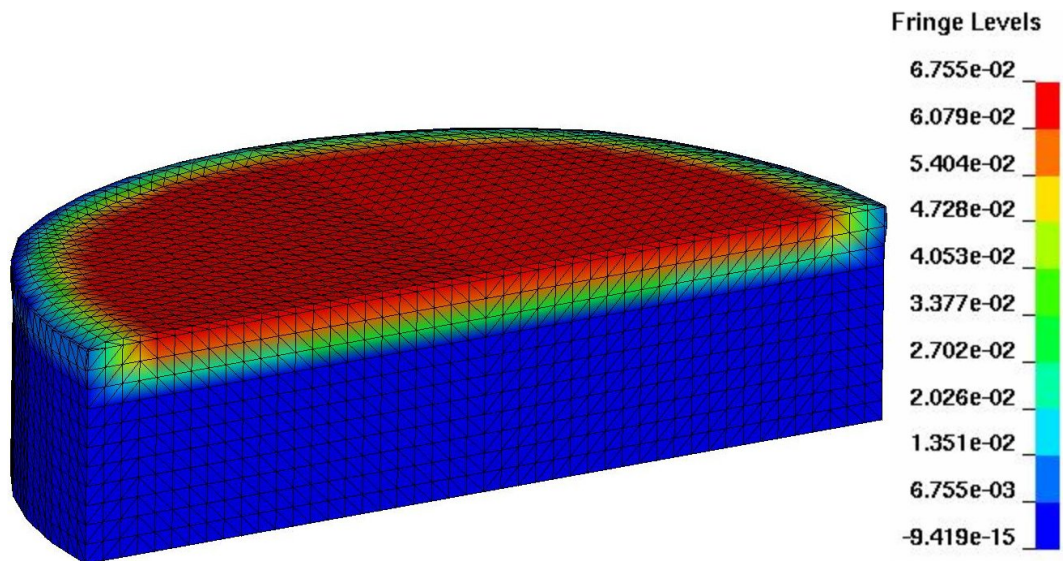


Figure 4.16: Unreacted material characterization simulation, pressure contours at time = $0.41 \mu\text{s}$.

4.1. SIMULATION OF UNREACTED MATERIAL CHARACTERIZATION TEST

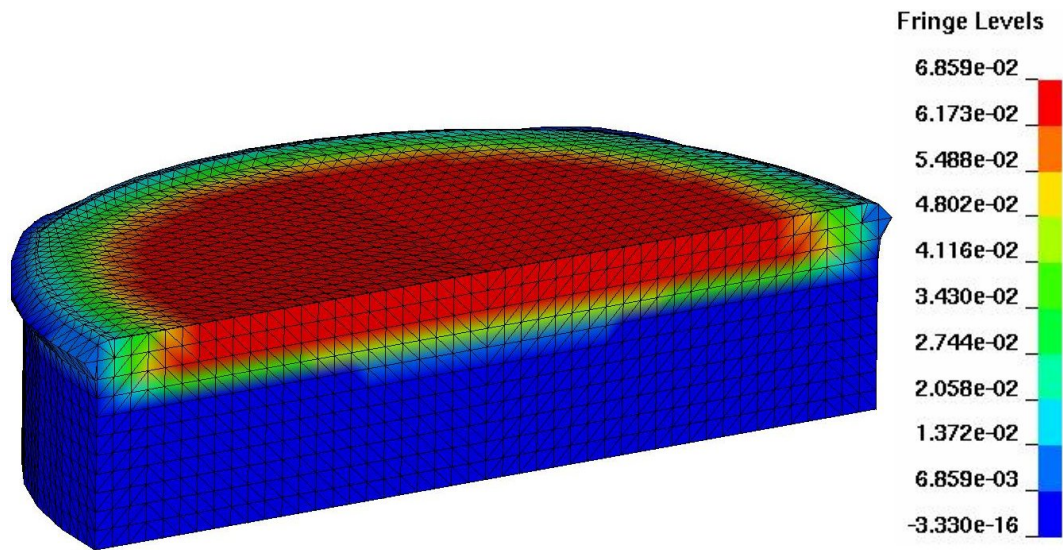


Figure 4.17: Unreacted material characterization simulation, pressure contours at time = 0.62 μs .

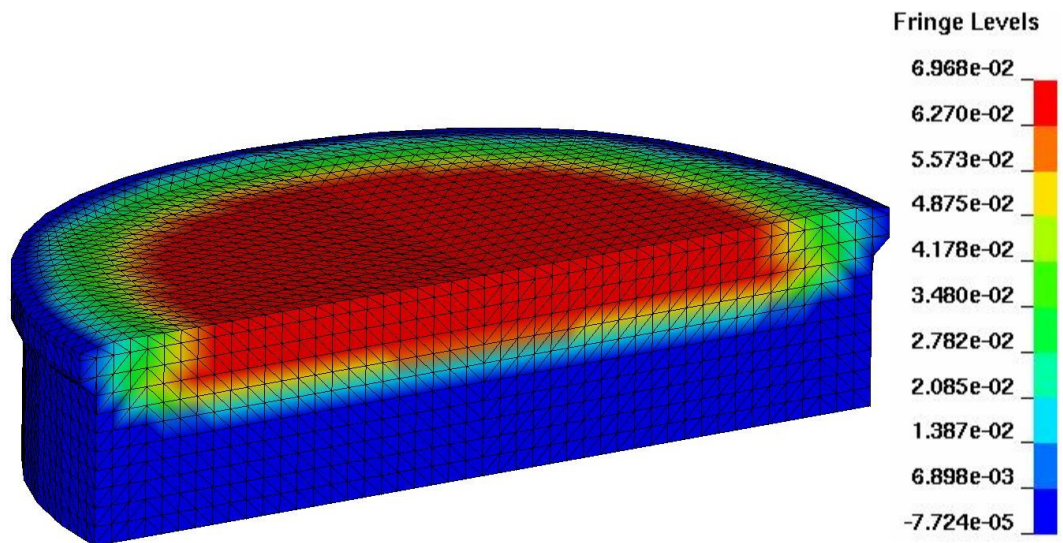


Figure 4.18: Unreacted material characterization simulation, pressure contours at time = 0.83 μs .

4.1. SIMULATION OF UNREACTED MATERIAL CHARACTERIZATION TEST

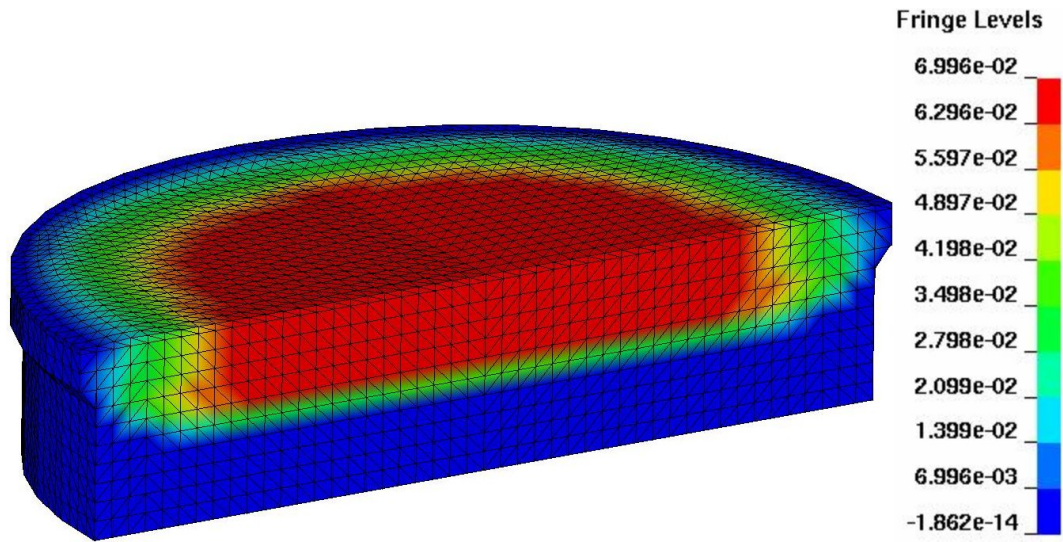


Figure 4.19: Unreacted material characterization simulation, pressure contours at time = $1.03 \mu s$.

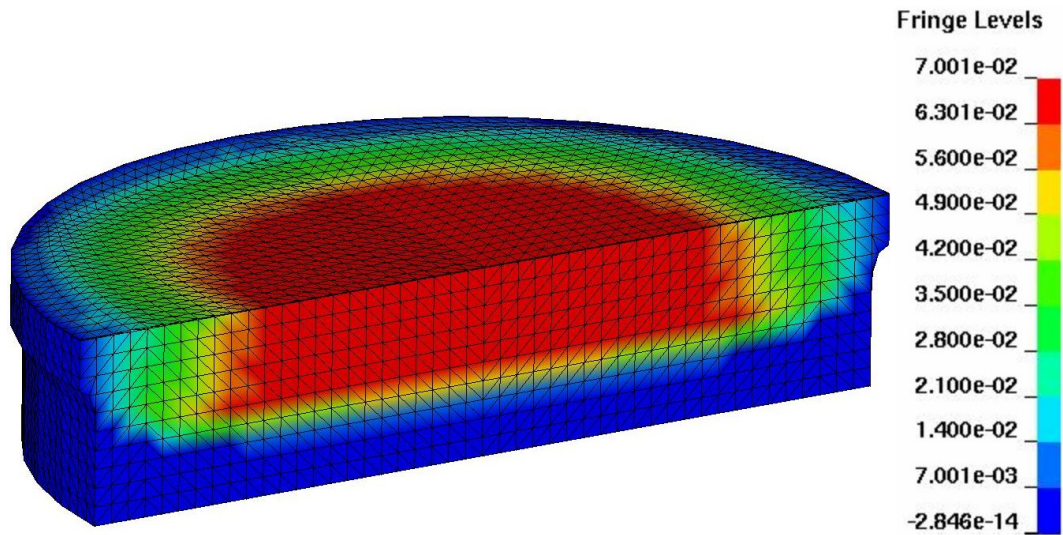


Figure 4.20: Unreacted material characterization simulation, pressure contours at time = $1.24 \mu s$.

4.1. SIMULATION OF UNREACTED MATERIAL CHARACTERIZATION TEST

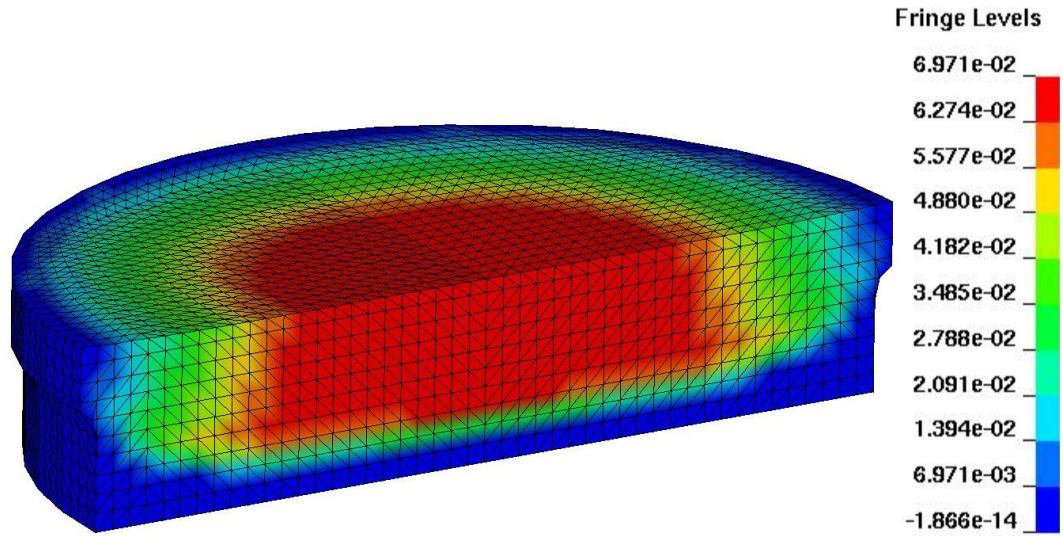


Figure 4.21: Unreacted material characterization simulation, pressure contours at time = 1.46 μs .

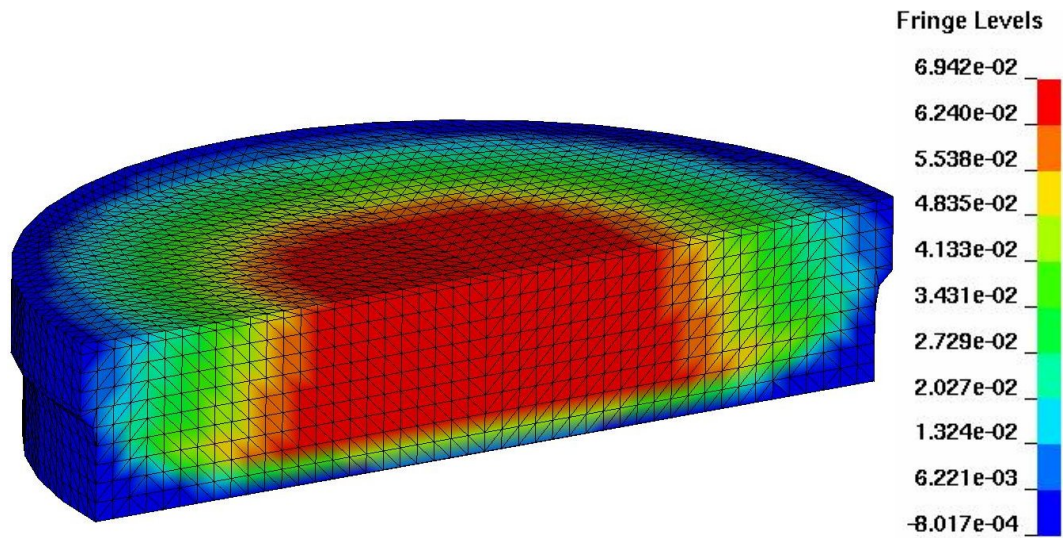


Figure 4.22: Unreacted material characterization simulation, pressure contours at time = 1.67 μs .

4.1. SIMULATION OF UNREACTED MATERIAL CHARACTERIZATION TEST

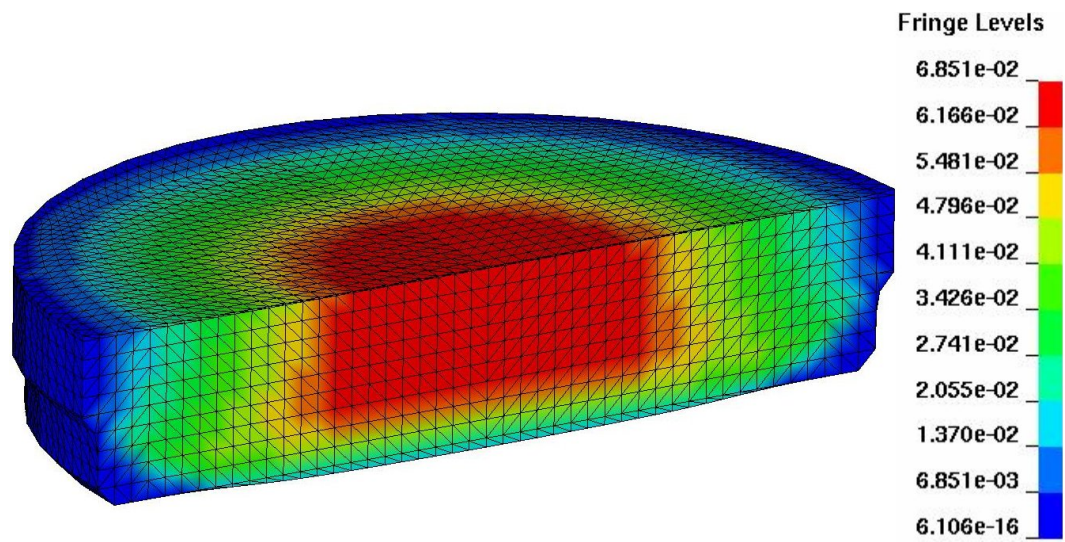


Figure 4.23: Unreacted material characterization simulation, pressure contours at time = 1.88 μ s.

4.1. SIMULATION OF UNREACTED MATERIAL CHARACTERIZATION TEST

In order to determine the particle velocity, or the velocity of the copper projectile, the volume fraction of an element originally containing the reactive material is plotted. When the volume fraction of the element that is copper is no longer zero, the copper projectile has arrived at the element. The particular element chosen for the measurement is 0.105 cm into the reactive cylinder, and the volume fraction plot is shown in Figure 4.24. The distance, 0.105 cm, divided by the time that the copper volume fraction ceased to be zero, 1.27 μs , gives the velocity of the projectile to be $8.28 \times 10^{-2} \frac{\text{cm}}{\mu\text{s}}$.

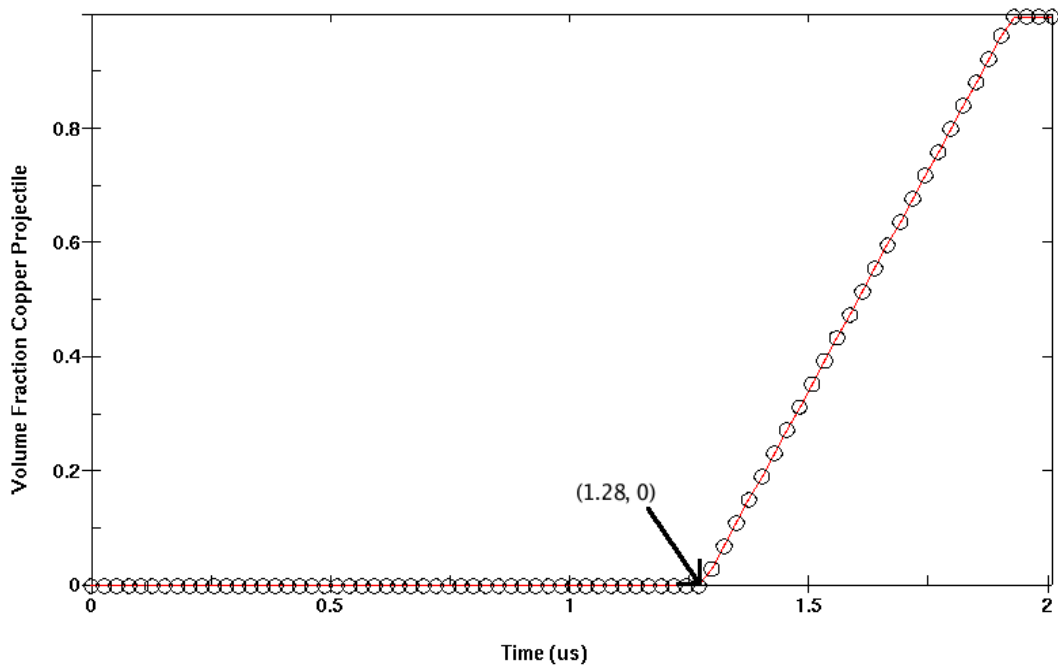


Figure 4.24: Volume fraction of an element 0.105 cm into the reactive cylinder.

The wave velocity was determined by plotting the acceleration of a node 0.58 cm into the material of the reactive cylinder. Where the acceleration at the node is at its peak we can say that the shock wave is passing. It is worth keeping in mind that the *CONTROL BULK VISCOSITY record smears the discontinuity of a shock out a little bit into a continuous change so that the macro effects of the shock can

4.1. SIMULATION OF UNREACTED MATERIAL CHARACTERIZATION TEST

be modeled accurately. The acceleration peaks at $1.61 \mu s$. The distance the wave traveled divided by its arrival time gives a wave velocity of $0.36 \frac{cm}{\mu s}$. This value matches the unreacted particle vs. wave velocity plot presented in Figure 2.4 and shows that the JWL parameters determined were implemented as expected.

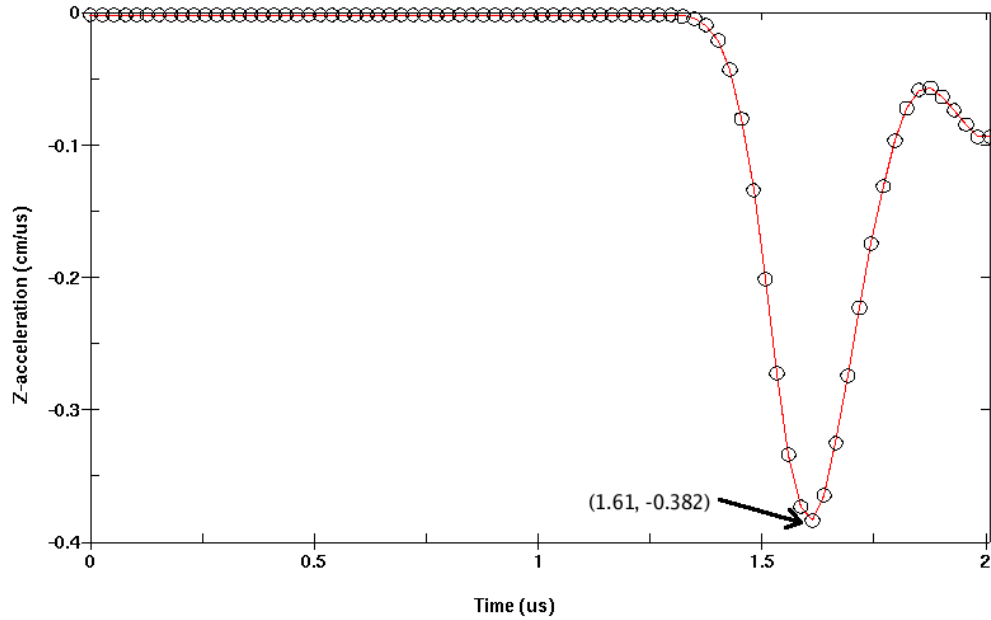


Figure 4.25: Acceleration curve of a node 0.58 cm into the reactive cylinder.

Reacted Material Characterization

This chapter describes a test with the purpose of characterizing the reacted state of the reactive material. A simulation of the characterization test is then performed to show that the equation of state developed in chapter 2 is modeling the reacted material as expected.

To validate the reacted portion of the I&G EOS, a cylinder test should be performed with the density of reactive material that is being characterized. This test consists of a 0.26 cm thick copper tube, with an inner diameter of 2.54 cm and a length of 29.99 cm, filled with reactive material. This tube is then shocked at one end, by an explosive charge, for example. The reactive material in the copper tube reacts as the pressure wave passes and the reaction products expand in the copper tube causing the copper tube to expand. At a point along the tube, the radial velocity of the expanding copper is measured until the copper ruptures. This rate of expansion translates into a cylinder wall energy that can be correlated with the C-J pressure[26]. For our purposes we simply want to compare the simulated cylinder test to an actual cylinder test to validate the simulation.

5.1 Simulation of the Reacted Material Characterization Test

This test was modeled as a coupled Euler-Lagrange problem. The Euler domain consists of a solid cylinder 35.99 cm high and 8.0 cm in diameter and is shown in Figure 5.1. Inside this cylinder is a Lagrangian copper tube and an Eulerian cylinder of reactive material. The close-up view shown in Figure 5.2 and the top view shown in Figure 5.3 illustrate these parts. The red represents the reactive material, the green is the copper tube, and the yellow is vacuum. The reactive cylinder is 2.54 cm in diameter and 29.99 cm long. The copper tube wraps around the reactive material and has a thickness of 0.26 cm. As shown in Figures 5.4 and 5.5 there is an additional part which represents the explosive that will create the pressure wave that will initiate the reactive material. This explosive material is placed in the model using LS-DYNA's `*INITIAL VOLUME FRACTION GEOMETRY` record. The Euler elements are all single point integration multi-material Euler elements. The Euler domain has no boundary conditions so material is free to flow out of the model through any of the sides of the domain. The outer material is a vacuum material described by the `*MAT VACUUM TITLE` record. The reactive and copper cylinders' material properties are described using LS-DYNA's `*MAT ELASTIC PLASTIC HYDRO TITLE` record. The copper cylinder is using a Grüneisen EOS defined by the `*EOS GRUNEISEN TITLE` and the reactive material is using the `*EOS IGNITION AND GROWTH OF REACTION IN HE TITLE` EOS created in Chapter 2. The shaped charge consists of C-4 whose material properties are described by the `*MAT HIGH EXPLOSIVE BURN` and has an equation of state described by the `*EOS JWL` record.

5.1. SIMULATION OF THE REACTED MATERIAL CHARACTERIZATION TEST

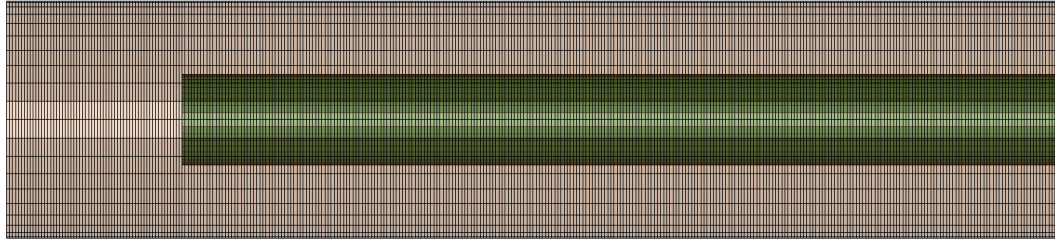


Figure 5.1: Reacted material characterization simulation euler mesh, full view.

The simulation begins with shaped charge being initiated at the tip using the *INITIAL DETONATION record. The plane pressure wave generated by the explosive moves down until it impacts the top of the reacted material and the cylinder. The simulation was run until the pressures in the reactive materials became so low as to indicate that the reaction was coming to a halt. Figures 5.6 through 5.16 depict the various material positions and shapes over time in a lengthwise cut of the Eulerian domain. The yellow is the Eulerian reactive material, the green is the Lagrangian copper tube, the red is the Euler shaped charge, and the beige is the surrounding vacuum. Keep in mind that the Euler materials can flow out of the Euler domain but, unlike the Lagrangian copper tube, they disappear from the simulation when they do. So once the copper tube or pieces of the copper tube leave the Euler domain they are no longer affected by the Euler materials.

5.1. SIMULATION OF THE REACTED MATERIAL CHARACTERIZATION TEST

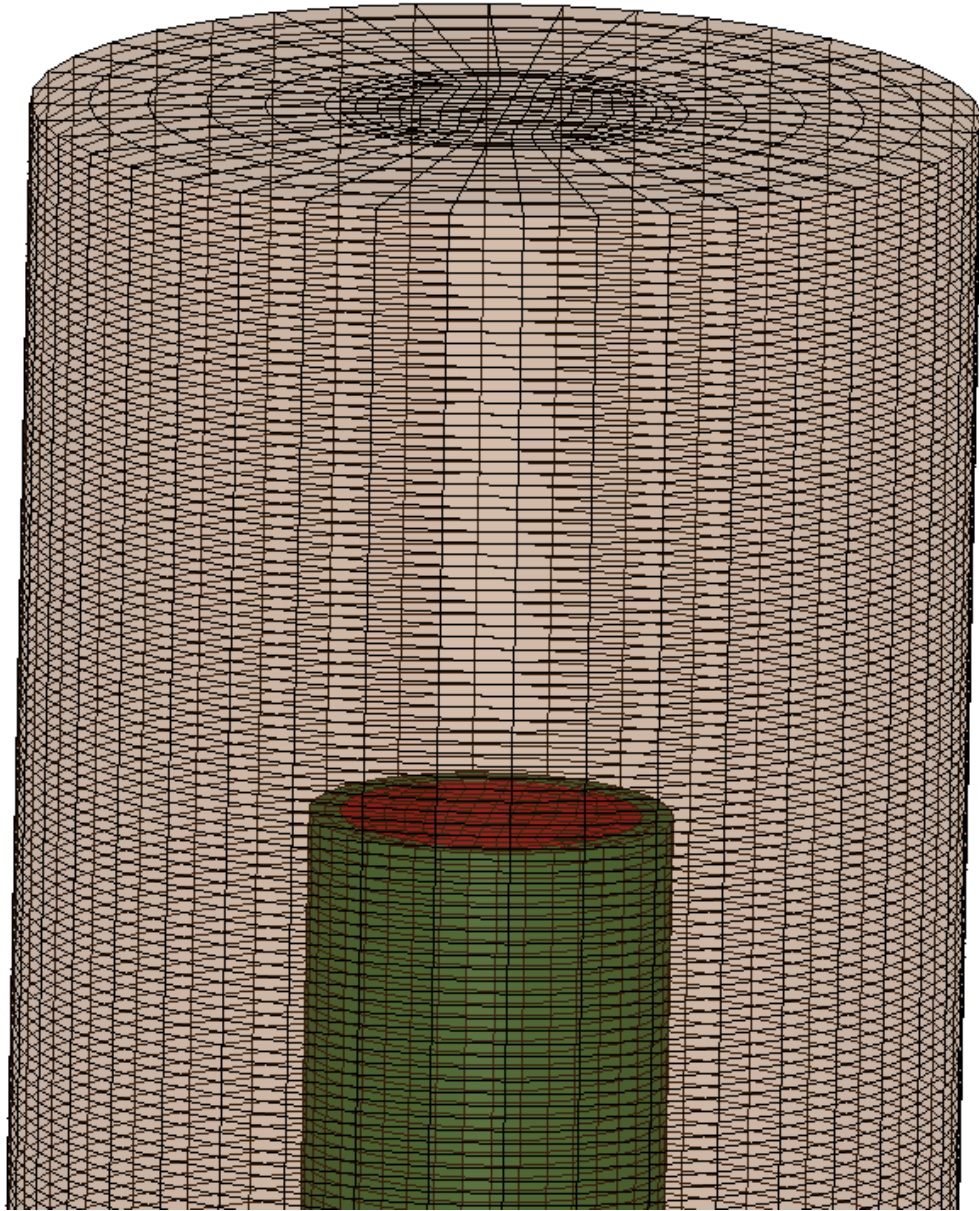


Figure 5.2: Reacted material characterization simulation euler mesh, close view.

5.1. SIMULATION OF THE REACTED MATERIAL CHARACTERIZATION TEST

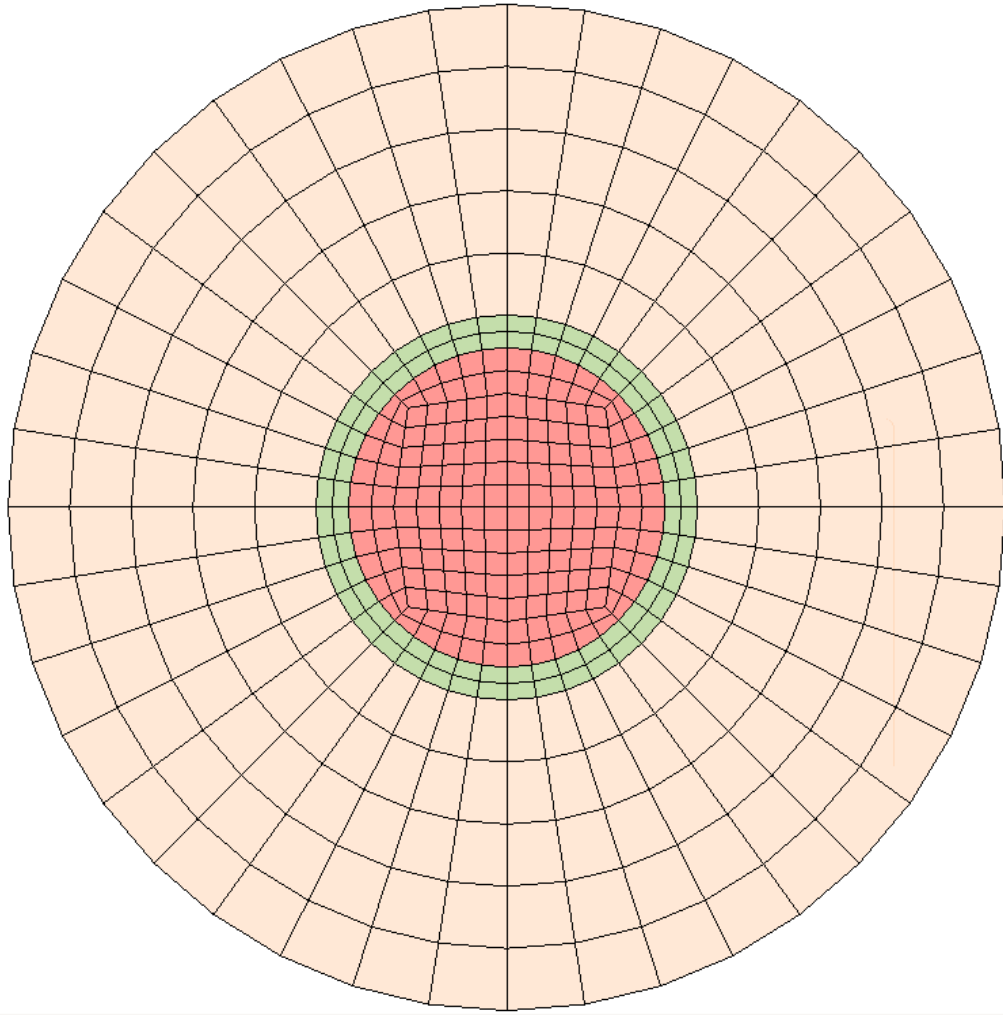


Figure 5.3: Reacted material characterization simulation euler mesh, top view.

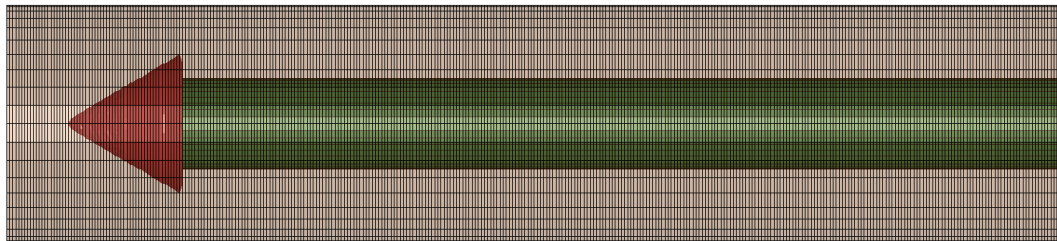


Figure 5.4: Reacted material characterization simulation euler parts, full view.

5.1. SIMULATION OF THE REACTED MATERIAL
CHARACTERIZATION TEST

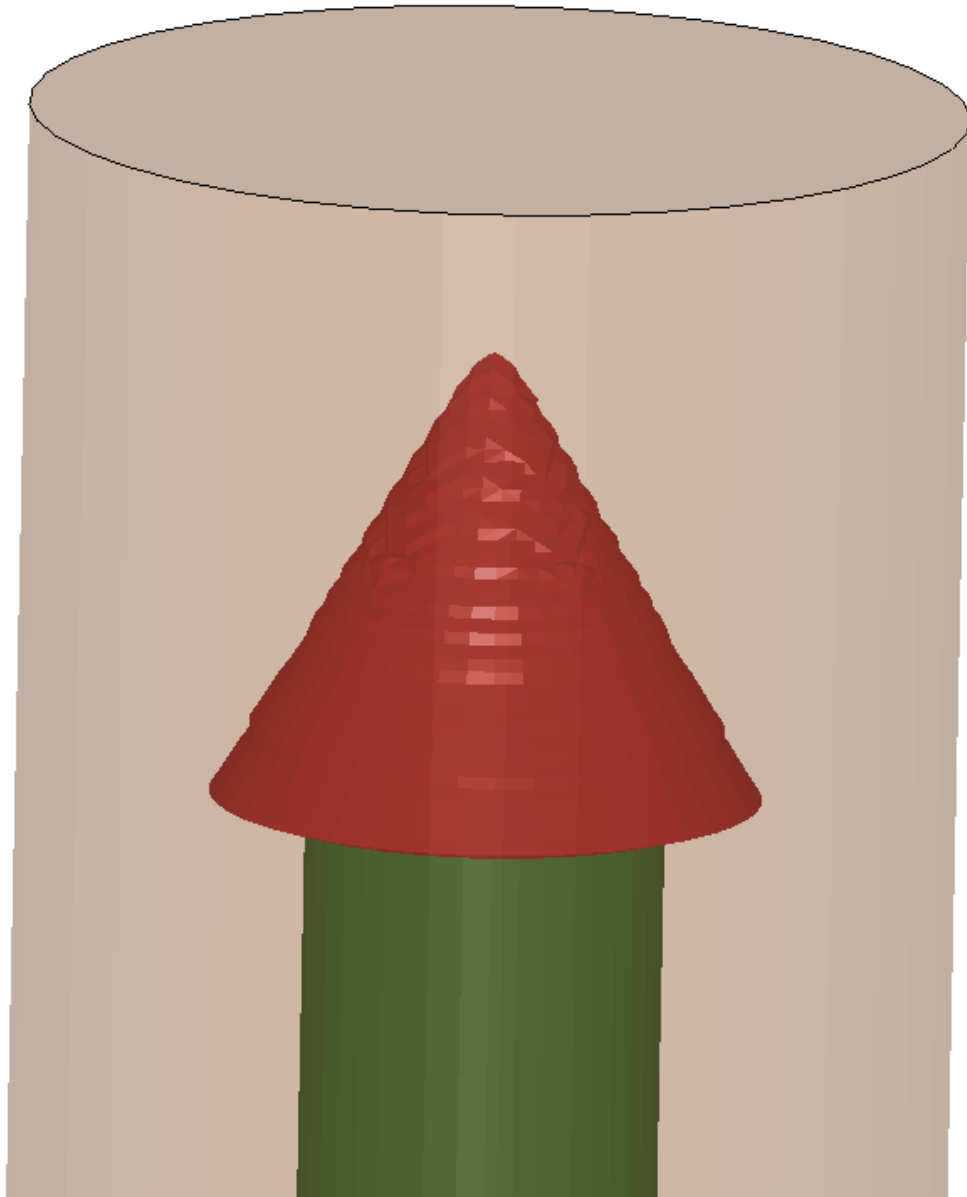


Figure 5.5: Reacted material characterization simulation euler parts, close view.

5.1. SIMULATION OF THE REACTED MATERIAL CHARACTERIZATION TEST

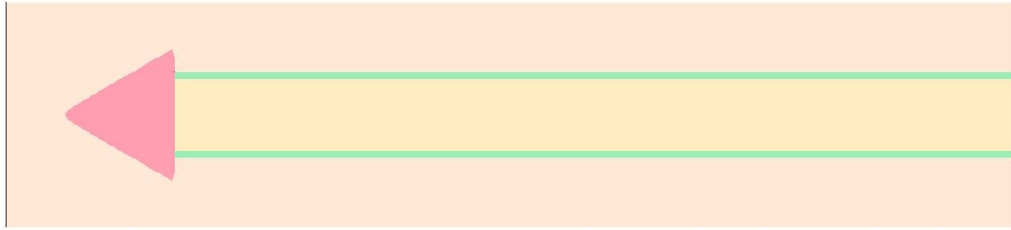


Figure 5.6: Reacted material characterization simulation, material locations at time = 00.00 μs .

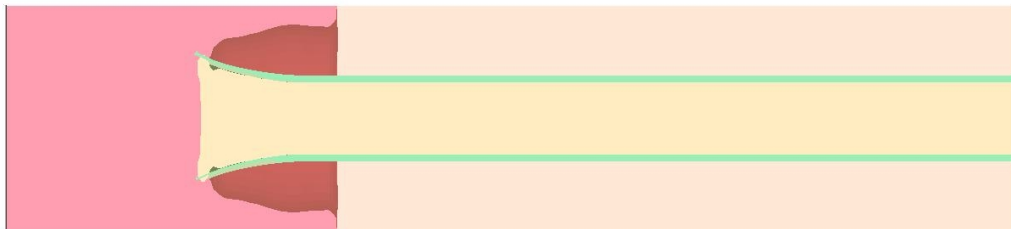


Figure 5.7: Reacted material characterization simulation, material locations at time = 19.40 μs .

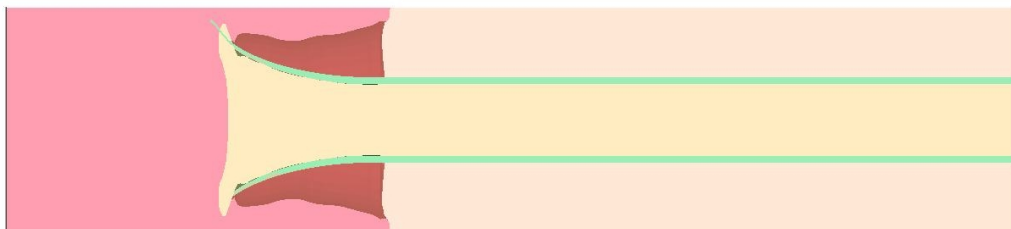


Figure 5.8: Reacted material characterization simulation, material locations at time = 38.80 μs .

5.1. SIMULATION OF THE REACTED MATERIAL CHARACTERIZATION TEST

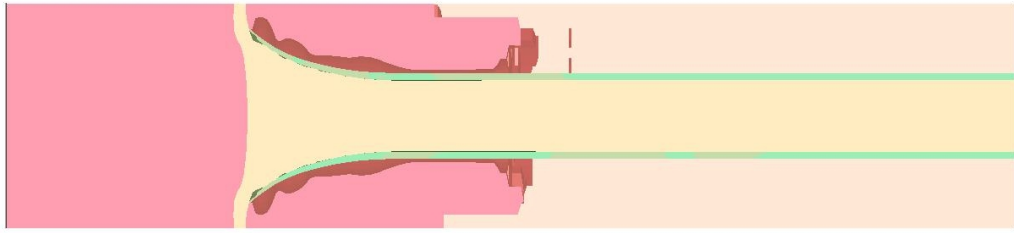


Figure 5.9: Reacted material characterization simulation, material locations at time = 58.20 μ s.



Figure 5.10: Reacted material characterization simulation, material locations at time = 77.60 μ s.

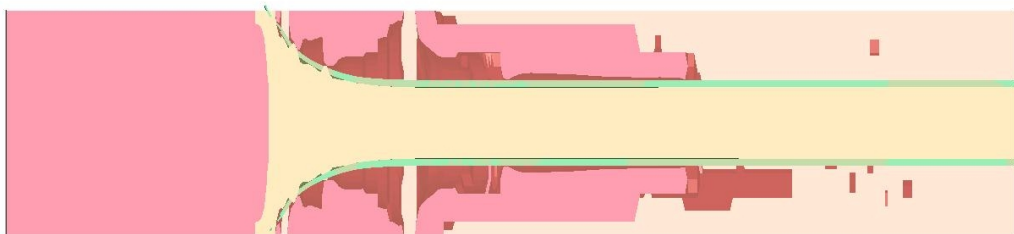


Figure 5.11: Reacted material characterization simulation, material locations at time = 97.00 μ s.

5.1. SIMULATION OF THE REACTED MATERIAL CHARACTERIZATION TEST



Figure 5.12: Reacted material characterization simulation, material locations at time = 116.4 μs .

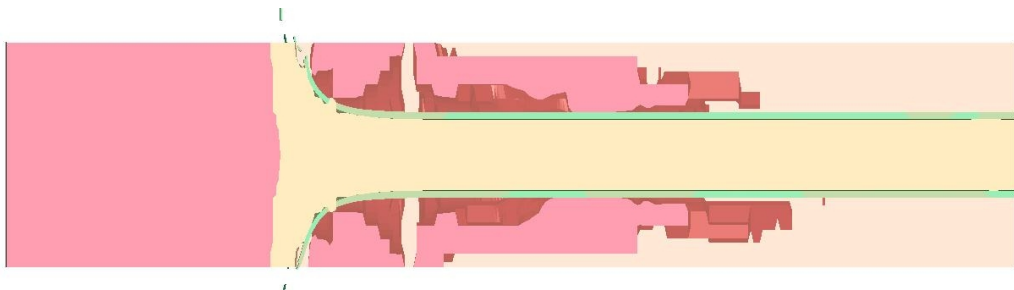


Figure 5.13: Reacted material characterization simulation, material locations at time = 135.8 μs .

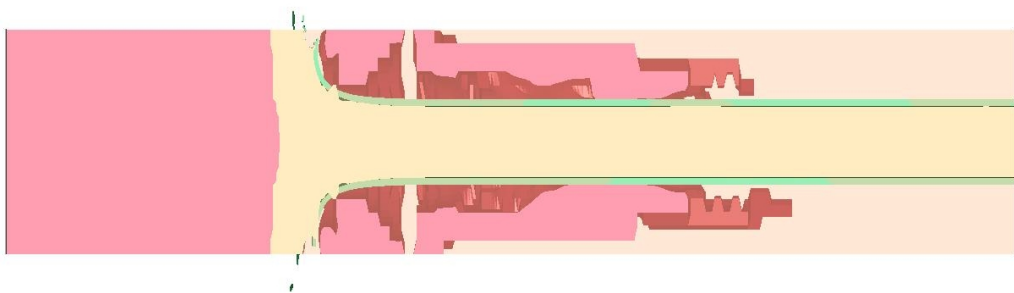


Figure 5.14: Reacted material characterization simulation, material locations at time = 155.2 μs .

5.1. SIMULATION OF THE REACTED MATERIAL CHARACTERIZATION TEST

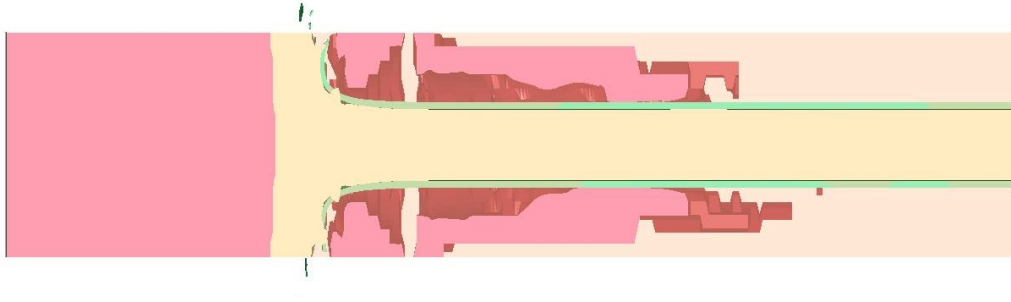


Figure 5.15: Reacted material characterization simulation, material locations at time = $174.6 \mu\text{s}$.

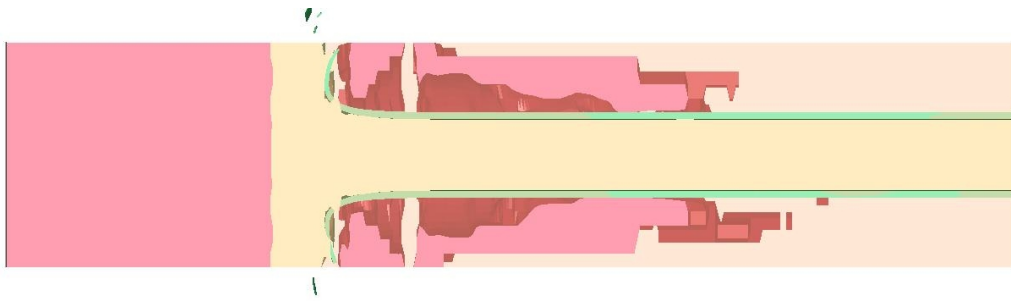


Figure 5.16: Reacted material characterization simulation, material locations at time = $194.0 \mu\text{s}$.

Figures 5.17 through 5.27 depict the pressure in the reactive material. The copper cylinder, C-4 explosive, and vacuum have been excluded from these plots for clarity. Please note that the pressure scales change with each time step to provide the maximum clarity.

5.1. SIMULATION OF THE REACTED MATERIAL CHARACTERIZATION TEST



Figure 5.17: Reacted material characterization simulation, pressure contours at time = 00.00 μs .



Figure 5.18: Reacted material characterization simulation, pressure contours at time = 19.40 μs .

5.1. SIMULATION OF THE REACTED MATERIAL CHARACTERIZATION TEST



Figure 5.19: Reacted material characterization simulation, pressure contours at time = 38.80 μs .

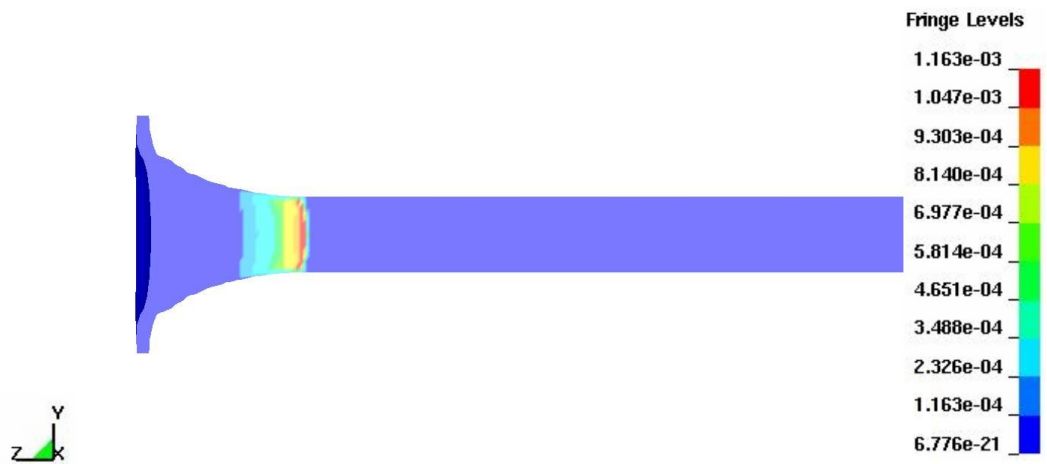


Figure 5.20: Reacted material characterization simulation, pressure contours at time = 58.20 μs .

5.1. SIMULATION OF THE REACTED MATERIAL CHARACTERIZATION TEST

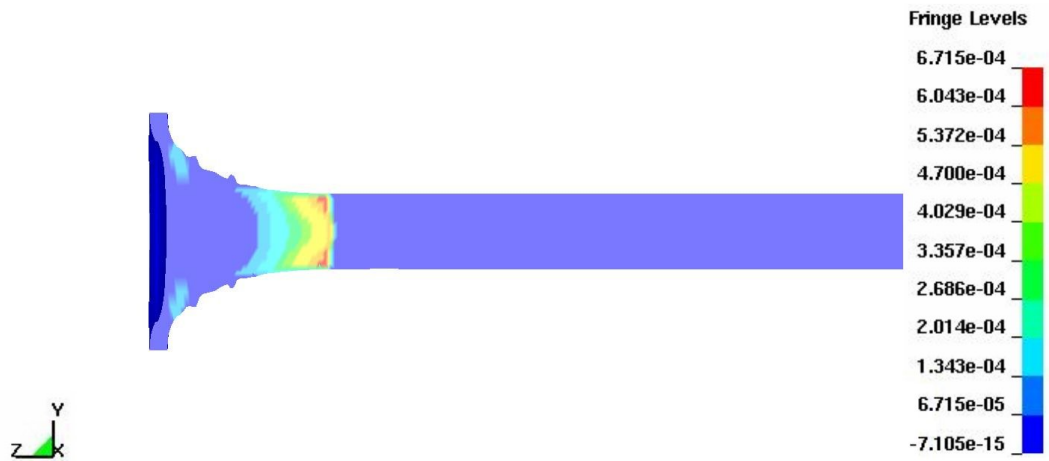


Figure 5.21: Reacted material characterization simulation, pressure contours at time $= 77.60 \mu\text{s}$.

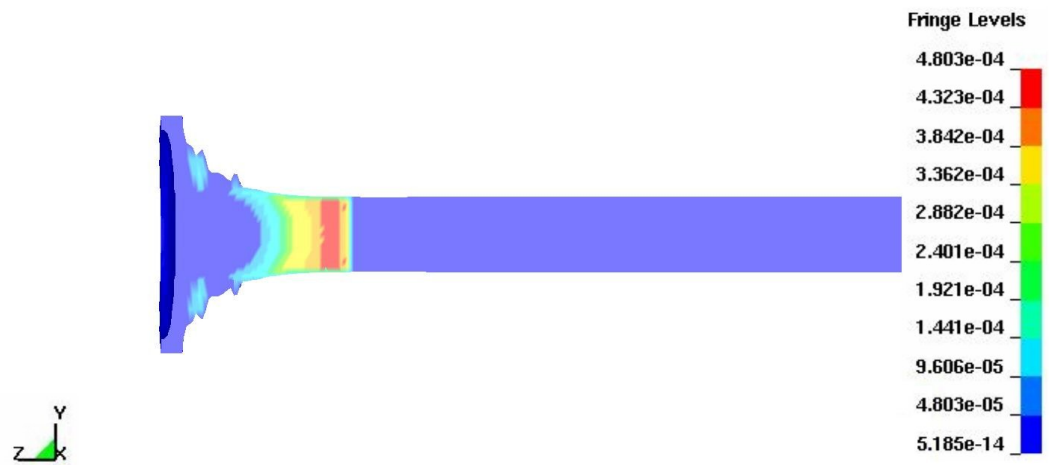


Figure 5.22: Reacted material characterization simulation, pressure contours at time $= 97.00 \mu\text{s}$.

5.1. SIMULATION OF THE REACTED MATERIAL CHARACTERIZATION TEST

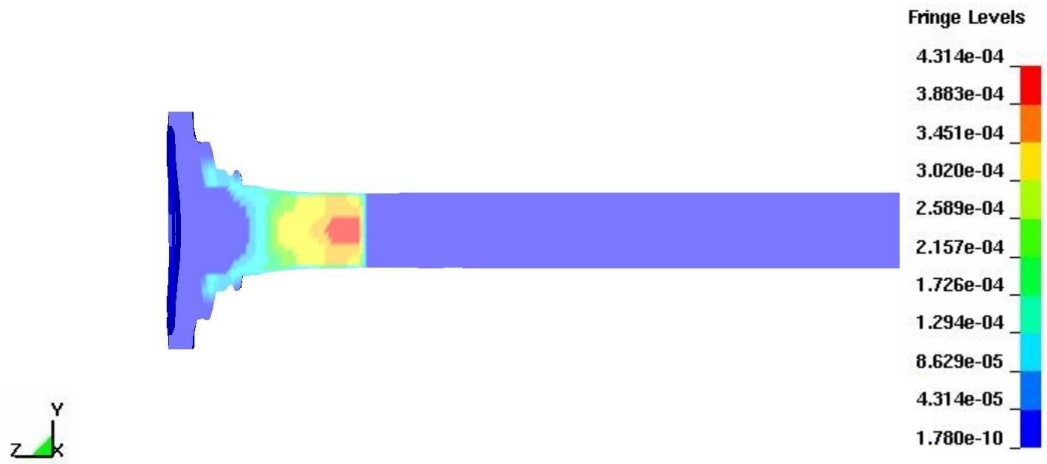


Figure 5.23: Reacted material characterization simulation, pressure contours at time = 116.4 μ s.

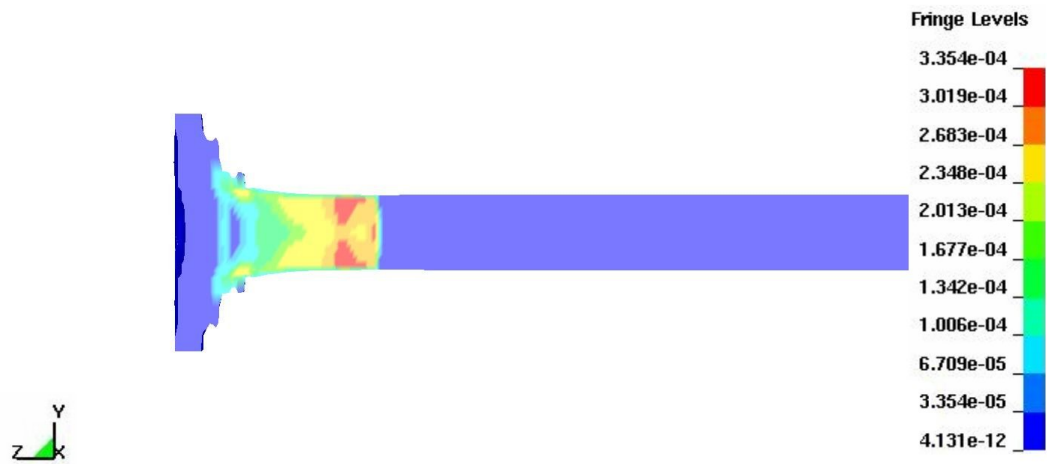


Figure 5.24: Reacted material characterization simulation, pressure contours at time = 135.8 μ s.

5.1. SIMULATION OF THE REACTED MATERIAL CHARACTERIZATION TEST

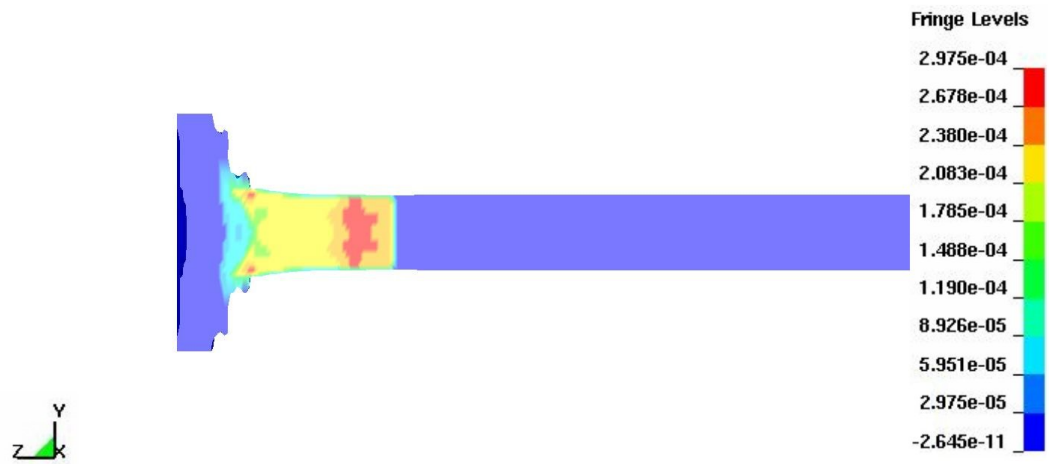


Figure 5.25: Reacted material characterization simulation, pressure contours at time = $155.2 \mu\text{s}$.

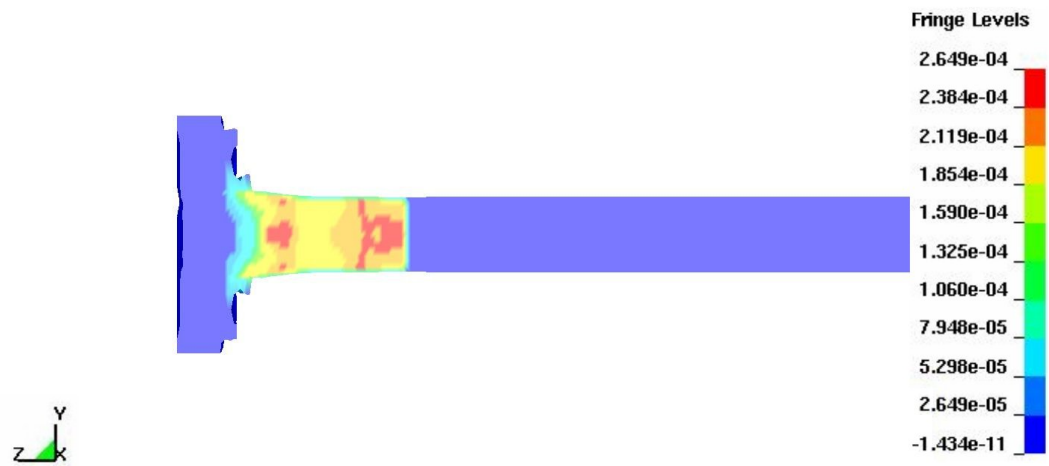


Figure 5.26: Reacted material characterization simulation, pressure contours at time = $174.6 \mu\text{s}$.

5.1. SIMULATION OF THE REACTED MATERIAL CHARACTERIZATION TEST

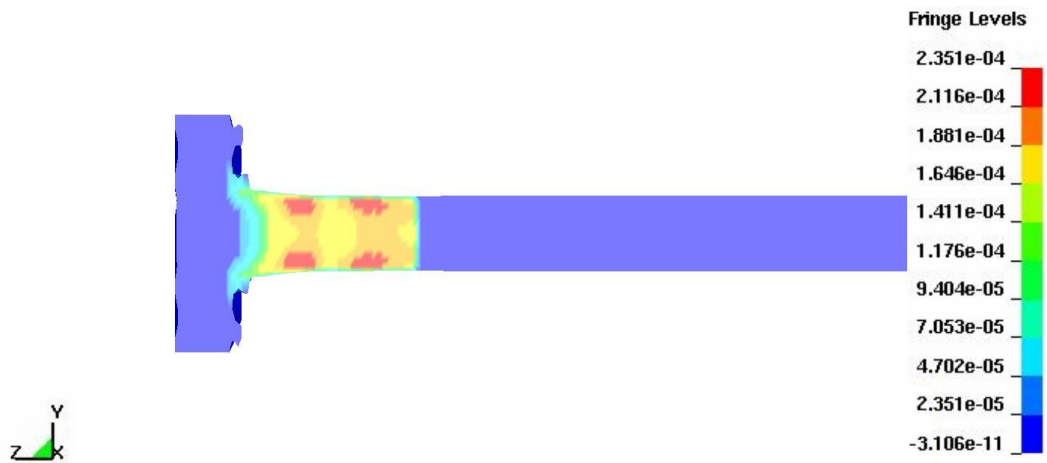


Figure 5.27: Reacted material characterization simulation, pressure contours at time = 194.0 μ s.

Figures 5.28 through 5.38 depict the percent of the reactive material in a given location that has been converted into reaction products. As with the pressure plots above, the copper cylinder, C-4 explosive, and vacuum have been excluded from these plots for clarity. Please note that the pressure scales change with each time step to provide the maximum clarity.

5.1. SIMULATION OF THE REACTED MATERIAL CHARACTERIZATION TEST



Figure 5.28: Reacted material characterization simulation, percent reacted at time = 00.00 μs .



Figure 5.29: Reacted material characterization simulation, percent reacted at time = 19.40 μs .

5.1. SIMULATION OF THE REACTED MATERIAL CHARACTERIZATION TEST



Figure 5.30: Reacted material characterization simulation, percent reacted at time = 38.80 μs .

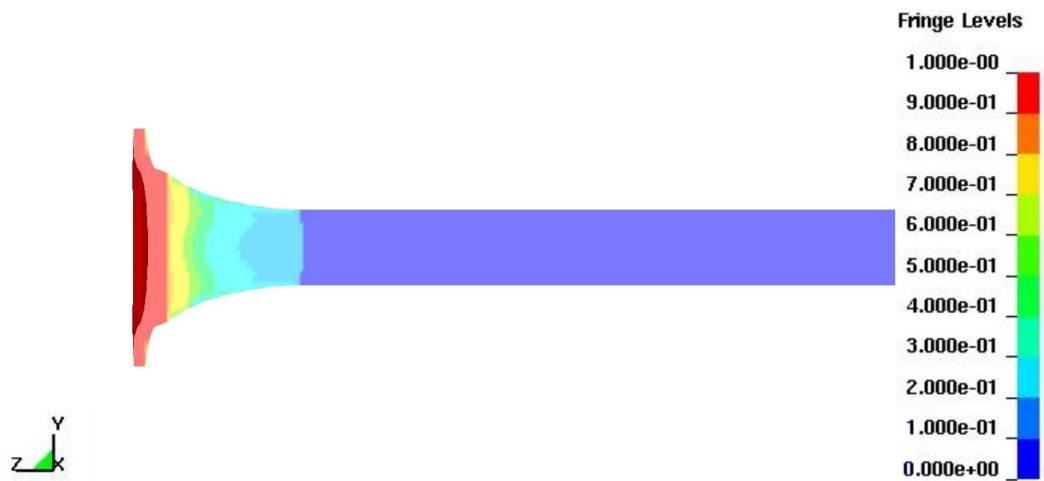


Figure 5.31: Reacted material characterization simulation, percent reacted at time = 58.20 μs .

5.1. SIMULATION OF THE REACTED MATERIAL CHARACTERIZATION TEST



Figure 5.32: Reacted material characterization simulation, percent reacted at time = $77.60 \mu\text{s}$.

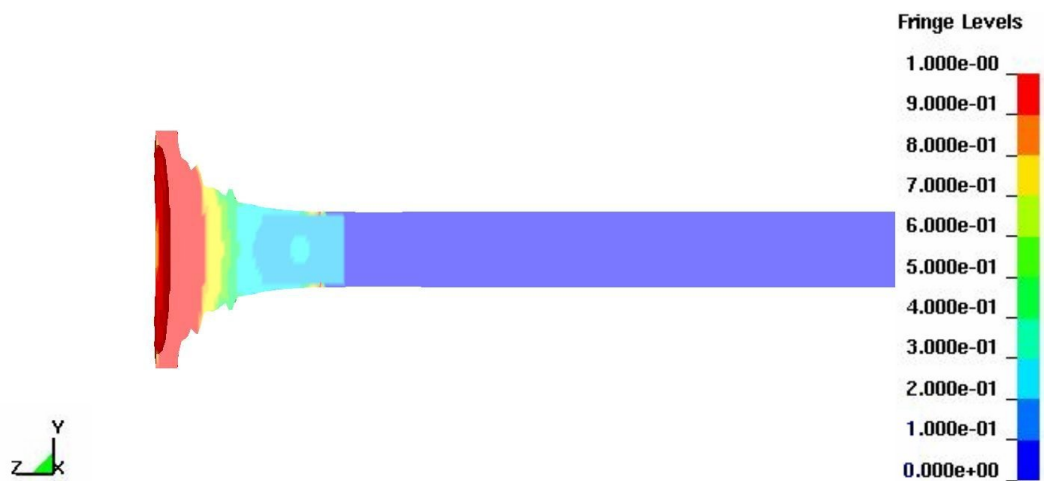


Figure 5.33: Reacted material characterization simulation, percent reacted at time = $97.00 \mu\text{s}$.

5.1. SIMULATION OF THE REACTED MATERIAL CHARACTERIZATION TEST

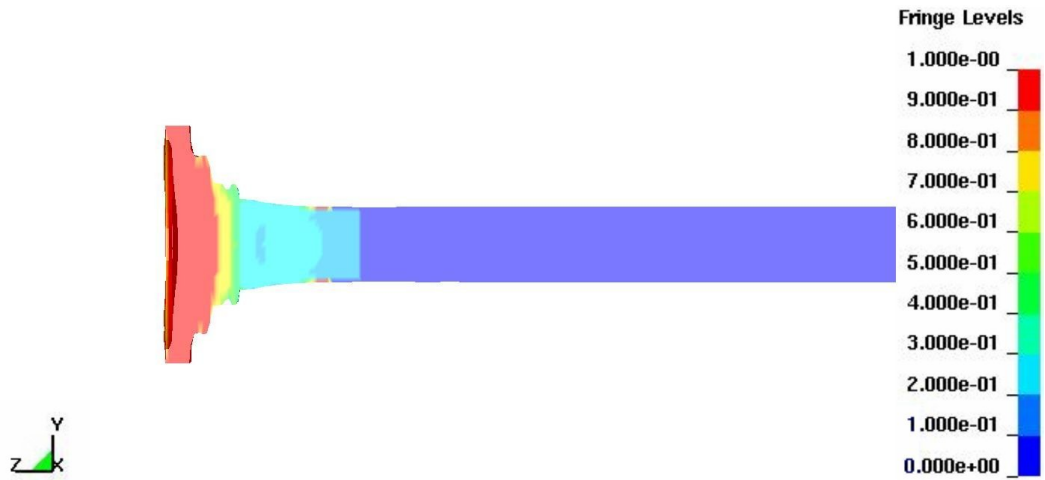


Figure 5.34: Reacted material characterization simulation, percent reacted at time = 116.4 μ s.

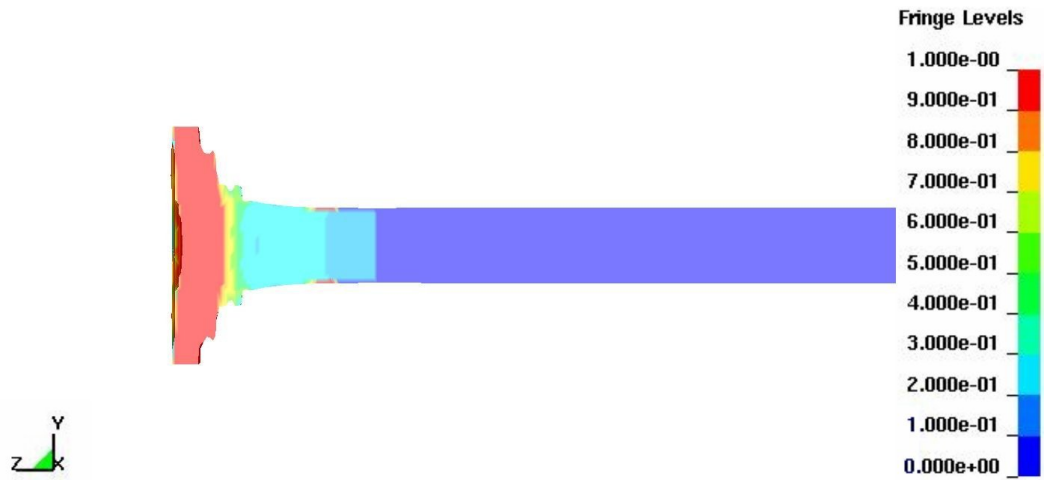


Figure 5.35: Reacted material characterization simulation, percent reacted at time = 135.8 μ s.

5.1. SIMULATION OF THE REACTED MATERIAL CHARACTERIZATION TEST

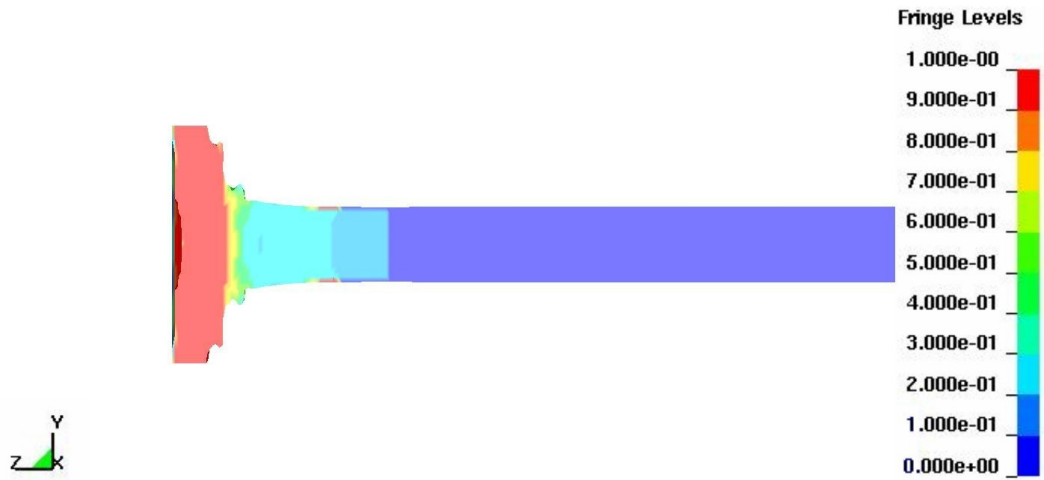


Figure 5.36: Reacted material characterization simulation, percent reacted at time = 155.2 μ s.

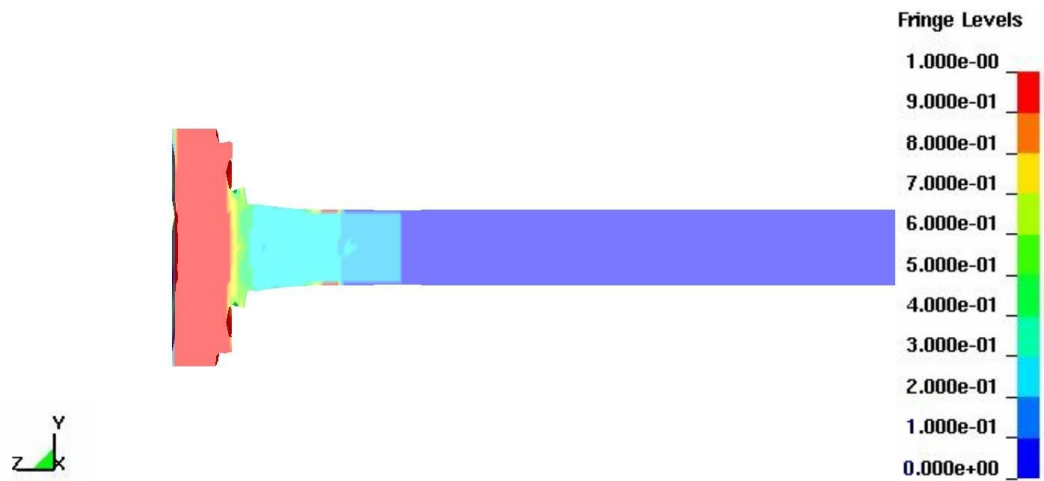


Figure 5.37: Reacted material characterization simulation, percent reacted at time = 174.6 μ s.

5.1. SIMULATION OF THE REACTED MATERIAL CHARACTERIZATION TEST

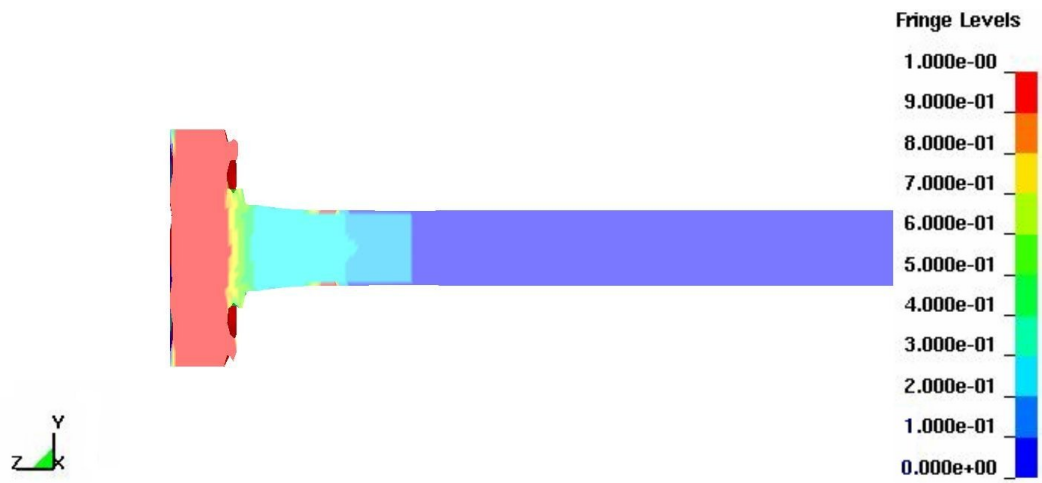


Figure 5.38: Reacted material characterization simulation, percent reacted at time = 194.0 μ s.

Reactive Material Box Test

General Sciences Inc. had performed several light gas gun tests of nonreacting steel projectiles and reactive material projectiles against targets that consisted of plate arrays in nitrogen and vacuum environments. This chapter describes one of their tests in detail. In addition this chapter describes a simulation of the test I created using the EOS developed in chapter 2. The results of the test and simulation are compared in chapter 7.

The sabots used for these tests were made from 7075 aluminum. Aluminum was chosen for its low density to keep projectile mass low, and for its low abrasive qualities to minimize gun barrel wear issues. A schematic of the projectile/sabot configuration along with relevant measurements are shown in Figure 6.1 and Table 6.1.

Table 6.1: Reactive projectile dimensions.

OD	1.27254	cm
ID	0.9525	cm
Wall Thickness	0.16002	cm
Height	2.06883	cm
Base Height	0.47625	cm
Base OD	1.27762	cm
Material Density	2.8	$\frac{\text{g}}{\text{cm}^3}$
Total Height	2.55	cm

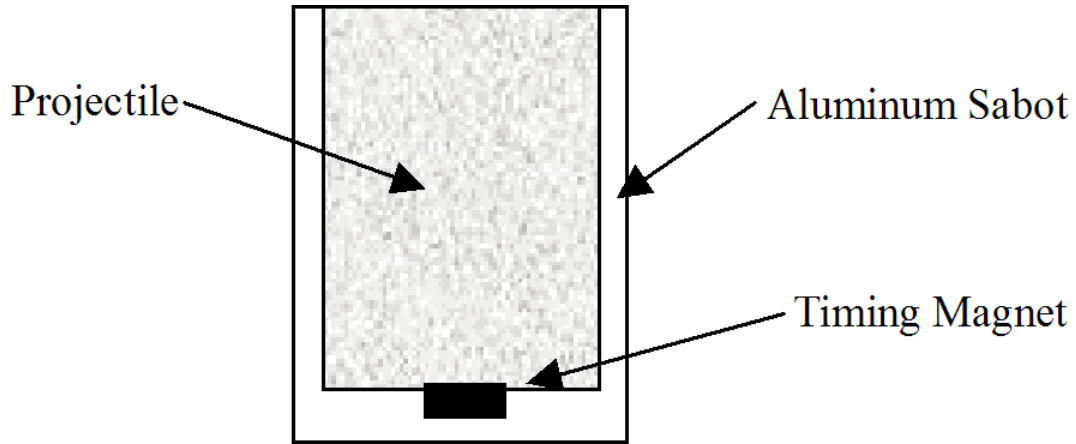


Figure 6.1: Projectile configuration.

The target box was 30.48 x 30.48 x 30.48 cm and consisted of an entrance and exit plate made of 0.3175 cm thick aluminum. Within each box was an array of three 0.1588 cm thick aluminum plates. The internal plates were connected together by four 0.9525 cm threaded rods with nuts holding the plates in position along the rods. The internal plate assembly was placed inside, but not attached to the external box. Lengths of threaded rod extending from the set of internal plates, in front and in back, kept the inner plates in position, in the box. The external plates of the box were tied together with three aluminum L-angles along each edge of the box. The L-angles were all attached to the interior of the box except for one of the side plates which was to be removable and attached with external L-angles. Three pressure and one temperature sensors were placed on the removable wall. A schematic showing the location of the sensors in relation to the plates and projectile path is shown in Figure 6.2. A photo of the target box is shown in Figure 6.3. The box was placed with the back of the box against a large steel I-beam to prevent it from flying away. Consequently, any damage done to the back of the box is not particularly interesting. The projectile was fired at the front plate of the box with an initial velocity of 3134 $\frac{\text{m}}{\text{s}}$.

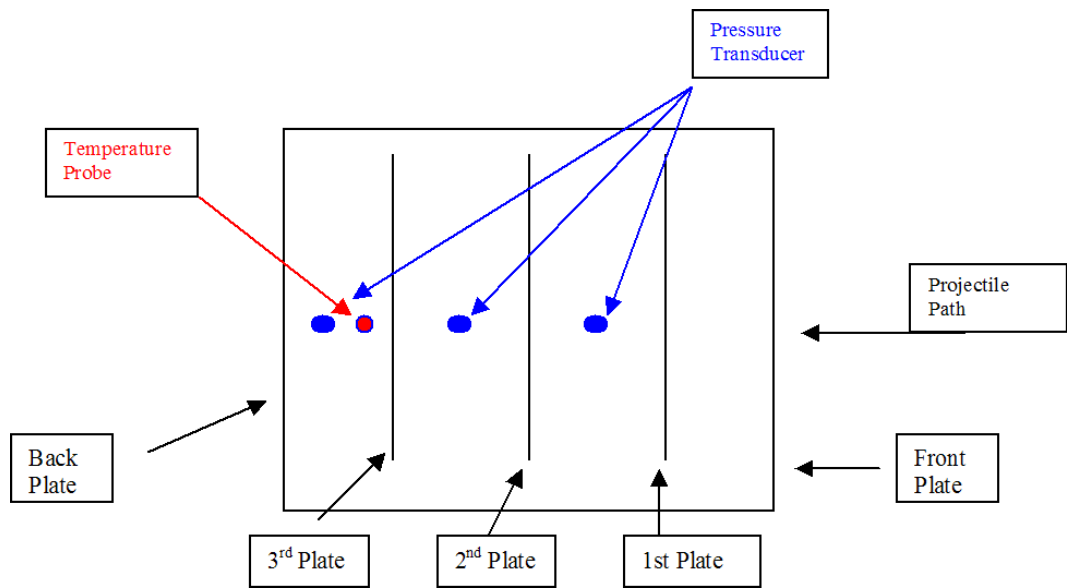


Figure 6.2: Box schematic.

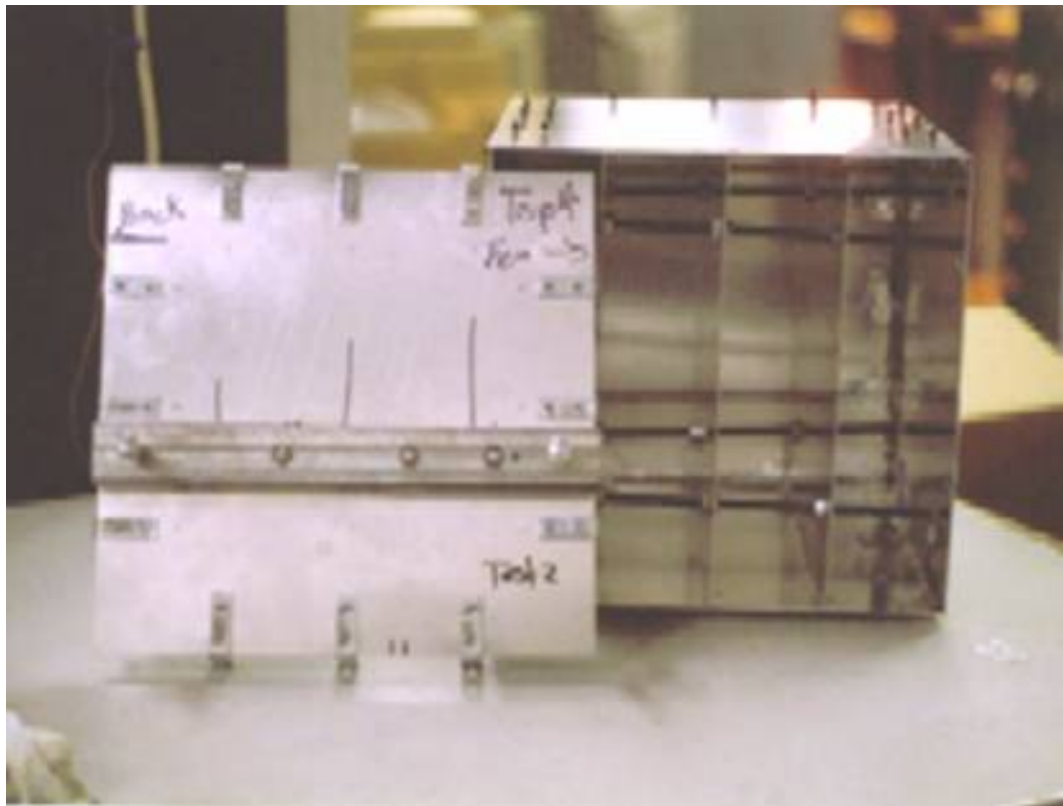


Figure 6.3: Box containing enclosed spaced plate array.

6.1 Simulation of a Reactive Projectile

vs. a Box

The box test simulation consists of both Euler and Lagrangian parts. The reactive material exists in the Euler domain while the sabot, box, plates, and rods are Lagrangian. Figure 6.4 shows the outside of the airmesh. The airmesh is the size of the box with a little extra space outside of the box to allow for the starting position of the projectile. The airmesh, reactive material mesh, plate, and sabot meshes are relatively well matched along the shot line to maximize the effectiveness of the Euler-Lagrange penalty coupling implemented with the *CONSTRAINED LAGRANGE IN SOLID record. A full view of the Lagrangian materials, the plates, threaded rods, and sabot, are shown in Figure 6.5. As is shown, the walls of the box were not modeled because of their distance from the shotline and the length of the simulation that would be required for them to play a significant role. In the actual testing, discussed in more detail in the next section, pressures were measured at the wall of the box and peak pressure didn't occur until approximately 0.012 seconds or 12,000 μs . This simulation was run over a period of approximately two weeks of constant run time for a total of approximately 500 μs . All of the plate meshes are the same with the exception of the front and back wall of the box which were thicker and slightly wider and taller, about two rows of elements, as per the original dimensions of the box. A close view of the mesh of the front plate is shown in Figure 6.6. As previously discussed, the projectile consists of some reactive material encased in an aluminum sabot. A picture of the reactive material portion of the airmesh and the sabot are shown in Figure 6.7. The reactive material mesh, and the airmesh in general, match up with the mesh of the plates. The mesh of the sabot is slightly smaller to accurately model the thin walls of the sabot. Figure 6.9 shows the full mesh of the reactive material. It is worth noting again that the reactive material is modeled in the Euler domain, so the elements

6.1. SIMULATION OF A REACTIVE PROJECTILE VS. A BOX

shown are merely the elements in which the reactive material initially resides. In the next time step the sabot (Lagrangian elements) will move forward while the reactive material will move to the next set of Euler elements along the shotline.

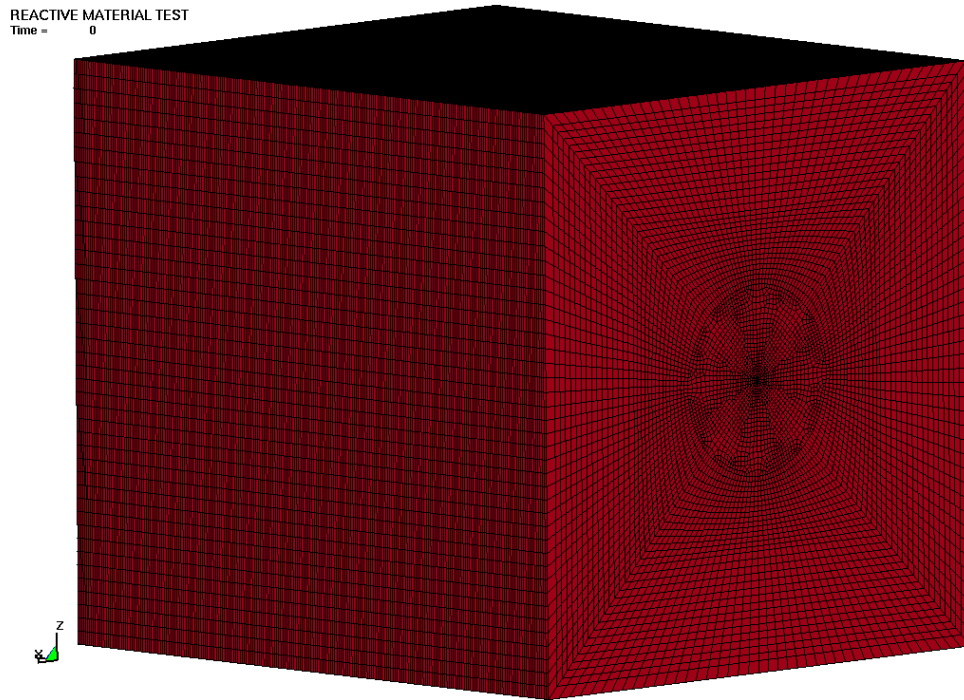


Figure 6.4: Airmesh used in the simulation of the box test.

6.1. SIMULATION OF A REACTIVE PROJECTILE VS. A BOX

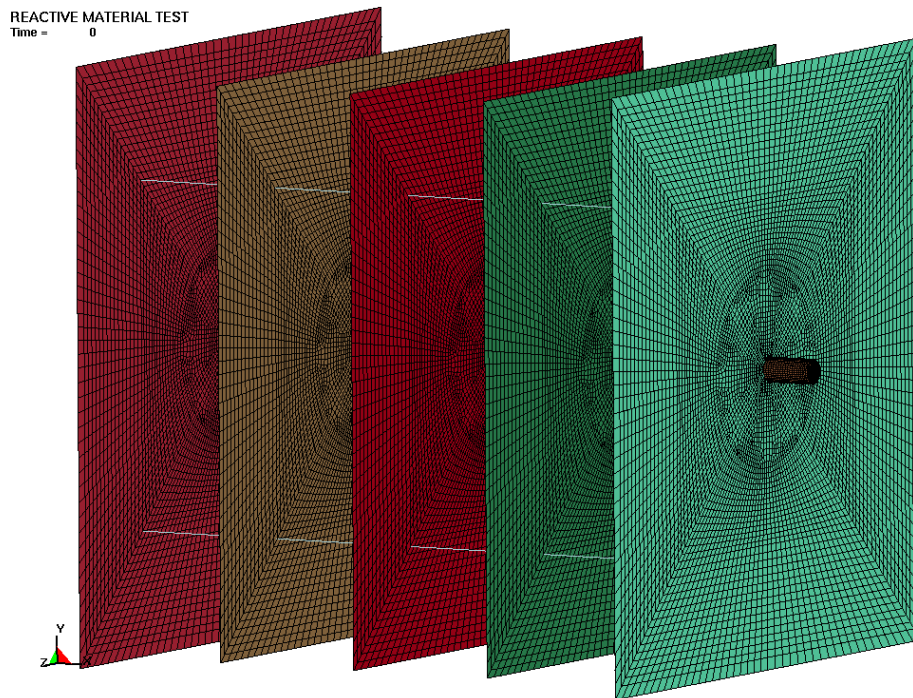


Figure 6.5: Plates and sabot used in the simulation of the box test.

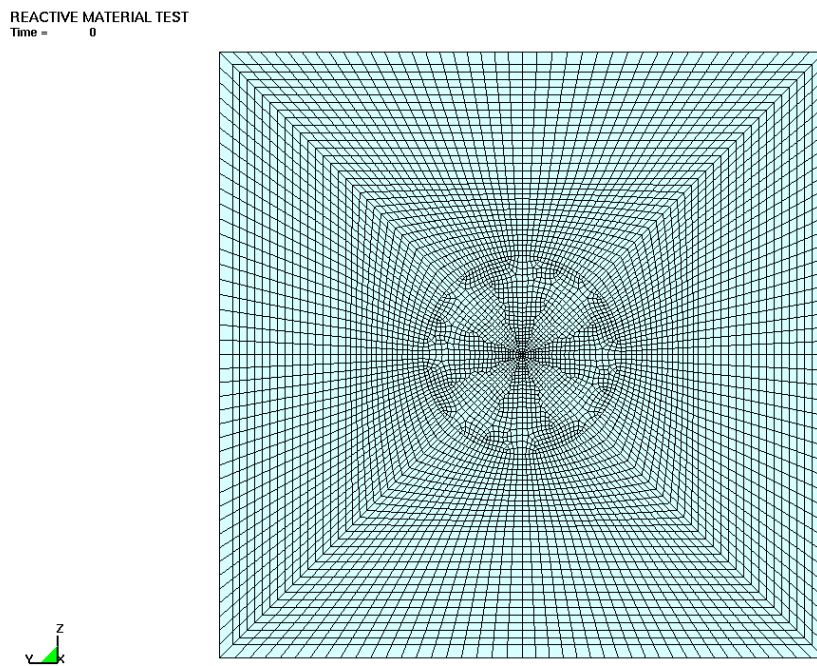


Figure 6.6: Plate mesh used in the simulation of the box test.

6.1. SIMULATION OF A REACTIVE PROJECTILE VS. A BOX

REACTIVE MATERIAL TEST
Time = 0

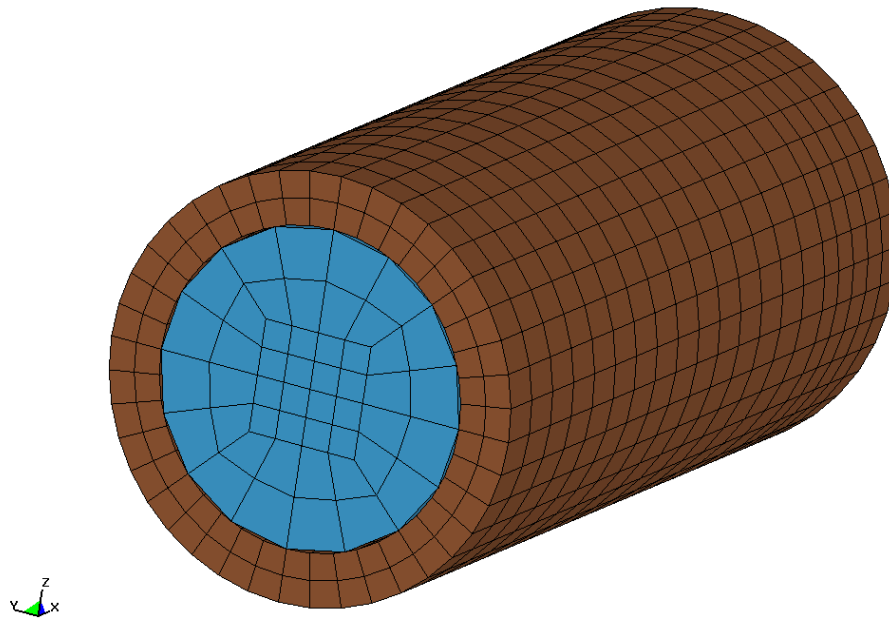


Figure 6.7: Projectile with reactive material used in the simulation of the box test.

REACTIVE MATERIAL TEST
Time = 0

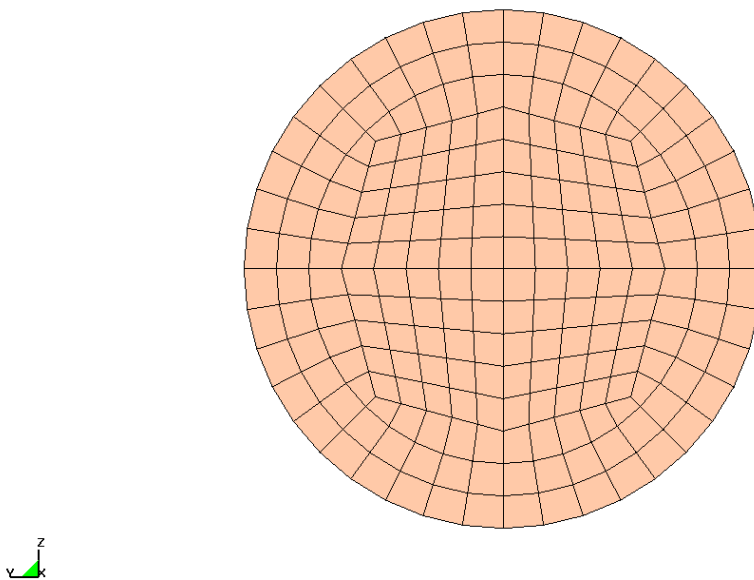


Figure 6.8: End view of the projectile sabot mesh.

6.1. SIMULATION OF A REACTIVE PROJECTILE
VS. A BOX

REACTIVE MATERIAL TEST
Time = 0

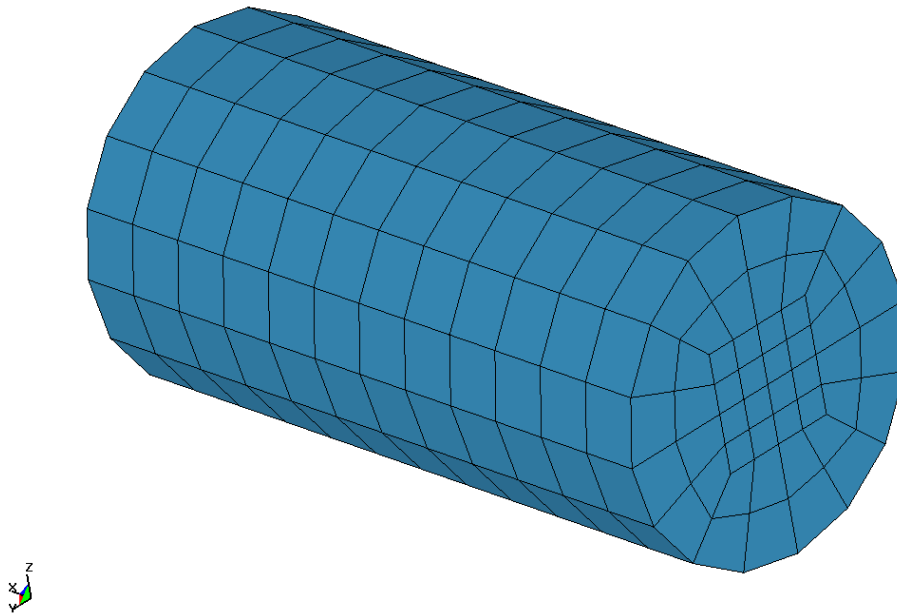


Figure 6.9: Eulerian mesh containing the reactive material at time = $0.0 \mu\text{s}$.

6.1. SIMULATION OF A REACTIVE PROJECTILE VS. A BOX

The Following pictures 6.10 through 6.20 show the Lagrangian materials of the box test. The Euler materials, like the reactive material or vacuum, are not shown so that the petaling of the walls and the disintegration of the sabot can clearly be seen. In the simulation the resulting damage to the plates, in terms of the measured area removed from the plate, was as follows: the front plate lost 1.622 cm², the first plate lost 74 cm², the second plate lost 380 cm², the third plate had yet to be damaged at the end of the current simulation. It appears that the damage to the third plate will not be related, like the previous plates, to the kinetic energy of the projectile so much as the ultimate overpressurization of the part of the box in front of the third plate, which will ultimately result in the failure of the third plate as the gasses attempt to fill the vacuum on the other side of the plate.

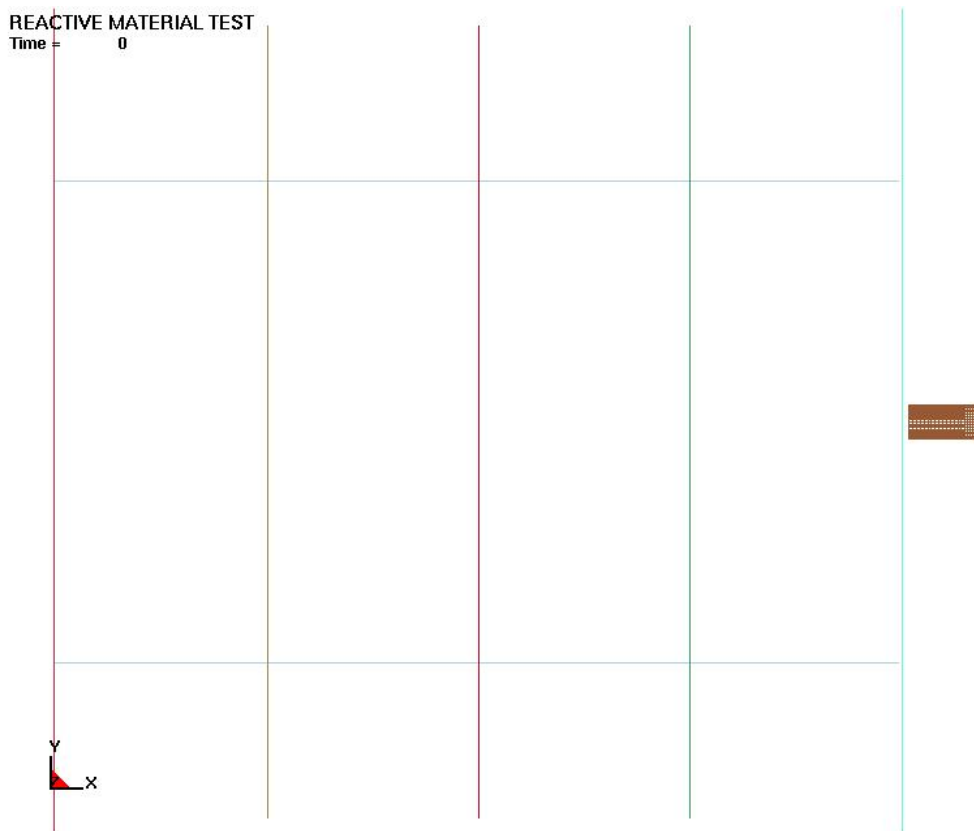


Figure 6.10: Box test, with no reactive material shown, at time = 0.0 μs .

6.1. SIMULATION OF A REACTIVE PROJECTILE
VS. A BOX



Figure 6.11: Box test, with no reactive material shown, at time = 25.0 μ s.

6.1. SIMULATION OF A REACTIVE PROJECTILE
VS. A BOX

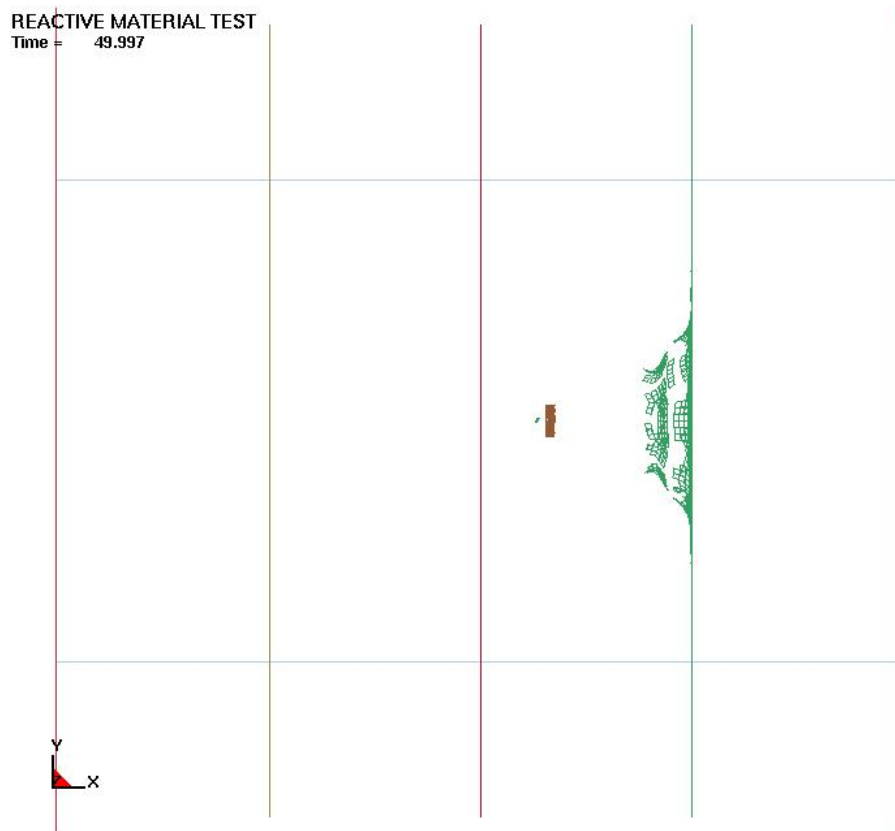


Figure 6.12: Box test, with no reactive material shown, at time = 49.997 μ s.

6.1. SIMULATION OF A REACTIVE PROJECTILE
VS. A BOX

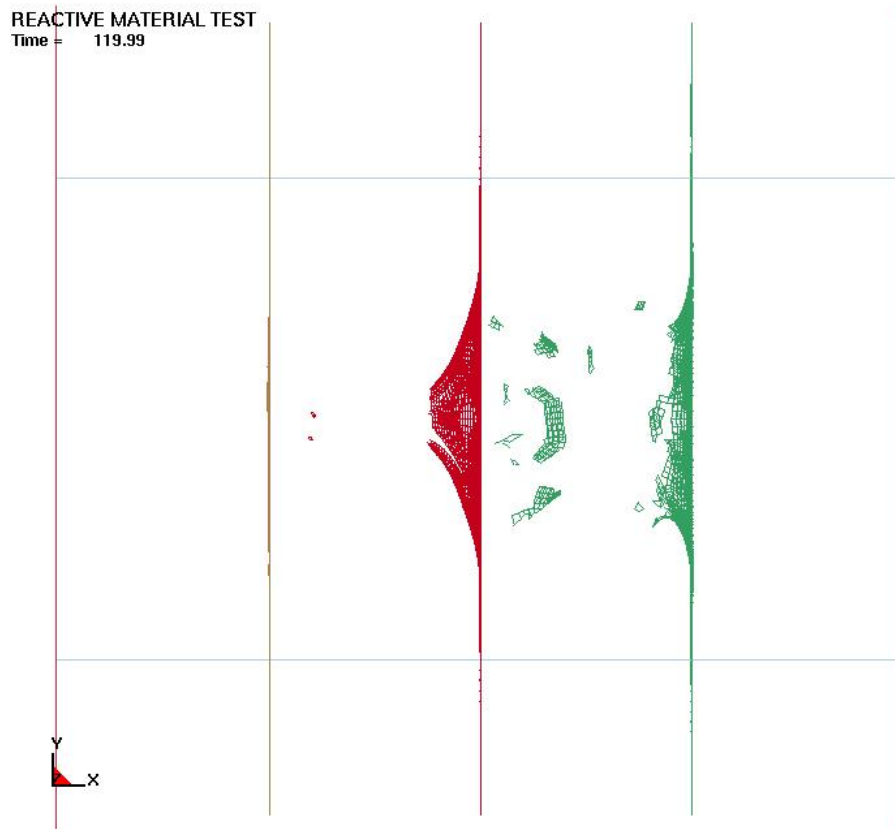


Figure 6.13: Box test, with no reactive material shown, at time = 119.99 μ s.

6.1. SIMULATION OF A REACTIVE PROJECTILE
VS. A BOX

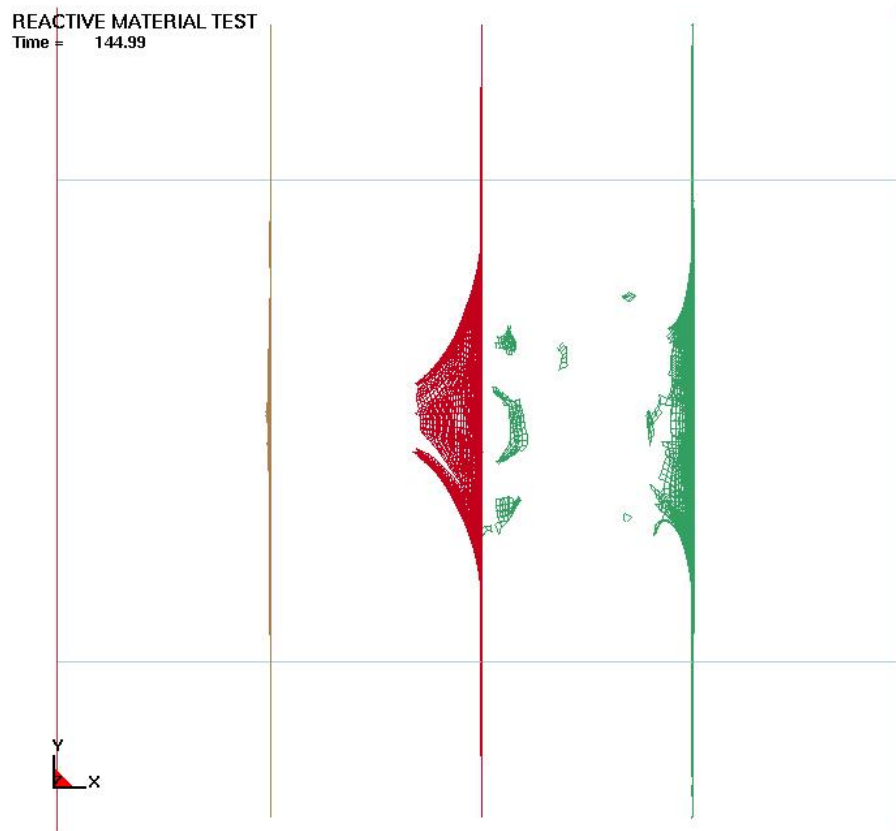


Figure 6.14: Box test, with no reactive material shown, at time = 149.99 μ s.

6.1. SIMULATION OF A REACTIVE PROJECTILE
VS. A BOX

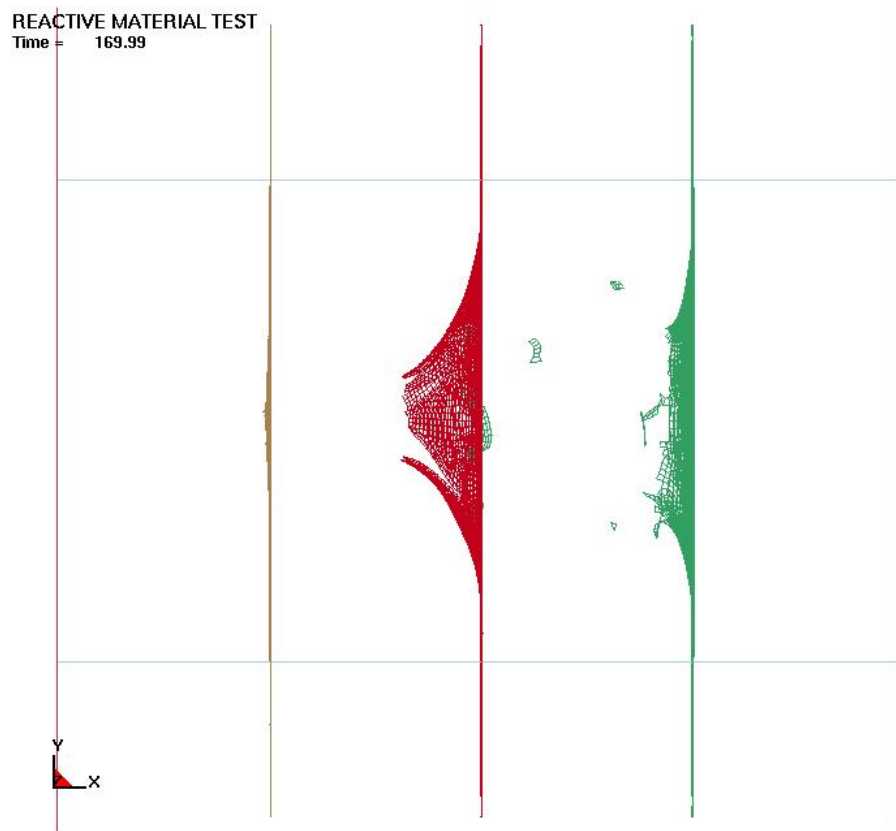


Figure 6.15: Box test, with no reactive material shown, at time = 169.99 μs .

6.1. SIMULATION OF A REACTIVE PROJECTILE
VS. A BOX

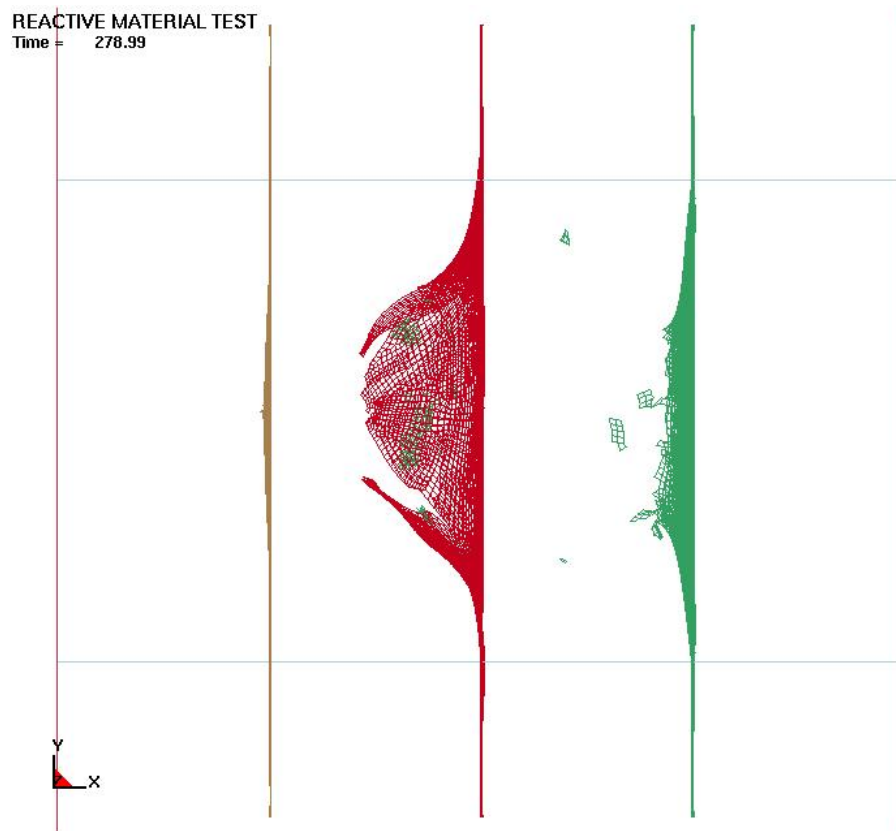


Figure 6.16: Box test, with no reactive material shown, at time = 278.99 μ s.

6.1. SIMULATION OF A REACTIVE PROJECTILE
VS. A BOX

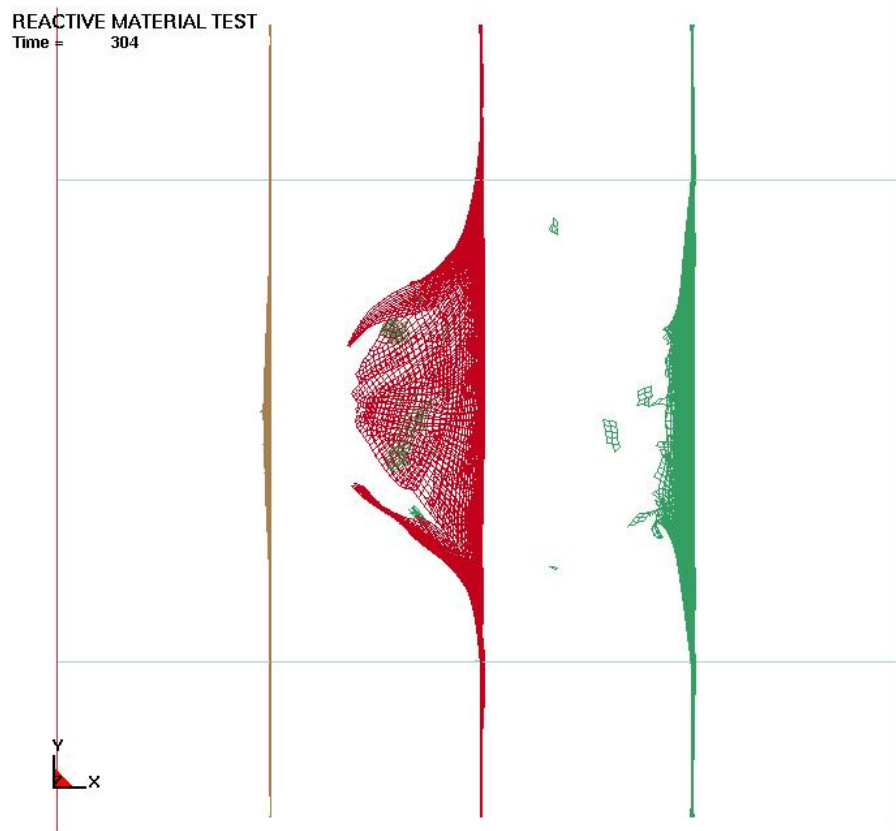


Figure 6.17: Box test, with no reactive material shown, at time = 304.0 μ s.

6.1. SIMULATION OF A REACTIVE PROJECTILE
VS. A BOX

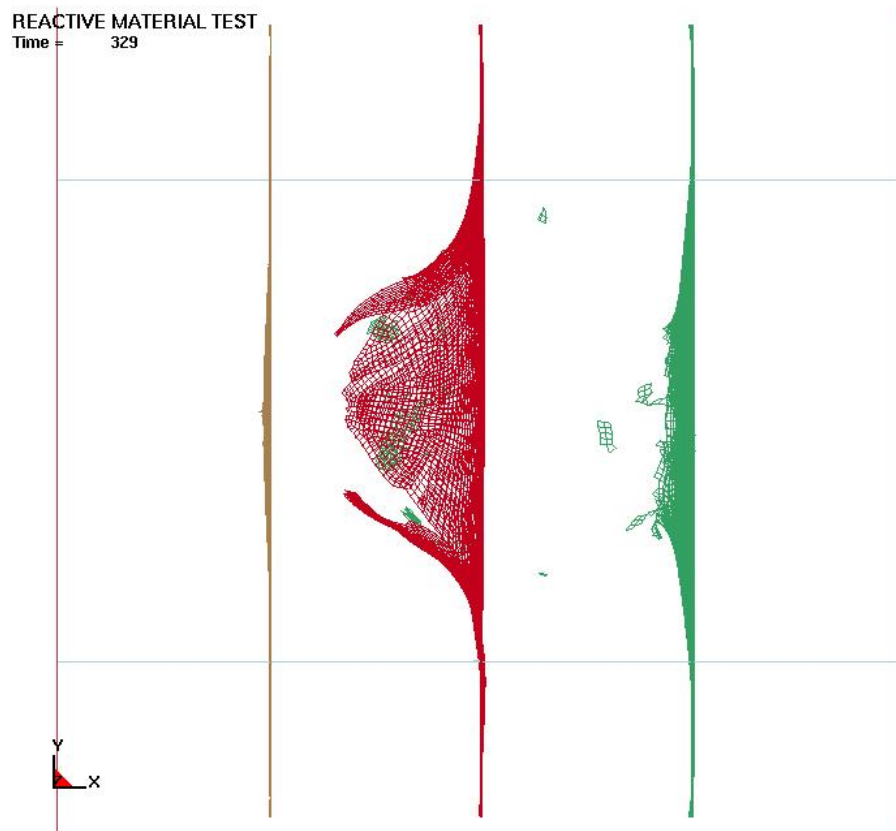


Figure 6.18: Box test, with no reactive material shown, at time = 329.0 μs .

6.1. SIMULATION OF A REACTIVE PROJECTILE
VS. A BOX

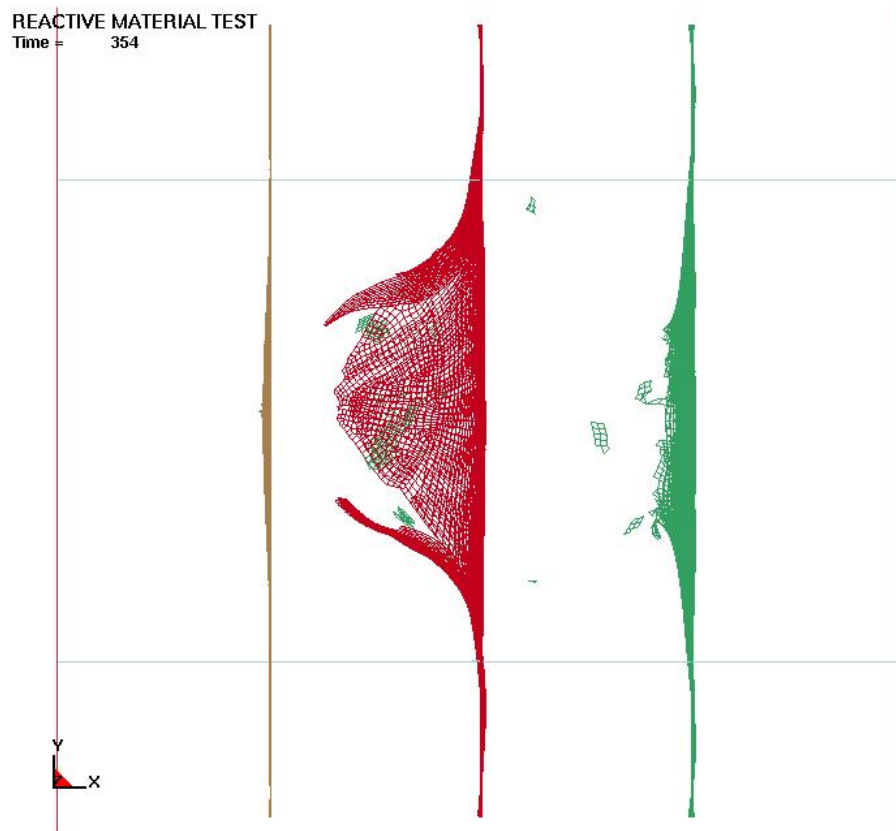


Figure 6.19: Box test, with no reactive material shown, at time = 354.0 μ s.

6.1. SIMULATION OF A REACTIVE PROJECTILE
VS. A BOX

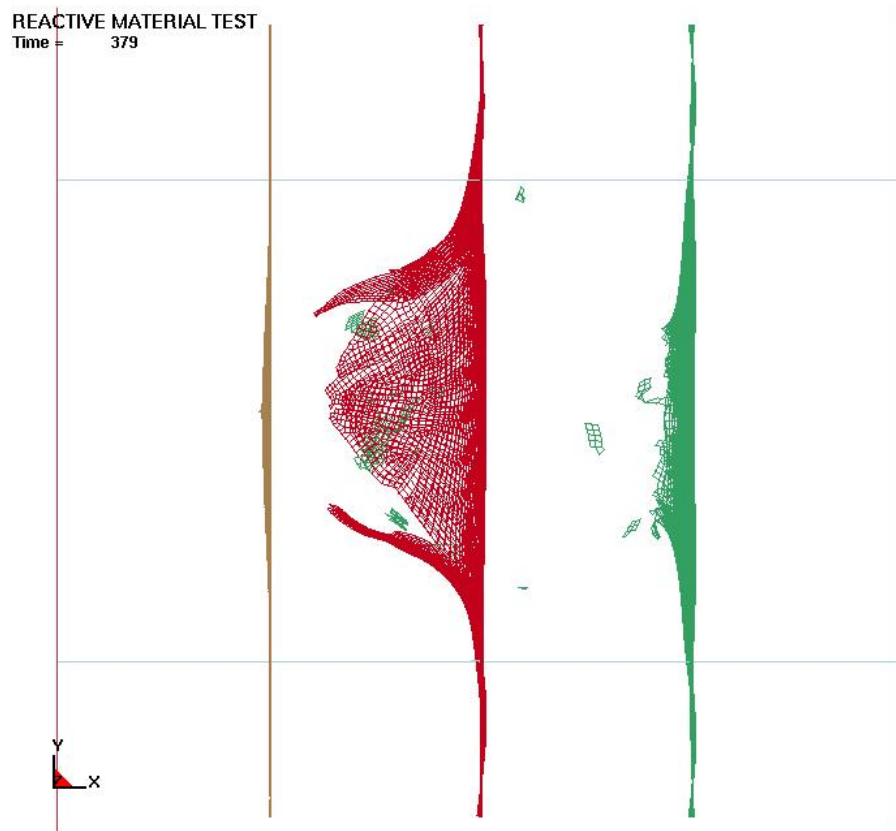


Figure 6.20: Box test, with no reactive material shown, at time = 379.0 μ s.

6.1. SIMULATION OF A REACTIVE PROJECTILE VS. A BOX

Finally pictures 6.21 through 6.31 show the same time sequence as the previous pictures, 6.10 through 6.20, but with the reactive material depicted. The reactive material was plotted using Ls-prepost's fluid display mode capability.

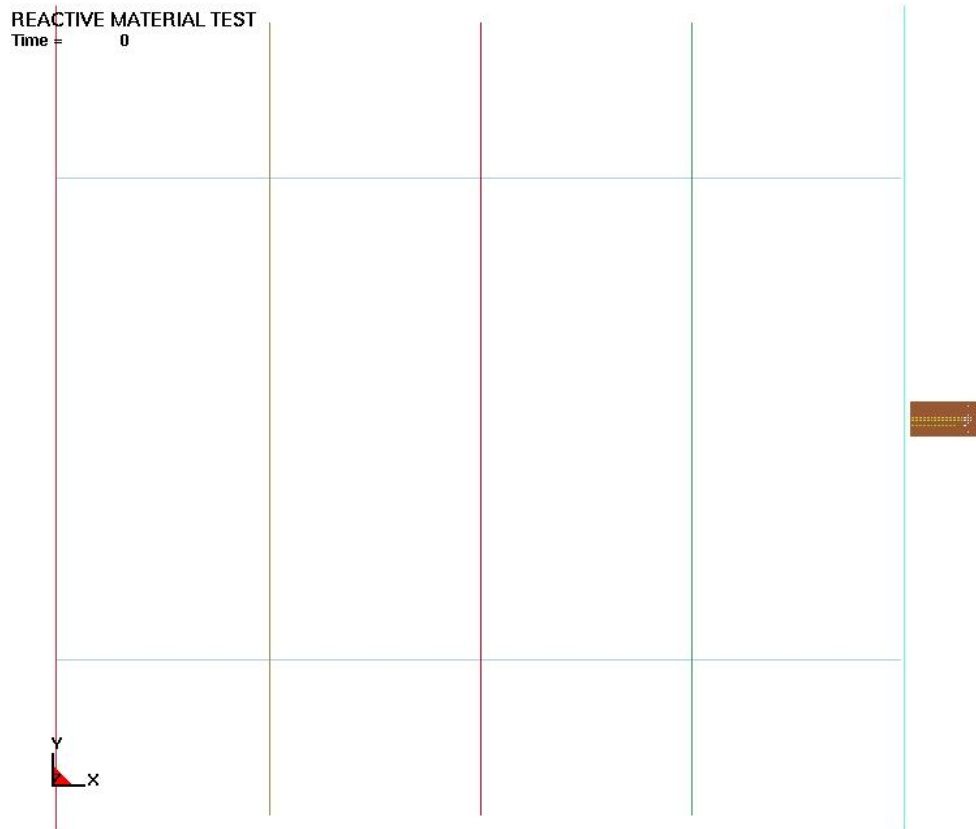


Figure 6.21: Box test, with reactive material shown, at time = 0.0 μ s.

6.1. SIMULATION OF A REACTIVE PROJECTILE
VS. A BOX



Figure 6.22: Box test, with reactive material shown, at time = 25.0 μ s.

6.1. SIMULATION OF A REACTIVE PROJECTILE
VS. A BOX

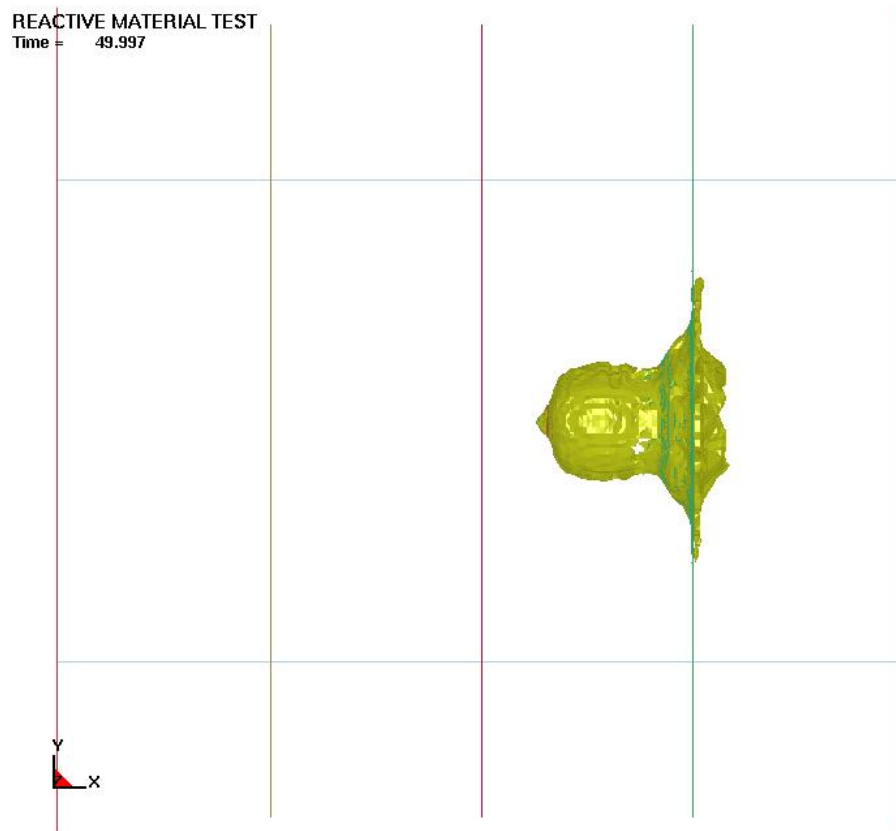


Figure 6.23: Box test, with reactive material shown, at time = 49.997 μs .

6.1. SIMULATION OF A REACTIVE PROJECTILE
VS. A BOX

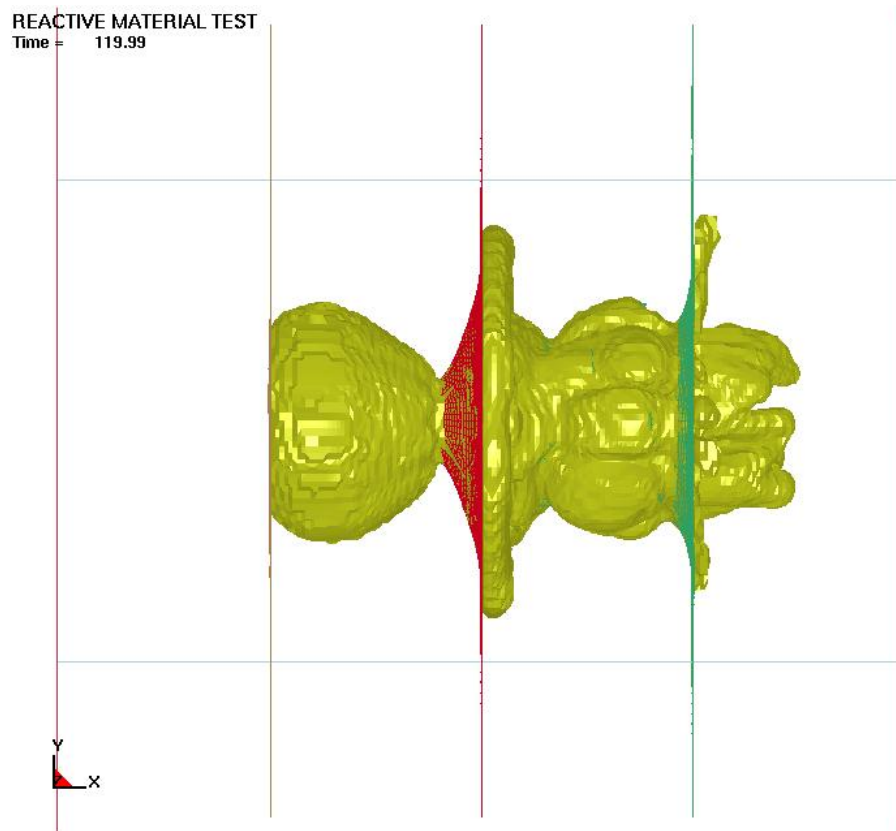


Figure 6.24: Box test, with reactive material shown, at time = 119.99 μs .

6.1. SIMULATION OF A REACTIVE PROJECTILE
VS. A BOX

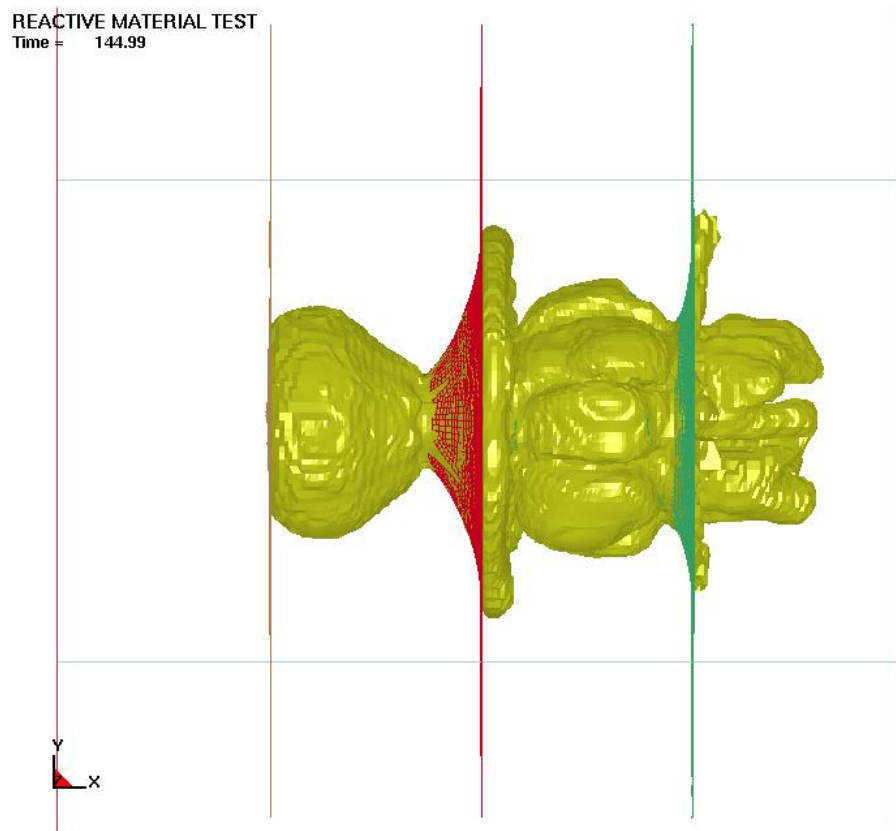


Figure 6.25: Box test, with reactive material shown, at time = 149.99 μ s.

6.1. SIMULATION OF A REACTIVE PROJECTILE
VS. A BOX

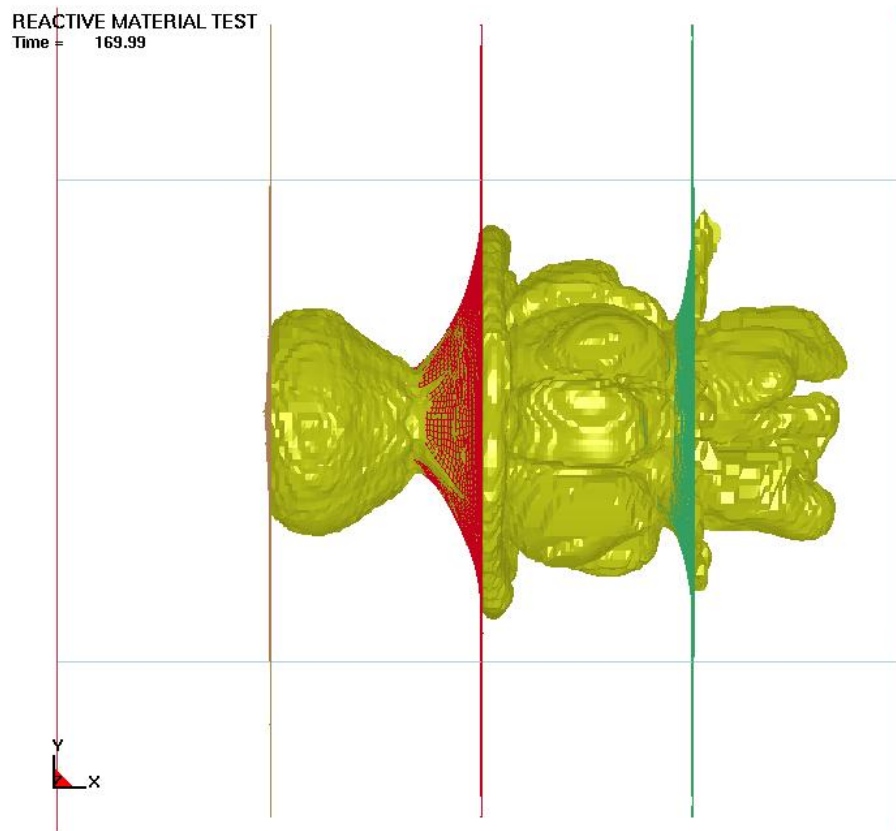


Figure 6.26: Box test, with reactive material shown, at time = 169.99 μ s.

6.1. SIMULATION OF A REACTIVE PROJECTILE
VS. A BOX

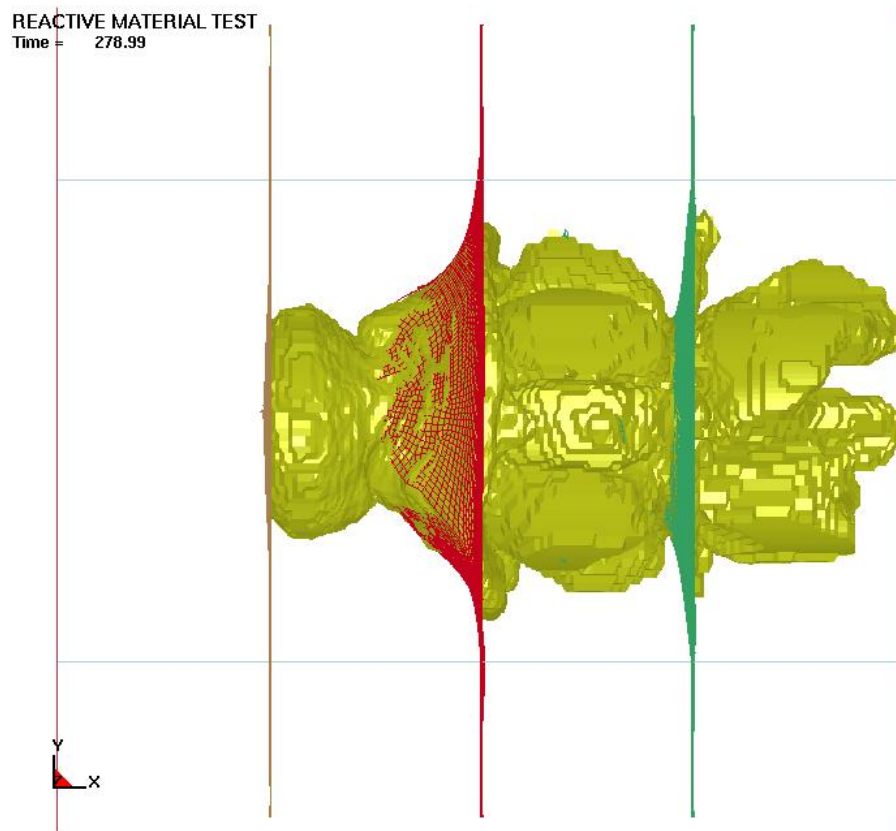


Figure 6.27: Box test, with reactive material shown, at time = 278.99 μs .

6.1. SIMULATION OF A REACTIVE PROJECTILE
VS. A BOX

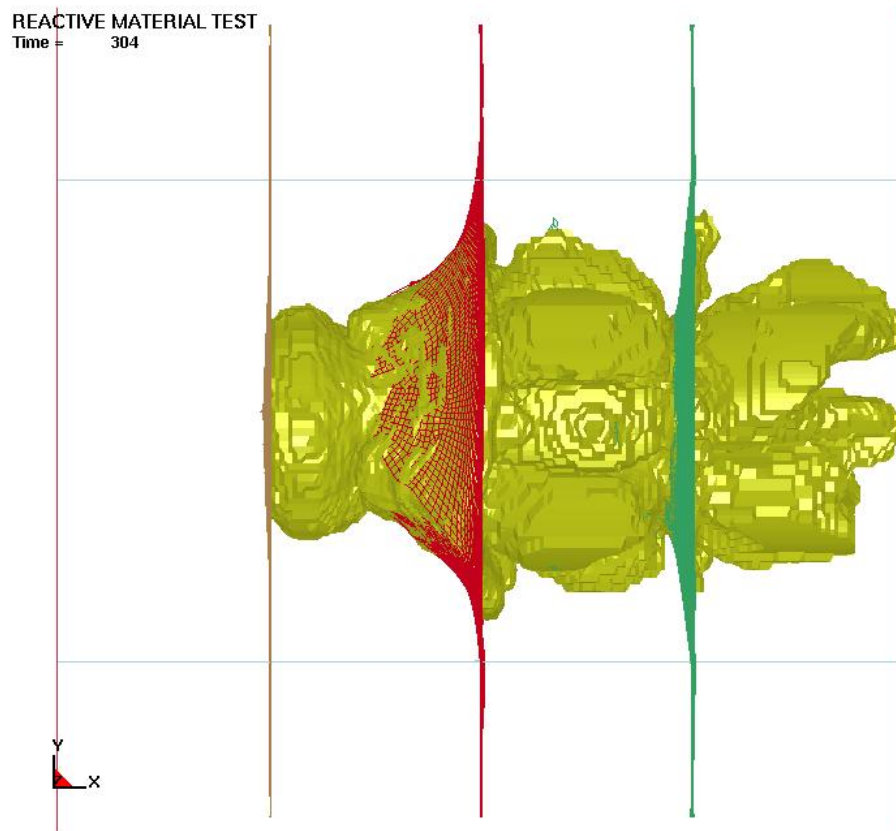


Figure 6.28: Box test, with reactive material shown, at time = 304.0 μ s.

6.1. SIMULATION OF A REACTIVE PROJECTILE
VS. A BOX

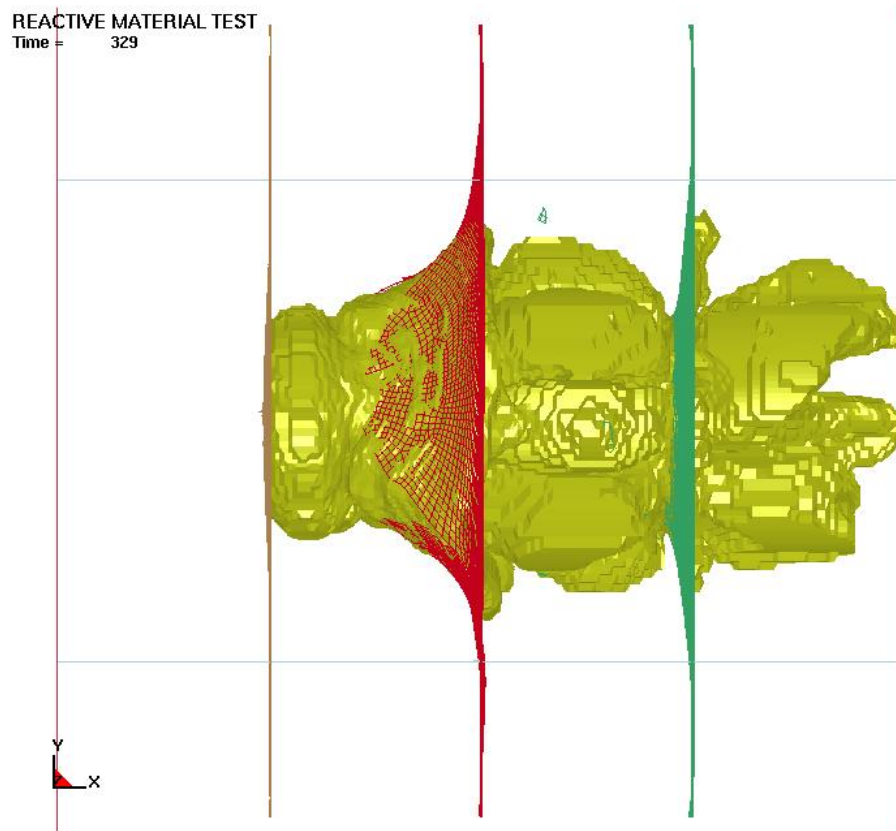


Figure 6.29: Box test, with reactive material shown, at time = 329.0 μ s.

6.1. SIMULATION OF A REACTIVE PROJECTILE
VS. A BOX

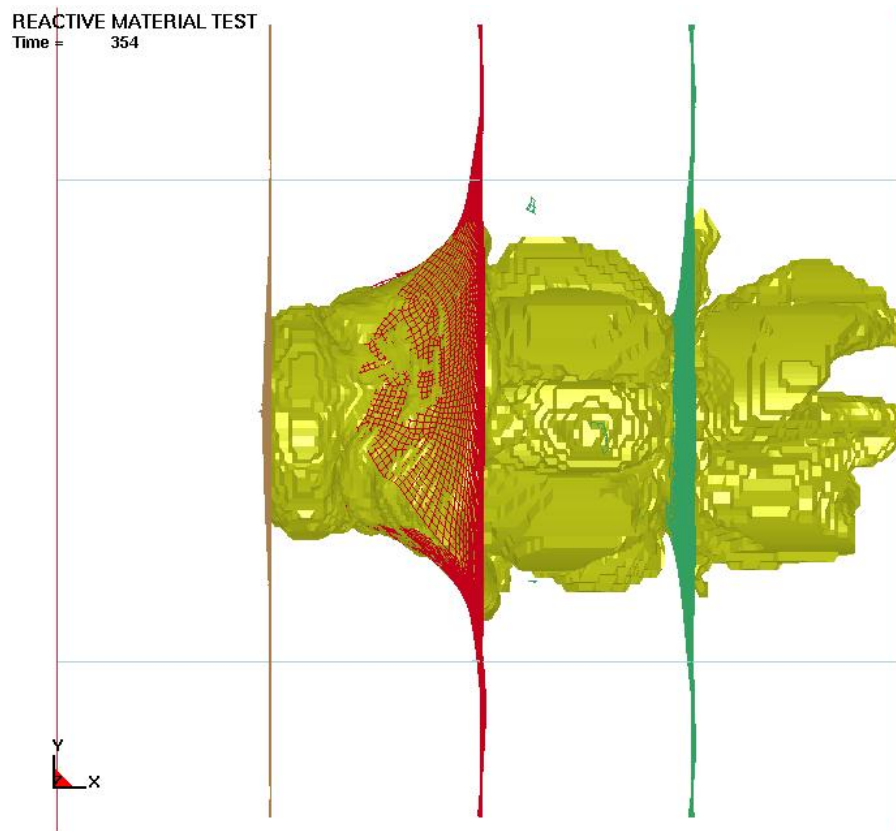


Figure 6.30: Box test, with reactive material shown, at time = 354.0 μ s.

6.1. SIMULATION OF A REACTIVE PROJECTILE
VS. A BOX

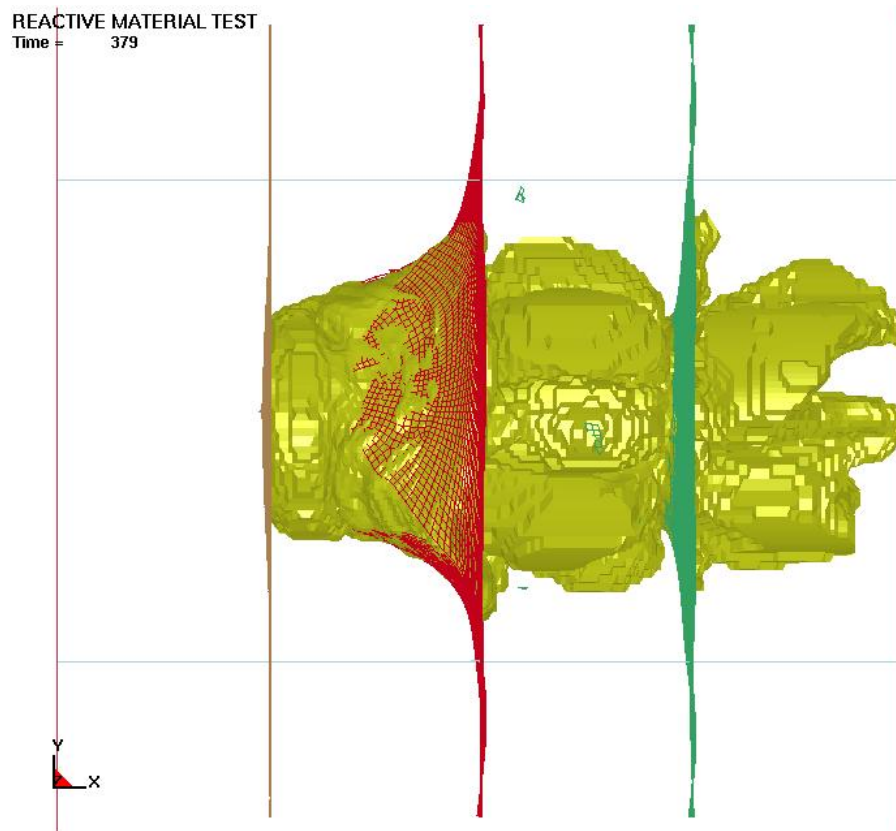


Figure 6.31: Box test, with reactive material shown, at time = 379.0 μ s.

6.2 Test Results of a Reactive Projectile

Impacting a Box

In the test the resulting damage to the plates, in terms of the measured area removed from the plate, was as follows: the front plate lost 2.52 cm², the first plate lost 76.13 cm², the second plate lost 366.26 cm², the third plate lost 451.61 cm². The damage to the back plate is not mentioned here because it was supported by a large I-beam, as mentioned previously. Figures 6.32 through 6.37 show pictures of the box after the test.

6.2. TEST RESULTS OF A REACTIVE PROJECTILE
IMPACTING A BOX



Figure 6.32: The front plate of the box.

6.2. TEST RESULTS OF A REACTIVE PROJECTILE
IMPACTING A BOX

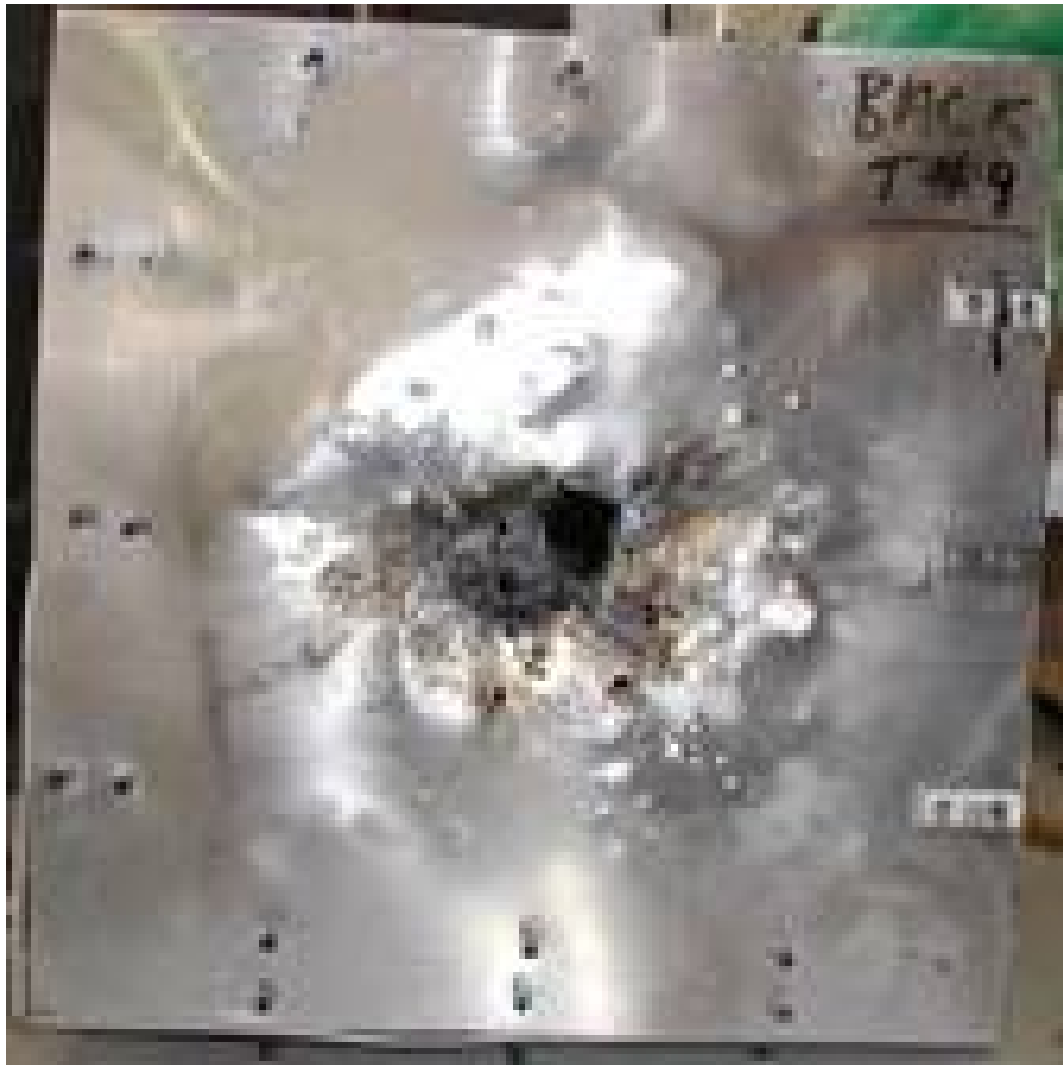


Figure 6.33: The back plate of the box.

6.2. TEST RESULTS OF A REACTIVE PROJECTILE
IMPACTING A BOX



Figure 6.34: The plate array inside the box.

6.2. TEST RESULTS OF A REACTIVE PROJECTILE
IMPACTING A BOX



Figure 6.35: The front of the first plate in the box.

6.2. TEST RESULTS OF A REACTIVE PROJECTILE
IMPACTING A BOX



Figure 6.36: The back of the third plate in the box.

6.2. TEST RESULTS OF A REACTIVE PROJECTILE
IMPACTING A BOX



Figure 6.37: Side view of the plate array inside the box.

Conclusions

Using the methodology developed in Chapter 2 and the ReactMat software developed as a part of this work and described in Chapter 3, an equation of state for an aluminum-PTFE mixture was created. This equation of state was used successfully to simulate characterization tests (Chapters 4 and 5) that could be used to validate the developed equation of state. The equation of state was also demonstrated in Chapter 6, where it was placed in a realistic projectile-target scenario. In this scenario the area removed from the first three plates is comparable to the damage achieved in the test presented. Damage to the fourth plate, like the side walls of the box appears to be damage that resulted from the box filling with reacted gas and exploding into the remaining vacuum areas of the target. Note that the third plate is nearly torn in half and the whole-plate bending seen in the simulation.

As a result of this project, a working methodology for the development of reactive material equations of state and software, ReactMat, to carry out this methodology were successfully developed. These equations of state can be used in conjunction with LS-DYNA to generate realistic performance data for a theoretical projectile made with the reactive material. With a sufficient database of realistic performance data for various reactive material mixtures, it will be possible to create a parametric model that could allow the development of even more effective reactive munitions.

In the future, additional work needs to be done to fully realize the end goal of a

parametric tool. On the validation side of this effort, additional work on the characterization test process to successfully collect material data and provide a real world check on the material properties used in the generation of the realistic performance data. Additionally, realistic tests need to be conceived that capture the desirable performance characteristics of a reactive munition or class of munitions. New reactive mixtures of interest could then be characterized analytically, validated using the characterization tests, and then run through the performance tests. Once sufficient performance data has been gathered on a variety of mixtures, the performance of mixtures with different constituent percentages could be extrapolated from the database in the search for a reactive material with the performance characteristics desired.

Unreacted Characterization Model

The following is the unreacted material characterization LS-DYNA model. The geometry has been excluded due to extreme length.

```
*KEYWORD
*TITLE
$# title
Unreacted Material Test
*CONTROL_ALE
$#   dct      nadv      meth      afac      bfac      cfac      dfac      efac
      3        1        3 -1.000000
$#   start      end      aafac      vfact      prit      ebc      pref      nsidebc
      0.0001.0000E+20  1.000000  1.0000E-6
*CONTROL_BULK_VISCOSITY
$#   q1      q2      type
      1.500000  0.060000
*CONTROL_ENERGY
$#   hgen      rwen      slnten      rylen
      2
*CONTROL_HOURLASS
$#   ihq      qh
      1  0.150000
*CONTROL_OUTPUT
$#   npopt      neecho      nrefup      iaccop      opifs      iprint      ikedit      iflush
      0        0        0        0        0.000      0        200      5000
$#   iprtf
      0
*CONTROL_PARALLEL
$#   ncpu      numrhs      const      para
      2        0        2
*CONTROL_TERMINATION
$#   endtim      endcyc      dtmin      endeng      endmas
      2.000000
*CONTROL_TIMESTEP
$#   dtinit      tssfacc      isdo      tslimt      dt2ms      lctm      erode      ms1st
      0.000  0.600000
$#   dt2msf      dt2mslc      imsc1
      0.000      0        0
*DATABASE_MATSUM
```

```

$#      dt      binary
      0.001000      1
*DATABASE_BINARY_D3DUMP
$# dt/cycl not used not used not used
      50      3
*DATABASE_BINARY_D3PLOT
$#      dt      lcdt      beam      npltc
      0.010000
$#  ioopt
      0
*DATABASE_EXTENT_BINARY
$#  neiph      neips      maxint      strflg      sigflg      epsflg      rltflg      engflg
      9
$#  cmpflg      ieverp      beamip      dcomp      shge      stssz      n3thdt      ialemat
      0      0      0      0      0      0      2
$#  nintsld      pkp_sen      sclp      null      msscl      therm
      0      0      0.000      0      0      0
*PART
$# title
Hammer
$#  pid      secid      mid      eosid      hgid      grav      adpopt      tmid
      9      3      2      2
*SECTION_SOLID
$#  secid      elform      aet
      3      11
*MAT_ELASTIC_PLASTIC_HYDRO_TITLE
Copper
$#  mid      ro      g      sigy      eh      pc      fs
      2      8.930000      0.447000      0.003590      0.000      0.000      1.000000
$#  eps1      eps2      eps3      eps4      eps5      eps6      eps7      eps8
      0.000      0.000      0.000      0.000      0.000      0.000      0.000      0.000
$#  eps9      eps10      eps11      eps12      eps13      eps14      eps15      eps16
      0.000      0.000      0.000      0.000      0.000      0.000      0.000      0.000
$#  es1      es2      es3      es4      es5      es6      es7      es8
      0.000      0.000      0.000      0.000      0.000      0.000      0.000      0.000
$#  es9      es10      es11      es12      es13      es14      es15      es16
      0.000      0.000      0.000      0.000      0.000      0.000      0.000      0.000
*EOS_GRUNEISEN_TITLE
Copper
$#  eosid      c      s1      s2      s3      gamao      a      e0
      2      0.394000      1.489000      0.000      0.000      1.990000
$#  v0
      1.000000
*PART
$# title
Air
$#  pid      secid      mid      eosid      hgid      grav      adpopt      tmid
      10      3      1
*MAT_VACUUM_TITLE
Vacuum
$#  mid      den
      1      1.3910E-6
*PART
$# title

```

```

Reactive Material
$#   pid   secid   mid   eosid   hgid   grav   adpopt   tmid
      11     3     3     3
*MAT_ELASTIC_PLASTIC_HYDRO_TITLE
Teflon-Aluminum
$#   mid   ro   g   sigy   eh   pc   fs
      3 2.391000 0.002089 1.1600E-4
$#   eps1   eps2   eps3   eps4   eps5   eps6   eps7   eps8
      0.000 0.000 0.000 0.000 0.000 0.000 0.000 0.000
$#   eps9   eps10  eps11  eps12  eps13  eps14  eps15  eps16
      0.000 0.000 0.000 0.000 0.000 0.000 0.000 0.000
$#   es1    es2    es3    es4    es5    es6    es7    es8
      0.000 0.000 0.000 0.000 0.000 0.000 0.000 0.000
$#   es9    es10   es11   es12   es13   es14   es15   es16
      0.000 0.000 0.000 0.000 0.000 0.000 0.000 0.000
*EOS_IGNITION_AND_GROWTH_OF_REACTION_IN_HE_TITLE
Teflon-Aluminum
$#   eosid   a   b   xp1   xp2   frer   g   r1
      3 4.7355E+5 30.620300 50.466801 4.927370 1.727100 4.5754E-6 2.293712
$#   r2     r3     r5     r6   fmxig   freq   grow1   em
      2.009256 7.7099E-5 45.292294 51.545380 0.000 11224.000 5.4521E+9 16.735001
$#   ar1    es1    cvp    cvr   eetal   ccrit   enq   tmp0
      0.000 1.002900 1.4570E-5 9.9300E-6 28.399000 1.0000E-6 0.013500
$#   grow2   ar2    es2    en   fmxgr   fmngr
      8.5990E+13 6.3067E-5 1.000200 26.962999
*INITIAL_VELOCITY_GENERATION
$#nsid/pid   styp   omega   vx   vy   vz
      9     2     0.000 0.000 0.000 -0.100000
$#   xc     yc     zc     nx   ny   nz   phase
      0.000 0.000 0.000 0.000 0.000 0.000 0
*DEFINE_CURVE_TITLE
init_vel_curve
$#   lcid   sidr   sfa   sfo   offa   offo   dattyp
      5     0   1.000000 1.0000E-4
$#   a1     o1
      0.000 1.00000000
      0.10000000 1.00000000
      400.00000000 1.00000000
*ALE_MULTI-MATERIAL_GROUP
$#   sid   idtype
      9     1
$#   sid   idtype
      10    1
$#   sid   idtype
      11    1
*END

```

Reacted Characterization Model

The following is the reacted material characterization LS-DYNA model. The geometry has been excluded due to extreme length.

```
*KEYWORD
*TITLE
$# title
Reactive Material Test
*CONTROL_ALE
$#   dct      nadv      meth      afac      bfac      cfac      dfac      efac
      3         1         2 -1.000000
$#   start      end      aafac      vfact      prit      ebc      pref      nsidebc
      0.0001.0000E+20  1.000000  1.0000E-6
*CONTROL_BULK_VISCOSITY
$#   q1      q2      type
      1.500000  0.060000
*CONTROL_ENERGY
$#   hgen      rwen      slnten      rylen
      2
*CONTROL_HOURLASS
$#   ihq      qh
      1  0.150000
*CONTROL_MPP_DECOMPOSITION_AUTOMATIC
*CONTROL_OUTPUT
$#   npopt      neecho      nrefup      iaccop      opifs      iprint      ikedit      iflush
      0         0         0         0         0.000      0         200      5000
$#   iprtf
      0
*CONTROL_PARALLEL
$#   ncpu      numrhs      const      para
      2         0         2
*CONTROL_TERMINATION
$#   endtim      endcyc      dtmin      endeng      endmas
      400.00000
*CONTROL_TIMESTEP
$#   dtinit      tssfacc      isdo      tslimt      dt2ms      lctm      erode      ms1st
      0.000  0.100000      0      0.000      0.000
$#   dt2msf      dt2mslc      imscl
      0.000      0         0
*DATABASE_MATSUM
$#   dt      binary
```

```

0.100000      1
*DATABASE_BINARY_D3DUMP
$# dt/cycl not used not used not used
      1000      3
*DATABASE_BINARY_D3PLOT
$#      dt      lcdt      beam      npltc
      0.100000
$#  ioopt
      0
*DATABASE_EXTENT_BINARY
$#  neiph      neips      maxint      strflg      sigflg      epsflg      rltflg      engflg
      9
$#  cmpflg      ieverp      beamip      dcomp      shge      stssz      n3thdt      ialemat
      0      0      0      0      0      0      2
$#  nintsld      pkp_sen      sclp      null      msscl      therm
      0      0      0.000      0      0      0
*PART
$# title
sample
$#  pid      secid      mid      eosid      hgid      grav      adpopt      tmid
      1      3      3      3
*SECTION_SOLID
$#  secid      elform      aet
      3      11
*MAT_ELASTIC_PLASTIC_HYDRO_TITLE
Teflon-Aluminum
$#  mid      ro      g      sigy      eh      pc      fs
      3      2.391000      0.002089      1.1600E-4
$#  eps1      eps2      eps3      eps4      eps5      eps6      eps7      eps8
      0.000      0.000      0.000      0.000      0.000      0.000      0.000      0.000
$#  eps9      eps10      eps11      eps12      eps13      eps14      eps15      eps16
      0.000      0.000      0.000      0.000      0.000      0.000      0.000      0.000
$#  es1      es2      es3      es4      es5      es6      es7      es8
      0.000      0.000      0.000      0.000      0.000      0.000      0.000      0.000
$#  es9      es10      es11      es12      es13      es14      es15      es16
      0.000      0.000      0.000      0.000      0.000      0.000      0.000      0.000
*EOS_IGNITION_AND_GROWTH_OF_REACTION_IN_HE_TITLE
Teflon-Aluminum
$#  eosid      a      b      xp1      xp2      frer      g      r1
      3      4.7355E+5      30.620300      50.466801      4.927370      1.727100      4.5754E-6      2.293712
$#  r2      r3      r5      r6      fmxig      freq      grow1      em
      2.009256      7.7099E-5      45.292294      51.545380      0.000000      11224.000      5.4521E+9      16.735001
$#  ar1      es1      cvp      cvr      eetal      ccrit      enq      tmp0
      0.000      1.002900      1.4570E-5      9.9300E-6      28.399000      1.0000E-6      0.013500
$#  grow2      ar2      es2      en      fmxgr      fmngr
      8.599E+13      6.3067e-5      1.0002      2.6963e1      0.000000      0.000000
*PART
$# title
Pipe
$#  pid      secid      mid      eosid      hgid      grav      adpopt      tmid
      3      4      4      4
*SECTION_SOLID
$#  secid      elform      aet
      4      2

```

```

*MAT_ELASTIC_PLASTIC_HYDRO_TITLE
Copper
$#   mid      ro      g      sigy      eh      pc      fs
      4  8.930000  0.447000  0.003590  0.000  0.000  1.000000
$#   eps1     eps2     eps3     eps4     eps5     eps6     eps7     eps8
      0.000  0.000  0.000  0.000  0.000  0.000  0.000  0.000
$#   eps9     eps10    eps11    eps12    eps13    eps14    eps15    eps16
      0.000  0.000  0.000  0.000  0.000  0.000  0.000  0.000
$#   es1      es2      es3      es4      es5      es6      es7      es8
      0.000  0.000  0.000  0.000  0.000  0.000  0.000  0.000
$#   es9      es10     es11     es12     es13     es14     es15     es16
      0.000  0.000  0.000  0.000  0.000  0.000  0.000  0.000
*EOS_GRUNEISEN_TITLE
Copper
$#   eosid      c      s1      s2      s3      gamao      a      e0
      4  0.394000  1.489000  0.000  0.000  1.990000
$#   v0
      1.000000
*PART
$# title
Air
$#   pid      secid      mid      eosid      hgid      grav      adpopt      tmid
      5        3        1
*MAT_VACUUM_TITLE
Vacuum
$#   mid      den
      1  1.3910E-6
*PART
$# title
c-4
$#   pid      secid      mid      eosid      hgid      grav      adpopt      tmid
      6        3        10      10
*MAT_HIGH_EXPLOSIVE_BURN
$#   MID      RO      D      PCJ      BETA      K      G      SIGY
$#   mid      ro      d      pcj      beta      k      g      sigy
      10  1.601000  0.819300  0.280000
*EOS_JWL
$#   EOSID      A      B      R1      R2      OMEG      E0      V0
$#   eosid      a      b      r1      r2      omeg      e0      vo
      10  6.097700  0.129510  4.500000  1.400000  0.250000  0.090000  1.000000
*INITIAL_DETONATION
$#   pid      x      y      z      lt
      6      0.000  0.000  34.152000
*INITIAL_VOLUME_FRACTION_GEOMETRY
$#   sid_ale      st_ale      group
      5        1        1
$#   geotype      in_opt      gr_fill
      4        0        3
$#   x0      y0      z0      x1      y1      z1      r1      r2
      0.000  0.000  30.000000  0.000  0.000  34.152000  2.397000
*SET_PART_LIST_TITLE
Lagrangian
$#   sid      da1      da2      da3      da4
      11

```

```

$#   pid1     pid2     pid3     pid4     pid5     pid6     pid7     pid8
      3
*SET_PART_LIST_TITLE
eularian
$#   sid      da1      da2      da3      da4
      12
$#   pid1     pid2     pid3     pid4     pid5     pid6     pid7     pid8
      1         5         6
*ALE_MULTI-MATERIAL_GROUP
$#   sid  idtype
      5      1
$#   sid  idtype
      1      1
$#   sid  idtype
      6      1
*CONSTRAINED_LAGRANGE_IN_SOLID
$#   slave  master  sstyp  mstyp  nquad  ctype  direc  mcoup
      11     12     0      0      -2     4      2
$#   start  end      pfac   fric   frcmin  norm  normtyp  damp
      0.0001.0000E+10 0.100000 0.000 0.500000
$#   cq     hmin    hmax   ileak  pleak  lcidpor  nvent  blockage
      0.000 0.000 0.000 0 0.010000
*END

```

Realistic Model

The following is the realistic LS-DYNA model. The geometry has been excluded due to extreme length.

```
*KEYWORD memory=450m
*TITLE
$# title
Reactive Material Test
*CONTROL_ALE
$#   dct      nadv      meth      afac      bfac      cfac      dfac      efac
      3        1        2 -1.000000
$#   start      end      aafac      vfact      prit      ebc      pref      nsidebc
      0.0001.0000E+20  1.000000  1.0000E-6  1.000000      2      0.000      2
*CONTROL_BULK_VISCOSITY
$#   q1      q2      type
      1.500000  0.060000
*CONTROL_CONTACT
$#   slsfac      rwpnal      islchk      shlthk      penopt      thkchg      orien      enmass
      0.100000      0.000      1      0      0      0      1
$#   usrstr      usrfrc      nsbcs      interm      xpene      ssthk      ecdt      tiedprj
      0      0      0      0      4.000000
$#   sfric      dfrc      edc      vfc      th      th_sf      pen_sf
      0.000      0.000      0.000      0.000      0.000      0.000      0.000
$#   ignore      frceng      skiprwg      outseg      spotstp      spotdel      spothin
      0      0      0      0      0      0      0.000
$#   isym      nserod      rwgaps      rwgth      rwksf
      0      0      0      0.000      1.000000
*CONTROL_ENERGY
$#   hgen      rwen      slnten      rylen
      2
*CONTROL_HOURLASS
$#   ihq      qh
      1      0.150000
*CONTROL_OUTPUT
$#   npopt      neecho      nrefup      iaccop      opifs      ipnint      ikedit      iflush
      0      0      0      0      0.000      0      200      5000
$#   iprtf
      0
*CONTROL_PARALLEL
$#   ncpu      numrhs      const      para
      1      0      2
```

```

*CONTROL_TERMINATION
$# endtim   endcyc   dtmin   endeng   endmas
   1000.0000
*CONTROL_TIMESTEP
$# dtinit   tssfacc   isdo    tslimt   dt2ms   lctm   erode   ms1st
   0.000   0.100000
$# dt2msf   dt2mslc   imsc1
   0.000     0       0
*DATABASE_MATSUM
$#   dt     binary
   0.100000     1
*DATABASE_BINARY_D3DUMP
$# dt/cycl  not used  not used  not used
   50        3
*DATABASE_BINARY_D3PLOT
$#   dt     lcdt     beam     npltc
   1.000000
$#  ioopt
   0
*DATABASE_EXTENT_BINARY
$#  neiph   neips   maxint   strflg   sigflg   epsflg   rtflg   engflg
   9
$#  cmpflg  ieverp   beamip   dcomp    shge     stssz   n3thdt   ialemat
   0        0       0       0       0       0       2
$#  nintsld  pkp_sen   sclp     null     mssc1    therm
   0        0       0.000   0       0       0
*CONTACT_AUTOMATIC_SINGLE_SURFACE
$#   cid
$#  ssid    msid     sstyp    mstyp    sboxid   mboxid   spr      title
   0        0       5
$#   fs     fd       dc       vc       vdc     penchk   bt      dt
   0.000   0.000   0.000   0.000   0.000   0       0.000   0.000
$#   sfs    sfm     sst     mst     sfst    sfmt     fsf     vsf
   1.000000 1.000000 0.000   0.000   1.000000 1.000000 1.000000 1.000000
$#   soft   sofsc1  lcdab   maxpar   sbopt   depth   bsort   frcfrq
   2
$#  penmax  thkopt   shlthk   snlog    isym    i2d3d   sldthk   sldstf
   0.000    0       0       0       0       0       0.000   0.000
*PART
$# title
Air
$#   pid    secid   mid     eosid    hgid    grav    adpopt   tmid
   1        3       1
*SECTION_SOLID
$#  secid   elform   aet
   3       11
*MAT_VACUUM_TITLE
Vacuum
$#   mid     den
   1 1.3910E-6
*PART
$# title
reactive projectile
$#   pid    secid   mid     eosid    hgid    grav    adpopt   tmid

```

```

      2      3      3      3
*MAT_ELASTIC_PLASTIC_HYDRO_TITLE
Teflon-Aluminum
$#   mid      ro      g      sigy      eh      pc      fs
      3  2.391000  0.002089  1.1600E-4
$#   eps1     eps2     eps3     eps4     eps5     eps6     eps7     eps8
      0.000    0.000    0.000    0.000    0.000    0.000    0.000    0.000
$#   eps9     eps10    eps11    eps12    eps13    eps14    eps15    eps16
      0.000    0.000    0.000    0.000    0.000    0.000    0.000    0.000
$#   es1      es2      es3      es4      es5      es6      es7      es8
      0.000    0.000    0.000    0.000    0.000    0.000    0.000    0.000
$#   es9      es10     es11     es12     es13     es14     es15     es16
      0.000    0.000    0.000    0.000    0.000    0.000    0.000    0.000
*EOS_IGNITION_AND_GROWTH_OF_REACTION_IN_HE_TITLE
Teflon-Aluminum
$#   eosid      a      b      xp1      xp2      frer      g      r1
      3  4.7355E+5  30.620300  50.466801  4.927370  1.727100  4.5754E-6  2.293712
$#   r2      r3      r5      r6      fmxig      freq      grow1      em
      2.009256  7.7099E-5  45.292294  51.545380  0.000000  11224.000  5.4521E+9  16.735001
$#   ar1      es1      cvp      cvr      eetal      ccrit      enq      tmp0
      0.000    1.002900  1.4570E-5  9.9300E-6  28.399000  1.0000E-6  0.013500
$#   grow2     ar2      es2      en      fmxgr      fmngr
      8.599E+13  6.3067e-5  1.0002  2.6963e1  0.000000  0.000000
*PART
$# title
Bullet Casing
$#   pid      secid      mid      eosid      hgid      grav      adpopt      tmid
      21      4      40      30
*SECTION_SOLID
$#   secid      elform      aet
      4      2
*MAT_ELASTIC_PLASTIC_HYDRO_TITLE
AL 7075
$#   mid      ro      g      sigy      eh      pc      fs
      40  2.813000  0.268900  0.004820  0.000    0.000  0.130000
$#   eps1     eps2     eps3     eps4     eps5     eps6     eps7     eps8
      0.000    0.000    0.000    0.000    0.000    0.000    0.000    0.000
$#   eps9     eps10    eps11    eps12    eps13    eps14    eps15    eps16
      0.000    0.000    0.000    0.000    0.000    0.000    0.000    0.000
$#   es1      es2      es3      es4      es5      es6      es7      es8
      0.000    0.000    0.000    0.000    0.000    0.000    0.000    0.000
$#   es9      es10     es11     es12     es13     es14     es15     es16
      0.000    0.000    0.000    0.000    0.000    0.000    0.000    0.000
*EOS_GRUNEISEN_TITLE
AL 7075
$#   eosid      c      s1      s2      s3      gamao      a      e0
      30  0.523000  1.320000  0.000    0.000  2.200000  0.000  0.007599
$#   v0
      1.000000
*PART
$# title
Front Plate
$#   pid      secid      mid      eosid      hgid      grav      adpopt      tmid
      29      6      80

```

```

*SECTION_SHELL
$CardName:0.25_INCHES
$  secid  elform  shrf  nip  propt  qr/irid  icomp  setyp
$#  secid  elform  shrf  nip  propt  qr/irid  icomp  setyp
      6      1 0.870000  5      2      0      0      1
$      t1      t2      t3      t4      nloc
$#      t1      t2      t3      t4      nloc      marea
      0.317500 0.317500 0.317500 0.317500
*MAT_PIECEWISE_LINEAR_PLASTICITY
$CardName:AL 7075
$  mid  ro  e  pr  sigy  etan  fail  tdel
$#  mid  ro  e  pr  sigy  etan  fail  tdel
      80 2.813000 0.710160 0.330000 0.004820 3.4473E-4 0.130000 0.001000
$  c  p  lcsc  lcsr  vp
$#  c  p  lcsc  lcsr  vp
      0.000 0.000 0 0 0.000
$  eps1  eps2  eps3  eps4  eps5  eps6  eps7  eps8
$#  eps1  eps2  eps3  eps4  eps5  eps6  eps7  eps8
      0.000 0.000 0.000 0.000 0.000 0.000 0.000 0.000
$  es1  es2  es3  es4  es5  es6  es7  es8
$#  es1  es2  es3  es4  es5  es6  es7  es8
      70000.000 75500.000
*PART
$# title
Inner Plate 1
$#  pid  secid  mid  eosid  hgid  grav  adpopt  tmid
      37      7      80
*SECTION_SHELL
$CardName:0.50_INCHES
$  secid  elform  shrf  nip  propt  qr/irid  icomp  setyp
$#  secid  elform  shrf  nip  propt  qr/irid  icomp  setyp
      7      1 0.870000  5      2      0      0      1
$      t1      t2      t3      t4      nloc
$#      t1      t2      t3      t4      nloc      marea
      0.158749 0.158749 0.158749 0.158749
*PART
$# title
Inner Plate 2
$#  pid  secid  mid  eosid  hgid  grav  adpopt  tmid
      38      7      80
*PART
$# title
Inner Plate 3
$#  pid  secid  mid  eosid  hgid  grav  adpopt  tmid
      39      7      80
*PART
$# title
Rear Plate
$#  pid  secid  mid  eosid  hgid  grav  adpopt  tmid
      40      6      80
*PART
$# title
Threaded Rods
$#  pid  secid  mid  eosid  hgid  grav  adpopt  tmid

```

```

41      5      5
*SECTION_BEAM_TITLE
threaded rods
$#  secid  elform  shrf  qr/irid  cst  scoor  nsm
      5      3
$#      a      iss      itt      irr      sa
0.952500
*MAT_PLASTIC_KINEMATIC_TITLE
steel
$#  mid      ro      e      pr      sigy      etan      beta
      5  7.860000  2.410000  0.320000  0.007240  0.045000
$#  src      srp      fs      vp
      0.000      0.000  10.300000
*INITIAL_VELOCITY
$#  nsid  nsidex  boxid  irigid
      1
$#  vx      vy      vz      vxr      vyr      vzr
-0.316600
*SET_PART_LIST_TITLE
LagrangeParts
$#  sid      da1      da2      da3      da4
      1
$#  pid1      pid2      pid3      pid4      pid5      pid6      pid7      pid8
      21      29      37      38      39      40
*SET_PART_LIST_TITLE
EulerParts
$#  sid      da1      da2      da3      da4
      2
$#  pid1      pid2      pid3      pid4      pid5      pid6      pid7      pid8
      1      2
*ALE_MULTI-MATERIAL_GROUP
$#  sid  idtype
      1      1
$#  sid  idtype
      2      1
*CONSTRAINED_LAGRANGE_IN_SOLID
$#  slave  master  sstyp  mstyp  nquad  ctype  direc  mcoup
      1      2      0      0      -2      4      3      1
$#  start  end  pfac  fric  frcmin  norm  normtyp  damp
      0.0001.0000E+10  0.100000  0.000  0.500000
$#  cq      hmin  hmax  ileak  pleak  lcidpor  nvent  blockage
      0.000      0.000  0.000      0  0.010000
*END

```

Bibliography

- [1] Aminov, Yu. A., Es'kov, N. S., and Nikitenko, Yu. R., "Modeling of Double Shock Initiation of TATB-Based Explosives," 12th International Detonation Symposium, Wyndham San Diego at Emerald Plaza, San Diego, California, (11-16 August 2002)
- [2] Baker, Ernest L., Capellos, Christos, and Stiel, Leonard I., "Jaguar Procedures For Detonation Properties of Aluminized Explosives," 12th International Detonation Symposium, Wyndham San Diego at Emerald Plaza, San Diego, California, (11-16 August 2002)
- [3] <https://pdc.usace.army.mil/software/blastx/>, BLAST-X User's Manual (March 2002)
- [4] Brown, L.L, Reed, C., ARA Project 0003, "First Look Evaluation of RIM/PTFE Projectiles", Final Report, October, 1999
- [5] <https://pdc.usace.army.mil/software/conwep/>, CONWEP User's Manual (March 2002)
- [6] Fickett, W., and Scherr, L. M., "Numerical Calculation of the Cylinder Test," Lawrence Livermore National Laboratory report UCRL-LA-5906 (March 1975)

BIBLIOGRAPHY

- [7] Fickett, W., "One-Dimensional Approximation to the Cylinder Test," Los Alamos Scientific Laboratory report UCRL-LA-6608, (January 1977)
- [8] Hallquist, John O., Stillman, Douglas W., Hughes, T. J. R., and Tarver, Craig, "Modeling of Airbags Using MVMA/DYNA3D," Livermore Software Technology Company (LSTC), (July 1990)
- [9] Holsapple, K. A., "What Do We Need To Know To Model Impact Processes?," 2003 Workshop on Impact Cratering, University of Washington, 352400, Seattle, WA 98195,(2003)
- [10] <http://www.nap.edu/openbook/0309091608/html/R1.html>, Advanced Energetic Materials (2004),Chapter 4, page 23, The National Academy of Sciences.
- [11] <http://www.ae.gatech.edu/research/sdssl/muri/muri.html>
- [12] Itoh, S., and Hamashima, H., "Determination of JWL Parameters From Underwater Explosion Test," 12th International Detonation Symposium, Wyndham San Diego at Emerald Plaza, San Diego, California, (11-16 August 2002)
- [13] James, H. R., and Lambourn, B. D., "A Continuum-Based Reaction Growth Model for the Shock Initiation of Explosives," Propellants, Explosives and Pyrotechnics, 26, pg. 246-256, (2001)
- [14] Kerley, Gerald I., "User's Manual for PANDA II: A Computer Code for Calculating Equations of State," Sandia National Laboratories report SAND88-2291, (June 1991)
- [15] Kerley, Gerald I., and Christian-Frear, Tracy L., "Prediction of Explosive Cylinder Tests Using Equations of State from the PANDA Code," Sandia National Laboratory report SAND93-2131, (September 28, 1993)

BIBLIOGRAPHY

- [16] Kerley, Gerald I., "A Reactive Equation of State Model for Teflon," NSWDC, Dahlgren Division, (October 1996)
- [17] Kerley, Gerald I., "Equations of State for Aluminum-Teflon Mixtures," NSWDC, Dahlgren Division, (November 1997)
- [18] Kerley, Gerald I., "A Study of Shock-Induced Reactive Behavior in Aluminum-PTFE Mixtures," NSWDC, Dahlgren Division, (December 1999)
- [19] Lee, E. L., and Tarver, C. M., "Phenomenological Model of Shock Initiation in Heterogeneous Explosives," *Phys. Fluids*, Vol. 23, No. 12, (December 1980)
- [20] Lee, E. L., Hornig, H. C., and Kury, J. W., "Adiabatic Expansion of High Explosive Detonation Products," Lawrence Livermore National Laboratory report UCRL-50422 (May 2, 1968)
- [21] "LS-DYNA Keyword User's Manual," Livermore Software Technology Corporation, (April 2003)
- [22] Lu, Jing Ping, Dorsett, Helen, and Kennedy, David L., "Simulation of Aquarium Tests for PBXW-115(AUST)," Weapons System Division Defense Science and Technology Organization, Edinburgh, South Australia
- [23] Lu, Jing Ping, and Kennedy, David L., "Modelling of PBXW-115 Using Kinetic CHEETAH and the DYNA Codes," DSTO Systems Sciences Laboratory, Edinburgh, South Australia, (September 2003)
- [24] Lu, J. P., Christo, F. C., Kennedy, D. L., "Detonation Modeling of Corner-Turning Shocks in PBXN-111," 15th Australasian Fluid Mechanics Conference, The University of Sydney, Sydney, Australia, (13-17 December 2004)

BIBLIOGRAPHY

- [25] Lu, Xia, and Hanagud, Sathya V., “Structural Phase Transitions and Equation of State of Aluminum from First-Principles”, School of Aerospace Engineering, Georgia Institute of Technology, Atlanta, GA
- [26] Charles L. Mader. *Numerical Modeling of Explosives and Propellants, 2nd edition*. CRC Press LLC, Boca Raton, FL, 1998
- [27] Marsh, Stanley P., ed., “LASL Shock Hugoniot Data,” University of California Press, Los Angeles, CA, (1980)
- [28] Marc A. Meyers. *Dynamic Behavior of Materials*. John Wiley & Sons, Inc., New York, NY, 1994
- [29] Morris, C. E., Fritz, J. N., and McQueen, R. G., “The Equation of State of Polytetrafluorethylene to 80GPa,” Los Alamos National Laboratory, Los Alamos, New Mexico, (1984)
- [30] Rowe, Adam, and Thadhani, Naresh, “Dynamic Mechanical Behavior of Two-phase $TiB_2 + Al_2O_3$ Ceramics,” Colorado School of Mines, Georgia Tech, (2002)
- [31] Souers, P. Clark, Anderson, Steve, Mercer, James, McGuire, Estella, and Vitello Peter, “JWL++: A Simple Reactive Flow Code Package For Detonation,” *Propellants, Explosives, Pyrotechnics*, 25, pg. 54-58, (2000)
- [32] Tarver, Craig M., Urtiew, Paul A., “Theoretical and Computer Models of Detonation in Solid Explosives,” Lawrence Livermore National Laboratory report UCRL-JC-128755 (October 1997)
- [33] Thoma, Klaus, Riedel, Werner, and Hiermaier, Stefan, “Mesomechanical Modeling of Concrete Shock Response Experiments and Linking to Macromechanics by Numerical Analysis,” ECCM '99, Munchen, Germany, (1999)

BIBLIOGRAPHY

- [34] Wilkins, M. L., “Modeling the Behavior of Materials,” Lawrence Livermore National Laboratory report UCRL-ID-113198 (March, 1993)

- [35] Wilkins, Mark L., Squier, Bailey, and Halperin, Bertram, “The Equation of State of PBX 9404 and LX04-01,” University of California Lawrence Radiation Laboratory report UCRL-7797 (April 27, 1964)

- [36] Wilkins, M. L., “A Method For Computer Simulation of Problems in Solid Mechanics and Gas Dynamics in Three Dimensions and Time,” Lawrence Livermore National Laboratory report UCRL-51574 Rev. 1 (May 30, 1975)

- [37] Zaug, J. M., Fried, L. E., Crowhurst, J. C., Hansen, D. W., Howard, W. M., Lee, G. S., Pagoria, P. F., and Abramson, E. H., “Experimental EOS and Chemical Studies of High-Pressure Detonation Products and Product Mixtures,” Lawrence Livermore National Laboratory report UCRL-JC-145159, (July 1, 2002)